OAK RIDGE NATIONAL LABORATORY LIBRARIES
3 4456 0555544 0

ORNL/TM-7128

ornl

OAK
RIDGE
NATIONAL
LABORATORY

UNION
CARBIDE

Neutronics Model of the Bulk Shielding Reactor (BSR): Validation by Comparison of Calculations with the Experimental Measurements

J. O. Johnson
L. F. Miller
F. B. K. Kam

OAK RIDGE NATIONAL LABORATORY
CENTRAL RESEARCH LIBRARY
CIRCULATION SECTION
4500N ROOM 175
LIBRARY LOAN COPY
DO NOT TRANSFER TO ANOTHER PERSON
If you wish someone else to see this report, send in name with report and the library will arrange a loan.
UCN-7969 3 9-77

OPERATED BY
UNION CARBIDE CORPORATION
FOR THE UNITED STATES
DEPARTMENT OF ENERGY

Printed in the United States of America. Available from
National Technical Information Service
U.S. Department of Commerce
5285 Port Royal Road, Springfield, Virginia 22161
NTIS price codes—Printed Copy: A06; Microfiche A01

This report was prepared as an account of work sponsored by an agency of the United States Government. Neither the United States Government nor any agency thereof, nor any of their employees, makes any warranty, express or implied, or assumes any legal liability or responsibility for the accuracy, completeness, or usefulness of any information, apparatus, product, or process disclosed, or represents that its use would not infringe privately owned rights. Reference herein to any specific commercial product, process, or service by trade name, trademark, manufacturer, or otherwise, does not necessarily constitute or imply its endorsement, recommendation, or favoring by the United States Government or any agency thereof. The views and opinions of authors expressed herein do not necessarily state or reflect those of the United States Government or any agency thereof.

ORNL/TM-7128

Contract No. W-7405-eng-26

OPERATIONS DIVISION

NEUTRONICS MODEL OF THE BULK SHIELDING REACTOR (BSR): VALIDATION BY COMPARISON OF CALCULATIONS WITH THE EXPERIMENTAL MEASUREMENTS

J. O. Johnson*
L. F. Miller
F. B. K. Kam

SPONSOR: J. A. Cox
Director, Operations Division

*Department of Nuclear Engineering
The University of Tennessee
Knoxville, Tennessee 37916

Date Published - May 1981

OAK RIDGE NATIONAL LABORATORY
Oak Ridge, Tennessee 37830
operated by
UNION CARBIDE CORPORATION
for the
DEPARTMENT OF ENERGY

OAK RIDGE NATIONAL LABORATORY LIBRARIES

3 4456 0555544 0

TABLE OF CONTENTS

ABSTRACT v

INTRODUCTION 1

DESCRIPTION OF BSR 2

DESCRIPTION OF THE EXPERIMENT 2

CALCULATIONAL FLOW PATH AND THEORY 3

DISCUSSION OF RESULTS 12

CONCLUSIONS 18

RECOMMENDATIONS 19

REFERENCES 20

APPENDIX A 21

APPENDIX B 84

ACKNOWLEDGEMENTS 102

DISTRIBUTION 103

ABSTRACT

A neutronics model for the Oak Ridge National Laboratory Bulk Shielding Reactor (ORNL-BSR) was developed and verified by experimental measurements.

A cross-section library was generated from the 218 group Master Library using the AMPX Block Code system. A series of one-, two-, and three-dimensional neutronics calculations were performed utilizing both transport and diffusion theory. Spectral comparison was made with ^{58}Ni(n,p) reaction.

The results of the comparison between the calculational model and other experimental measurements showed agreement within 10% and therefore the model was determined to be adequate for calculating the neutron fluence for future irradiation experiments in the ORNL-BSR.

INTRODUCTION

In the past several years, there has been a growing concern in the industry to be able to predict the irradiation damage to the pressure vessel and core support structure of some of the early Light Water Reactors (LWR) without in-place test specimens. Therefore, in an effort to obtain further insight into irradiation damage of LWRs, the Nuclear Regulatory Commission (NRC) has established the LWR Irradiation Surveillance Improvement Program. The primary goals of this program are to establish consistent and accurate dosimetry and damage analysis techniques, both experimental and analytical, to correlate changes in material properties with the characteristics of the neutron radiation field. With respect to these goals, several experiments are being performed. Along with these experiments, computational models are being formed using the experiments as a guide to the accuracy of the model. Once an acceptable model has been validated, important parameters, such as fluences and reaction rates can be accurately calculated for similar systems. These calculated parameters can be compared with irradiation damage measurements to obtain points on a trend curve relating fluence to irradiation damage. This will facilitate better prediction of the irradiation damage to the reactor pressure vessel and core support structure for specific configurations of interest.

The work reported within this document is funded by the Naval Research Laboratories (NRL). They are primarily interested in the characteristics of the steel and in the core support structure of the various types of reactors as a function of irradiation. This report, however, is limited to the determination of an accurate neutronics model of the Oak Ridge National Laboratory Bulk Shielding Reactor (ORNL-BSR).

The procedure for formulating the computational model of the ORNL-BSR involved many calculations. Physical data pertaining to the core and experimental configurations were obtained to construct input for the models used in the neutronics calculations. A 40 neutron energy group working library was generated that included cell-weighted and self-shielded core cross sections. This library was used in a series of

one-, two-, and three-dimensional neutronics calculations to obtain a variety of results. Relative fluxes above 0.1, 0.5, and 1.0 MeV, as well as the spectrum, were calculated to obtain spectral averaged cross sections for the $^{54}Fe(n,p)$, $^{58}Ni(n,p)$ reactions and the average displacement cross section for Fe. Spatial distributions of measured and calculated activities were compared to evaluate the calculated spatial distributions. Measured and calculated reaction rate ratios were compared to evaluate the calculated spectrum at various locations.

DESCRIPTION OF BSR

The BSR is a pool reactor used in research that makes use of ordinary water as a moderator, a coolant, and a shield. The design is remarkably simple and consists of a lattice of Materials Test Reactor (MTR) type fuel elements immersed in a large pool of water. The reactor operates at a maximum power of 2 MW with forced convection cooling and has the main advantages of low costs, safety, flexibility, and accessibility.

The standard MTR-type fuel element consist of eighteen aluminum clad plates of 93% enriched uranium-aluminum alloy. Each element has the dimensions of 2.996 in. × 3.069 in. × 24.625 in. with an active fuel length of 23.625 in. centered in the axial direction. Each element has a metal-to-water ratio of about 0.72. The reactivity of the BSR is controlled by the use of six control elements. These control elements contain a control blade slot that replaces the center nine plates of a standard fuel element. The control blades are composed of B_4C and stainless steel.

DESCRIPTION OF THE EXPERIMENT

The experimental phase of this project was performed on two separate core loadings of the BSR. Core 37 contained a single NRL irradiation position as shown in Fig. 1. The weights of the elements used in core 37 (in terms of grams of ^{235}U) are shown in Table 1. Core 54 contained two NRL irradiation positions as shown in Fig. 2. Table 2, likewise, contains the weights of the fuel elements used in core 54. These are the two cores used in the dosimetry capsule irradiations of the flux monitor wires,

but are not the cores used in the actual metallurgical test specimen irradiations. However, the cores used in the test specimen irradiations are very similar in loading with differences only in the fuel element burnup.

The dosimetry capsules for BSR cores 37 and 54 are shown in Figs. 3 and 4, respectively. Each capsule is designed to fit in a standard MTR-type fuel element with all center plates removed and the side plate constructued of aluminum. Aluminum spacers of approximately 1.75 in. and 3.625 in. were used in the bottom of the experimental elements in cores 37 and 54, respectively, to position the NRL dosimetry capsules in the axial direction. Table 3 details the various axial irradiation positions and other axial positions of interest for the two experimental elements. Flux monitor wires of iron and nickel were inserted in the irradiation tubes (cf. Figs. 3 and 4) of the dosimetry capsules. Segments of the wire were cut out at the axial irradiation positions shown in Table 3. Count rate measurements of these wire segments gave the absolute experimental reaction rates with which the computational results were compared.

CALCULATIONAL FLOW PATH AND THEORY

The development of the computational model for the ORNL-BSR utilized a wide variety of computer codes and was considered adequate enough to calculate the parameters measured in the experiments. The Criticality Safety 218 Group Master Library[1] was used to generate the various cross-section sets utilized in the neutronics calculations. The 40 group reference cross-section library was generated by executing various modules of the AMPX-II[2] code system. Fig. 5 depicts the generation of the 40 neutron energy group library. Table 4 explains the footnote on the various modules in Fig. 5. Figs. 6 through 8 show the neutronics calculations performed on each sub-library created from the reference 40 group library. Table 4, again, explains the footnote on the various modules.

AJAX, an AMPX-II module, was used to create a master library of those elements needed in the calculations. This smaller library was less cumbersome to manage and utilize in the calculations for this project. MALOCS utilized a Fission-1/E-Maxwellian spectrum to weight the cross sections and collapse them to 40 neutron energy groups. Resonance information from the 218 group Master Library is retained in the 40 group Master Library. The equations used to calculate the Fission-1/E-Maxwellian spectrum are given below:

Fission Tail $$\chi(E) = .77E^{1/2}e^{-.776E} \quad (1)$$

1/E $$F(E) = 1/E \quad (2)$$

Maxwellian distribution $$n(E) = \frac{2\pi}{(\pi kT)^{3/2}} E^{1/2} e^{-E/kt} \quad . \quad (3)$$

The 40 group Master Library generated by MALOCS was used as input into NITAWL which is an acronym for Nordheim Integral Treatment And Working Library production. NITAWL is employed for reading these general ENDF/B formats, performing resonance self-shielding calculations, and collecting data into workable arrangements such as the format required by the other AMPX-II modules.

The Nordheim Integral Treatment utilizes the balance equation that describes neutron slowing down in an infinite, homogeneous medium and generalizes this equation to account for a heterogeneous fuel cell. Energy-dependent first-flight escape probabilities $P_{Fo}(E)$ and $P_{Mo}(E)$ are key parameters in the heterogeneous cell treatment. The treatment also interprets the flux in the fuel $\phi_F(E)$ and the flux in the moderator $\phi_M(E)$ to obtain the volume averaged fluxes in the fuel and moderator, respectively. These characterizations set forth give a set of coupled balance relations for the fuel and moderator given by equations 4 and 5, respectively.[3]

$$V_F \sum_t^F(E)\ \phi_F(E) = V_F[1 - P_{Fo}(E)] \int_E^{E/\alpha_F} \frac{dE'\ \sum_S^F(E')\ \phi_F(E')}{(1 - \alpha_F)\ E'}$$

$$+ V_M\ P_{Mo}(E) \int_E^{E/\alpha_M} \frac{dE'\ \sum_S^M(E')\ \phi_M(E')}{(1 - \alpha_M)\ E'} \tag{4}$$

$$V_M \sum_t^M(E)\ \phi_M(E) = V_M[1 - P_{Mo}(E)] \int_E^{E/\alpha_M} \frac{dE'\ \sum_S^M(E')\ \phi_M(E')}{(1 - \alpha_M)\ E'}$$

$$+ V_F\ P_{Fo}(E) \int_E^{E/\alpha_F} \frac{dE'\ \sum_S^F(E')\ \phi_F(E')}{(1 - \alpha_F)\ E'} \tag{5}$$

In the above equations, F denotes fuel, M denotes moderator and alpha (α) is just

$$\alpha = \left(\frac{A - 1}{A + 1}\right)^2 . \tag{6}$$

To decouple these equations, a few approximations are necessary. First, one must utilize the flat source approximation of uniform isotropic neutrons to compute the escape probabilities. Secondly, the narrow resonance approximation for the moderator must be instituted to allow the flux in the moderator to be replaced by its asymptotic form:

$$\phi_M(E) \sim 1/E \tag{7}$$

Then, substituting the above assumptions into equations 4 and 5 allow for the equations to be decoupled. Once $P_{Fo}(E)$ is known, the fuel equation can be solved for $\phi_F(E)$ and the effective resonance integral can be calculated

$$I = \int_{E_o} dE\ \sigma_\gamma^F(E)\ \phi_F(E) \quad . \tag{8}$$

The multi-group cross sections in the resonance region can then be calculated from the appropriate resonance integrals. It should be noted that this program does not take into effect the interference due to resonances of different nuclides.

With the resonance calculations performed, the AMPX-II working library has been formed and the next step was to cell-weight the cross sections. The module within AMPX-II normally used for these calculations is XSDRNPM which is an acronym for X-Section Dynamics for Reactor Neutronics with Petrie Modifications.

The model used in the cell-weighting calculations is shown in Fig. 9. This model is a typical fuel plate in a MTR-type element and half the water channel on each side of the plate. A repeating boundary condition was applied to the two water channel boundaries. The cell-weighted

cross sections were produced according to the equation:

$$\overline{\sigma_G}^{Cell} = \frac{\sum_{j=1}^{IZM} N_j \sum_{i\varepsilon j} \Delta V_i \sum_{g\varepsilon G} \phi_g(i)\ \sigma_g(i)}{\left[\sum_{j=1}^{IZM} N_j \sum_{i\varepsilon j} \Delta V_i\right]\left[\frac{1}{V} \sum_{i=1}^{IM} \Delta V_i \sum_{g\varepsilon G} \phi_g(i)\right]} \quad , \tag{9}$$

where IZM is the total number of zones, j is a zone index, N_j is the number density in zone j, i is a spatial interval index, ΔV_i is the volume of interval i, g is a group index, $\sigma_g(j)$ is the group value of the microscopic cross section, IM is the total number of intervals, V is the total cell volume, and $\phi_g(i)$ is the flux for spatial interval i defined by:

$$\phi_g(i) = \int_{E\varepsilon g} dE\ \phi(E,\overline{r}) \quad . \tag{10}$$

This produces an "average" value of the cross section and not a point value. The averaging codes in XSDRNPM assume some characteristic flux shape, such as 1/E or fission spectrum, across a group to arrive at the fine-group values.

Since the cross-section set out of XSDRNPM only contained the fuel element cross sections, NITAWL was used again to merge the XSDRNPM cell-weighted cross section with the previous NITAWL self-shielded cross sections to form the final reference 40 group working weighted library to be used in all subsequent calculations.

Up to this point, all calculations were performed on a 40 neutron energy group structure because results of a previous study have shown this group structure adequate for the resonance and cell-weighting calculations.[4] However, since the remaining calculational flow paths

(Figs. 6 through 8) involve two- and three-dimensional calculations, such a group structure would be too costly to employ in terms of time and money. Therefore, the 40 group working weighted library formed by NITAWL was again used as input to XSDRNPM for the purpose of "zone" weighting and collapsing to 40, 27, 15, and 7 neutron energy groups. As stated above, one reason for performing this calculation was to cut cost and computer time. A second reason for performing the "zone" weighting calculation was to check for any perturbations that group structure would have on the results.

The "zone" weighted cross sections were produced by the equation:

$$\bar{\sigma}_g^{Zone_j} \bar{\phi}_G^{\,j} V_j = \sum_{i \varepsilon j} \Delta V_i \sum_{g \varepsilon G} \phi_g(i)\, \sigma_g(i), \qquad (11)$$

where $\bar{\phi}_G^{\,j}$ is the average flux in zone j group G, and V_j is the volume of zone j. Since XSDRNPM is a one-dimensional code, the zones were set up as rows of elements. Referencing to Figs. 1 and 2, there were two outside zones of water, one on each side, and the core was divided into eight individual zones. Zone 2 was core positions 85 through 89, zone 3 was core positions 75 through 79, and so on down to zone 9 being core positions 15 through 19. This calculation produces a separate set of core cross sections for each zone and, therefore, each set was more representative of the spectrum in that region of the core.

After the "zone" weighting, the cross-section sets were collapsed to the 40, 27, 15, and 7 neutron energy group structures shown in Tables 5 through 8. These four libraries were the basic libraries used in all the transport and diffusion calculations depicted in Figs. 6 through 8.

Figs. 6 through 8 indicate that a variety of one-, two-, and three-dimensional transport and diffusion calculations were performed. The cross section format was in the proper form for the one-dimensional transport calculations (XSDRNPM) since they were generated in the AMPX-II system. However, the cross section format was incorrect for VENTURE[5] and DOT 4.2[6] because these codes are separate from AMPX-II. For this purpose,

the AMPX-II CONTAC was used. CONTAC is an AMPX-II utility module which converts an AMPX-II working library into a library for other code systems. In the case of DOT 4.2, CONTAC converted the AMPX-II 7 group library to an ANISN format (Fig. 8). DOT 4.2 is a two-dimensional discretized transport code. In the case of VENTURE, CONTACT converted the AMPX 40, 27, 15, and 7 group libraries into ISOTXS format. VENTURE is a multi-dimensional code block consisting of several special processors which solves the multi-group diffusion equation.

The calculations involved both the use of transport and diffusion theory. One reason for this is that transport theory was needed to show the validity of the diffusion theory calculations. Furthermore, the only three-dimensional calculation that could be done at ORNL was a diffusion theory calculation. XSDRNPM (one-dimensional) and DOT 4.2 (two-dimensional) both solve a time dependent form of the Boltzmann Transport Equation shown below:[7]

$$\frac{1}{v}\frac{\partial\phi(\bar{r},E,\bar{\Omega},t)}{\partial t} = -\bar{\Omega}\circ\nabla\phi(\bar{r},E,\bar{\Omega},t) - \Sigma_t(\bar{r},E)\,\phi(\bar{r},E,\bar{\Omega},t)$$
$$+\,\chi(E)\int_0^\infty dE'\int_0^{4\pi} d\bar{\Omega}'\,\nu\,\Sigma_f(\bar{r},E')\,\phi(\bar{r},E',\bar{\Omega}',t) \qquad (12)$$
$$+\int_0^\infty dE'\int_0^{4\pi} d\bar{\Omega}'\,\Sigma(E'\to E,\bar{\Omega}'\to\bar{\Omega})\,\phi(\bar{r},E',\bar{\Omega}',t).$$

Both codes use the discrete ordinates method to discretize the direction variable $\bar{\Omega}$ in the neutron transport equation. This produces a coupled set of N equations of the form:

$$\bar{\Omega}_n\times\nabla\phi_n + \Sigma_t\,\phi_n(r,E) = \sum_{n=1}^{N} w_{n'}\int_0^\infty dE'\,\Sigma_S(E'\to E,\bar{\Omega}_{n'}\to\bar{\Omega}_n)\,\phi_{n'}(r,E')$$
$$+\,S_n(r,E) \qquad (13)$$

where n = 1 . . . N while

$$\phi_n(r,E) \equiv \phi(r,E,\bar{\Omega}_n) \ . \tag{14}$$

The codes further discretize the energy variable to form a coupled set of multi-group S_N equation of the form:

$$\Omega_n \times \nabla\phi_n^g + \Sigma_{tg}\ \phi_n^g = \sum_{n'} w_{n'} \sum_{g'} \Sigma_{S_{n'\to n}^{g'\to g}}\ \phi_{n'}^{g'} + S_n^g \ , \tag{15}$$

n = 1 . . . N, g = 1 . . . G, and w_n are the appropriately chosen quadrature weights for the particular numerical integration scheme used to handle the angular integrals.

VENTURE solves the steady-state equation with the diffusion approximation to transport for the neutron flux at geometric location r and energy E given below:

$$\begin{aligned} -\nabla D(r,E)\ \nabla\ \phi(r,E) + \left[\Sigma_a(r,E) + \Sigma_S(r,E) + D(r,E)\ B_1^2(E)\right] \phi(r,E) \\ = \int_{E'} \left[\Sigma(r,E'\to E) + \frac{1}{K_e}\ \chi(r,E)\ \nu\Sigma_f(r,E')\right] \phi(r,E')\ dE' \ . \end{aligned} \tag{16}$$

The continuous energy spectrum is divided into discrete energy groups, and usually a simplification is made in the transport term to give:

$$\begin{aligned} -D_g(r)\ \nabla^2\ \phi_g(r) + \left[\Sigma_{a_g}(r) + \sum_n \Sigma_{S_{g\to n}}(r) + D_g(r)\ B_{1_g}^2\right] \phi_g(r) \\ = \Sigma_n \left[\Sigma_{S_{n\to g}}(r) + \frac{1}{K_e}\ \chi_g(r)\ \nu\ \Sigma_{f_g}(r)\right] \phi_g(r) \ , \end{aligned} \tag{17}$$

where $D_g(r)$ is the diffusion coefficient, normally one-third of the reciprocal of the transport cross section.

As was stated earlier, the three-dimensional calculation could have been quite large and costly had not a smaller group structure been utilized. However, it was found that this alone would not make the problem manageable. Therefore, a study was performed on the two-dimensional VENTURE calculations with respect to the perturbations of the results due to assumptions about core symmetry.

In the analysis of core symmetry, quarter, half, and full core symmetries were considered. The quarter core symmetry model for both cores 37 and 54 mocked-up the top right quarter of Figs. 1 and 2, respectively. The half core symmetry model for core 37 mocked-up the top half of Fig. 1 because of the position of the NRL experiment. The half core symmetry model for core 54 mocked-up the right half of Fig. 2 due to symmetry about the long axis. The full core symmetry model for both cores mocked-up the entire core. The results of these studies will be discussed in the next section. The three-dimensional calculations used the quarter core symmetry model to ease the computer cost and decrease the size of the problem.

Upon finishing all the neutronics calculations, WINDOWS[8] was used to perform the analysis of the flux spectra and calculate the various parameters outlined in the introduction.

Finally, the DISSPLA[9] system was used to plot some of the results of the various calculations.

DISCUSSION OF RESULTS

With such a complex calculational flow diagram as that set forth in Figs. 5 through 8, and with the various added calculations of determining adequate group structures and core geometry for the models, a large volume of results were generated. Thus, a representative sample of results are presented for discussion and for support of the conclusions and recommendations.

The results are discussed in an order first showing the overall validity of the calculations and then the various perturbations are investigated. Finally, the selected parameters mentioned in the introduction are discussed.

In discussing the overall validity of the calculations, the reader is referred to Figs. 10 through 12 for core 37 with the tabular equivalent data in Tables 9 through 12. Figs. 13 through 17 illustrate data for core 54 and tabular equivalent data are given in Tables 13 through 20.

As stated earlier for both cores, quarter core symmetry was used for the three-dimensional calculations to cut cost and computer time. This assumption appears to be very good with respect to the neutron flux spectrum. However, since neither core was symmetric in its fuel loading or its power distribution, the absolute power of the reactor could not be calculated accurately. Therefore, the calculational results were normalized using a least squares fitting technique to the experimental measurements. One normalization factor was used for each element and a separate factor was used for each core. The reasons behind this were: 1) the two cores had different loadings and therefore two different spectra, and 2) if both the iron and nickel reaction rates would have been utilized in the same normalization constant, both power and spectral effects would have been factored into the normalization factor.

This spectral effect is measured by the ratio of the experimental nickel to iron ratio to the calculated nickel to iron ratios. These ratios differed by less than 1% for core 37; however, for core 54 the ratios differed by approximately 7%. Therefore, in order to maintain consistency between spatial and spectral effects, separate normalization factors were computed for iron and nickel.

The figures and tables mentioned above indicate that the axial distributions of the reaction rates obtained experimentally and by calculations are very close. For core 37, the effect of the aluminum block in the center of the steel blocks of the dosimetry capsule is seen more sharply in the experimental results mainly because of the breakdown in diffusion theory at material interfaces. It can also be seen that in general for core 37 the calculated fluxes were high in the top of the core. The justification behind this result is that in using the quarter core symmetry model, the effects of the partially inserted control rods are not seen. In core 37 approximately 65% of the power is generated in the lower half of the core (Fig. 1), and also the control rods in core positions 66 and 68 are fully withdrawn. These facts coupled with the amount of aluminum and water in the top half of the core caused the fluxes to be high and therefore the absolute activities.

In the case of core 54, the results looked very good in the axial distribution for all irradiated tubes except tube 2 (cf. Fig. 14). The discrepancies seen in Fig. 14 are due to an error in the model. Core position 89 in Fig. 2 was mocked-up as a solid aluminum block. This interpretation of the core loading was erroneous since this element was an aluminum can filled with water. With water instead of aluminum present in that position, the values of the flux along that portion of the experimental assembly would have been higher and thus closer to the experimental measurements. The same effect is slightly seen for tube 3 (cf. Fig. 15) which is also along that side of the experimental assembly (Fig. 2).

In general for both cores, the calculational results were found to fall off slower than the experimental results. There are two main reasons for this discrepancy: 1) the axial fuel distribution of the elements, which had a moderate degree of burnup, was limited to an empirical relationship, and 2) no allowance was made for the aluminum grid plate at the core bottom. Therefore, mocking-up pure water raised the value of the fluxes and decreased the fall-off rate slightly.

Despite the discrepancies discussed above, the overall results showed the calculational model predicted the axial distribution of the reaction rate within 10%. Therefore, it is safe to assume the model is a valid one for calculating the ORNL-BSR.

The experimental and calculated ratios of the ^{58}Ni(n,p) reaction and ^{54}Fe(n,p) reaction are compared in Tables 21 and 22 for cores 37 and 54, respectively. Since the two cores were so different in the loadings, each core is discussed separately.

The comparison of the ratios of ^{58}Ni(n,p) reaction to ^{54}Fe(n,p) reaction in Table 21 indicates very good agreement between the calculations and the experiment. Excluding plane 10 for the three-dimensional VENTURE calculation, the calculated ratios were within 5% of the experimental ratios. (The experimental ratio at plane 10 was approximately 13% different from any other experimental ratios and is therefore believed to be a bad experimental data point.) This result requires a little more comment in that it is the author's belief that a cancellation of factors affecting the spectrum has taken place. The factors in question are the ENDF/B-IV fission spectrum, the unsymmetric core loading of core 37, and the associated unsymmetric power distribution. Current work performed at ORNL has shown the ENDF/B-IV fission spectrum to give discrepancies in calculating reaction rates for threshold foils in the high energy end of the spectrum. Since these results show less discrepancy than would be expected from other current calculations at ORNL, it was concluded that a cancellation of factors has taken place.

The comparison of the ratio of $^{58}Ni(n,p)$ reaction to $^{54}Fe(n,p)$ reaction in Table 22 indicates a systematic error of approximately 7.5%. As discussed previously with core 37, this effect is primarily due to the ENDF/B-IV fission spectrum. The effects of core loading, power distribution, and the aluminum can in core position 89 (cf. Fig. 2) discussed previously also contribute to the discrepancy but are not large factors because of a better core loading for core 54. The results shown in Table 22 are closer to what the author believes the calculated ratios should be. The spectral results of core 54 were very similar to those of core 37 except the effects of core loading were smaller.

In general for both cores, the spectral shift across the element in the high energy groups of interest is seen to be less than 7% and sometimes even negligible (cf. Tables 21 and 22).

The final results to be analyzed in the calculations are the tables of the spectral averaged cross sections. Tables 23 through 49 show the values of the total flux, flux greater than 0.1, 0.5, and 1.0 MeV, and the spectral averaged cross sections for the $^{54}Fe(n,p)$ reaction, $^{58}Ni(n,p)$ reaction, and the average displacement cross section for iron.

There are two general characteristics which are noticeable when viewing these tables of spectral averaged cross sections. One very important characteristic seen in both cores is that even though seven groups appeared adequate for the spectral shape, it was not adequate for the calculation of these parameters in WINDOWS. WINDOWS uses a direct unfolding method with log-log interpolation between two groups. With such a broad group structure, WINDOWS will have a larger degree of error in the unfolded spectrum. Therefore, all seven group results except the average displacement cross section for iron are obtained from direct folding of group fluxes and cross sections. Another general characteristic seen for the two cores is that the numbers remained fairly consistent from calculation to calculation, especially for core 54. Core 37 had some discrepancy (approximately 9%) between the two-dimensional transport calculations (DOT 4.2, Table 25) and the two-dimensional diffusion calculations (VENTURE, Table 26). The reason for this discrepancy is not apparent from the models used in the calculations.

The differences in the spectra in the various tubes are seen in the numbers in the tables of cross sections. The changes in the group structure were found to have very little effect on the spectral averaged cross sections presented in Tables 23 and 24 for core 37, and Tables 35 and 36 for core 54. For core 37, Tables 32 through 34 show the cross sections for the various axial positions of tubes 3, 4, and 5. One can see the spectral shift of approximately 7% from tubes 3 and 4 to tube 5. This shift is partially due to the breakdown of diffusion theory in a strong absorber (steel) and partially due to the nonsymmetric core loading. Also, one can see the effects of the aluminum in planes 5 and 6. With aluminum replacing steel in the experimental capsule, the thermal flux in particular is seen to increase substantially. This is due to the lower neutron absorption of aluminum, therefore allowing for the neutron population in the experiment to increase raising the flux in this section of the core. These two spectral effects are greatest for the value of the total cross section, and decrease in size as you limit the spectrum to the high-energy region. For core 54, Tables 45 through 49 show a 7 to 9% spectral shift across the experimental capsule for the various irradiation planes in the three-dimensional calculation. It is seen largely in the thermal groups (total cross sections) and much less in the fast groups which are of primary interest in the model. The reason behind this result is the placement of the experimental elements (cf. Fig. 2). Core 37 (Fig. 1) has the experimental capsule placed on the core centerline where core 54 has the experimental capsule offset from the centerline. Tubes 1 and 2 are on the side of the experiment facing the outside edge of the reactor, and tubes 3 and 4 are on the side closest to the core centerline. Therefore, tubes 1 and 2 should have a lower thermal flux than tubes 3 and 4. This result is seen in Tables 45 through 49.

One characteristic discussed before and seen clearly in these spectral cross section results also is the effect of core loading on the results. The spectral cross section tables of the different core symmetries assumed show relatively small differences for core 54 (cf. Tables 37 through 44). Core 37, on the other hand shows large variations of ±20%

in proceeding from quarter to full core symmetry calculations (cf. Tables 25 through 31). This reaffirms the lack of symmetry in core 37 as a prime source of discrepancy, and also established the importance of a symmetric power distribution in an analysis involving assumptions on core symmetry.

The group fluxes for the two-dimensional full core symmetry VENTURE calculation using 15 neutron energy groups are presented in Tables 50 through 53. Table 50 presents the center point group fluxes for each core position in BSR core 54 (see Fig. 2), and Tables 51 through 53 present the center point group fluxes by core position along the north, east, and west faces of the BSR core, respectively.

These flux values are based on the measured reaction rate of $^{54}Fe(n,p)^{54}Mn$ divided by the spectrum averaged cross section for ^{54}Fe based on the calculated flux above 1 MeV. In mathematical notation, the spectrum averaged cross section above 1 MeV is defined as

$$\bar{\sigma}(E_R) = \frac{\int_0^\infty \sigma(E)\ \phi_c(E)\ dE}{\int_{E_R}^\infty \phi_c(E)\ dE} \tag{18}$$

where E_R is the reference energy (1 MeV), and $\phi_c(E)$ is the calculated flux. Therefore, the flux based on the measurement is just

$$\phi(E) = \frac{\int_0^\infty \sigma(E)\ \phi_M(E)\ dE}{\bar{\sigma}(E_R)} \tag{19}$$

where the term in the integral is the measured reaction rate. From the results in Tables 50 through 53, the nonsymmetric core loading (i.e., power distribution) is seen in the magnitude of the flux values.

CONCLUSIONS

The results of this analysis show that the computational model set forth in this report is an adequate model for calculating the ORNL-BSR based on the desired parameters obtained during the course of this work. This conclusion is based on the comparison of the experimental and computational reaction rates and the ratio of these reaction rates as a function of axial position and also on the consistency of the calculated parameters.

The correct method of cross section generation is problem dependent. However, the methods used for self-shielding and cell-weighting has proven to be adequate for this type of problem.

The use of diffusion theory was proven valid with one- and two-dimensional comparisons with transport theory, even though there were slight discrepancies in the center tubes of the steel capsules and at the aluminum-steel interfaces.

The 40 neutron energy group structure was adequate for performing the resonance self-shielding calculations and cell-weighting calculations.

The group structure used in the neutronic calculations were adequate in predicting the spectral shape and the spectral averaged cross sections. However, use of the ENDF/B-IV fission spectrum probably introduced the systematic error in the reaction rate ratios.

The use of quarter or half core symmetry for core 54 caused negligible perturbations to the spectrum where for core 37 the spectrum was greatly affected. This is due to the nonsymmetric core loading.

The spectral averaged cross sections were consistent from calculation to calculation and were primarily sensitive to core symmetry and power distribution.

RECOMMENDATIONS

Based on the preceeding results and conclusions, the author would like to make the following recommendations for better results.

1. Either use the 218-group Criticality Master Library with the ENDF/B-V fission spectrum, or use the 171-group Vitamin C Library [10] with the associated ENDF/B-V fission spectrum.
2. If the 171-group Vitamin C Library is used, an experiment should be performed using 10 groups instead of 7. This will allow for added groups in the 6 to 20 MeV energy range while retaining the other groups.
3. Either load the reactor in a more symmetrical fashion to obtain a symmetric power distribution or extend the three-dimensional calculation to at least half core symmetry.
4. Include the effects of fission product poisoning which were left out of this model.
5. Correct the composition mistakes found in the model and discussed in the result section (i.e. the aluminum can and the core bottom grid plate).
6. Use a coarse-mesh three-dimensional diffusion code which is economical enough to handle an increased problem size to verify the results.

The above recommendations should help to clear up the discrepancies in this report and give a set of results closer to the experimental values.

REFERENCES

1. W. E. Ford III, C. C. Webster, and R. M. Westfall, A 218-Group Neutron Cross Section Library in the AMPX Mater Interface Format for Criticality Safety Studies, ORNL/CSD/TM-4 (July 1976).

2. N. M. Greene et al, AMPX - A Modular Code System to Generate Multi-group Neutron-Gamma Cross Sections from ENDF/B, ORNL-3706 (March 1976)

3. L. W. Nordheim, "The Theory of Resonance Absorption", Proceedings of Symposia in Applied Mathematics, Vol. X1, pg. 58, Garret Birhoff and Eugene E. Wagner, Eds., Am. Math. Soc. (1961).

4. J. O. Johnson, Neutronics Model Evaluation for the Light Water Reactor Pressure Vessel Irradiation Surveillance Improvement Program, (Available from the University of Tennessee Nuclear Engineering Dept.) .

5. D. R. Vondy, T. B. Fowler, and G. W. Cunningham, VENTURE - A Code Block for Solving Multigroup Neutronics Problems Applying the Finite-Difference Diffusion-Theory Approximation to Neutron Transport, ORNL-5026 (April 1975).

6. W. A. Rhoades and D. B. Simpson, The DOT 4.2 Two-Dimensional Discrete Ordinates Transport Code, (Not published yet).

7. N. M. Greene and C. W. Craven, Jr., XSDRN: A Discrete Ordinates Spectral Averaging Code, ORNL/TM-2500 (July 1969).

8. F. W. Stallmann, J. F. Eastham, and F. B. K. Kam, WINDOWS - A Program for the Analysis of Spectral Data Foil Activation Measurements, ORNL/TM-6656 (December 1978).

9. Integrated Software Systems Corporation, DISSPLA - Display Integrated Software System and Plotting Language, (July 1975).

10. R. W. Roussin, et al, VITAMIN-C 171 Neutron, 36 Gamma-Ray Group Cross Sections in AMPX and CCCC Interface Formats for Fusion and LMFBR Neutronics, DLC-41 (March 1978).

APPENDIX A

Table 1. Fuel Elements Utilized in Core No. 37.

Core Position	Element Number	Element Weight (^{235}U g)
15	Aluminum Plug	-
16	M-9-H	176
17	M-18-H	202
18	M-8-H	179
19	BSF-28	123
25	M-196-D	155
26	BSF-S-11	62 (Control Rod)
27	M-12-H	185
28	BSF-S-12	61 (Control Rod)
29	M-323-H	153
35	M-20-H	199
36	M-10-H	172
37	M-16-H	181
38	M-11-H	171
39	M-19-H	200
45	BSF-39	132
46	BSF-S-13	80 (Control Rod)
47	M-17-H	187
48	BSF-S-14	79 (Control Rod)
49	BSF-40	128
55	M-13-H	181
56	M-194-D	132
57	M-3-H	157
58	M-14-H	178
59	M-195-D	134
65	M-1-H	162

Table 1. Fuel Elements (Cont'd).

Core Position	Element Number	Element Weighting (^{235}U g)
66	BSF-S-9	59 (Control Rod)
67	NRL Exp. I	-
68	BSF-S-10	59 (Control Rod)
69	M-2-H	160
75	Aluminum Plug	-
76	Aluminum Plug	-
77	M-4-H	158
78	M-7-H	178
79	M-6-H	178
85	Aluminum Plug	-
86	Fission Chamber	-
87	Aluminum Plug	-
88	Aluminum Plug	-
89	M-15-H	199

Table 2. Fuel Elements Utilized in Core No. 54

Core Position	Element Number	Element Weight (^{235}U g)
15	Aluminum Plug	-
16	M-9-H	161
17	M-3-H	141
18	M-8-H	161
19	Aluminum Plug	-
25	M-16-H	153
26	BSF-S-13	69 (Control Rod)
27	M-19-H	174
28	BSF-S-14	68 (Control Rod)
29	M-6-H	158
35	M-13-H	159
36	M-10-H	145
37	YZP-003W	183
38	M-11-H	143
39	M-14-H	153
45	YZP-0048	193
46	BSF-S-15	88 (Control Rod)
47	M-20-H	168
48	BSF-S-16	88 (Control Rod)
49	YZP-003Y	193
55	M-7-H	161
56	M-1-H	141
57	YZP-0044	187
58	M-2-H	138
59	YZP-003X	184
65	YZP-0040	200

Table 2. Fuel Elements (Cont'd)

Core Position	Element Number	Element Weight (^{235}U g)
66	B-198-C	67 (Control Rod)
67	M-15-H	183
68	B-199-C	68 (Control Rod)
69	YZP-0041	195
75	M-12-H	172
76	NRL Exp. I	-
77	Aluminum Plug	-
78	NRL Exp. II	-
79	YZP-0047	180
85	Fission Chamber	-
86	YZP-0042	184
87	M-18-H	180
88	YZP-0046	185
89	Aluminum Plug	-

Table 3. Axial Positions of Interest Given as Distance from Core Bottom

Core No. 37		Core No. 54	
Axial Position	Approximate Distance from Core Bottom (in.)	Axial Position	Approximate Distance from Core Bottom (in.)
Top of Core	24.625	Top of Core	24.625
Top of Dosimetry Capsule	19.000	Top of Dosimetry Capsule	20.875
Irradiation Position 1	17.000	Irradiation Position 1	19.800
2	16.000	2	18.800
3	14.500	3	17.800
4	13.000	4	16.800
Core Centerline	12.313	5	15.300
Irradiation Position 5	11.500	6	13.800
6	8.700	Core Centerline	12.313
7	7.200	Irradiation Position 7	12.300
8	5.700	8	10.800
9	4.200	9	9.300
10	3.200	10	8.300
Bottom of Dosimetry Capsule	1.750	11	7.300
		12	6.300
		13	5.300
		Bottom of Dosimetry Capsule	3.625

Table 4. Footnotes to the Block Diagrams in Figs. 5-8

[a]AMPX 218-group master library containing only neutron data

[b]Broad-group AMPX master library containing only neutron data (40-groups)

[c]AMPX microscopic working library (40-groups)

[d]AMPX microscopic working/cell-weighted library (40-groups)

[e]AMPX microscopic working/zone-weighted library (40-, 27-, 15-, 7-groups)

[f]CCCC ISOTXS microscopic library created for the VENTURE system (40-, 27-, 15-, 7-groups)

[g]ANISN formatted microscopic library created for use in AXMIX (7-groups; Binary)

[h]GIP (group independent) macroscopic library created for DOT 4.2 (7-groups)

[i]AJAX manages AMPX master libraries by merging, collecting, assembling, reordering, reidentifying and/or copying data sets.

[j]MALOCS collapses fine-group master libraries to a broad-group master library.

[k]NITAWL resonance self-shields AMPX master data sets, produces both "regular" ANISN libraries and ANISN sensitivity cross sections, and produces AMPX working libraries. NITAWL can be used to merge working libraries.

[ℓ]XSDRNPM - Given a working library, XSDRNPM performs a one-dimensional discrete ordinate (S_n) calculation with general anisotropic scattering. The module can be used to spatially weight and to collapse cross sections. Weighted cross section can be produced in working, CCCC's, ISOTXS, or ANISN formats.

[m]CONTAC - Converts an AMPX working library to either an ANISN or a CCCC's ISOTXS cross section library

[n]WINDOWS - Performs the analysis of spectral data foil activation measurements

[o]VENTURE - A modular code system developed to do reactor core analysis using multi-group, multi-dimensional diffusion theory.

[p]AXMIX - Manages ANISN-type cross section data sets and libraries by mixing, changing table lengths, making scattering order adjustments, adjointing, and making transport corrections.

[q]DOT 4.2 - A code presently in the Discrete Ordinates System (DOS) which performs 2-D discrete ordinates, diffusion, or P_1 theory neutronics.

Table 5. Energy Boundaries for the 40-Group Library

Group Number	Energy Boundary (eV)
1	2.00(7)
2	6.43(6)
3	4.80(6)
4	3.00(6)
5	2.48(6)
6	2.36(6)
7	1.50(6)
8	1.36(6)
9	1.25(6)
10	1.01(6)
11	8.75(5)
12	8.20(5)
13	4.99(5)
14	3.30(5)
15	2.70(5)
16	2.00(5)
17	1.50(5)
18	1.00(5)
19	8.50(4)
20	1.30(4)
21	2.58(3)
22	3.04(2)
23	1.22(2)
24	8.98(1)
25	2.76(1)
26	9.10(0)
27	3.06(0)
28	1.86(0)

Table 5. Energy Boundaries (Cont'd)

Group Number	Energy Boundary (eV)
29	1.68(0)
30	1.24(0)
31	1.13(0)
32	9.78(-1)
33	7.47(-1)
34	5.48(-1)
35	3.75(-1)
36	3.01(-1)
37	2.00(-1)
38	8.96(-2)
39	3.99(-2)
40	2.52(-2)
41	1.00(-5)

Table 6. Energy Boundaries for the 27-Group Library

Group Number	Energy Boundary (eV)
1	2.00(7)
2	6.43(6)
3	4.80(6)
4	2.48(6)
5	1.50(6)
6	1.36(6)
7	1.01(6)
8	4.99(5)
9	1.00(5)
10	1.30(4)
11	2.58(3)
12	3.04(2)
13	8.98(1)
14	2.76(1)
15	9.10(0)
16	3.06(0)
17	1.68(0)
18	1.24(0)
19	1.13(0)
20	9.78(-1)
21	7.47(-1)
22	3.75(-1)
23	3.01(-1)
24	2.00(-1)
25	8.96(-2)
26	3.99(-2)
27	2.52(-2)
28	1.00(-5)

Table 7. Energy Boundaries for the 15-Group Library

Group Number	Energy Boundary (eV)
1	2.00(7)
2	6.43(6)
3	4.80(6)
4	3.00(6)
5	2.36(6)
6	1.36(6)
7	1.01(6)
8	4.99(5)
9	3.30(5)
10	1.62(5)
11	1.00(5)
12	1.30(4)
13	1.22(2)
14	1.86(0)
15	5.48(-1)
16	1.00(-5)

Table 8. Energy Boundaries for the 7-Group Library

Group Number	Energy Boundaries (eV)
1	2.00(7)
2	1.25(6)
3	1.01(6)
4	4.99(5)
5	3.30(5)
6	1.00(5)
7	3.06(0)
8	1.00(-5)

Table 9. Comparison of Experimental and Calculated $^{54}Fe(n,p)$ Reaction Rates for the NRL Dosimetry Capsule in Position 67 of Core No. 37, Tube 3

Axial Position	Experimental Value (dps/target atom)	Calculated Value (dps/target atom)
1	$4.86(10^{-13})$*	5.13
2	4.76	5.17
3	4.88	5.24
4	4.85	5.32
5	5.50	5.51
6	5.39	5.12
7	4.59	4.68
8	4.18	4.28
9	3.66	3.83
10	3.47	3.51

*Read 4.86×10^{-13}

Table 10. Comparison of Experimental and Calculated $^{54}Fe(n,p)$ Reaction Rates for the NRL Dosimetry Capsule in Position 67 of Core No. 37, Tube 4

Axial Position	Experimental Value (dps/target atom)	Calculated Value (dps/target atom)
1	$6.08(10^{-13})$*	6.29
2	6.29	6.40
3	6.51	6.52
4	6.69	6.58
5	7.18	6.67
6	6.99	6.25
7	6.35	5.78
8	5.88	5.29
9	5.00	4.70
10	4.56	4.24

*Read 6.08×10^{-13}

Table 11. Comparison of Experimental and Calculated $^{54}Fe(n,p)$ Reaction Rates for the NRL Dosimetry Capsule in Position 67 of Core No. 37, Tube 5

Axial Position	Experimental Value (dps/target atom)	Calculated Value (dps/target atom)
1	$5.04(10^{-13})$*	5.49
2	5.15	5.54
3	5.14	5.63
4	5.50	5.71
5	5.96	5.92
6	5.85	5.50
7	5.15	5.01
8	4.51	4.57
9	3.91	4.07
10	3.46	3.73

*Read 5.04×10^{-13}

Table 12. Comparison of Experimental and Calculated $^{58}Ni(n,p)$ Reaction Rates for the NRL Dosimetry Capsule in Position 67 of Core No. 37, Tube 5

Axial Position	Experimental Value (dps/target atom)	Calculated Value (dps/target atom)
1	-	7.16
2	$6.76(10^{-13})$*	7.22
3	7.05	7.33
4	7.49	7.44
5	7.74	7.72
6	-	7.17
7	6.94	6.53
8	6.16	5.96
9	-	5.31
10	5.04	4.86

*Read 6.76×10^{-13}

Table 13. Comparison of Experimental and Calculated $^{54}Fe(n,p)$ Reaction Rates for the NRL Dosimetry Capsule in Position 78 of Core No. 54, Tube 1

Axial Position	Experimental Value (dps/target atom)	Calculated Value (dps/target atom)
1	$3.02(10^{-13})$*	3.02
2	3.17	3.28
3	3.40	3.47
4	3.48	3.62
5	3.65	3.78
6	3.68	3.87
7	3.72	3.88
8	3.65	3.83
9	3.51	3.70
10	3.44	3.58
11	3.16	3.46
12	2.94	3.25
13	2.69	3.05

*Read 3.02×10^{-13}

Table 14. Comparison of Experimental and Calculated $^{54}Fe(n,p)$ Reaction Rates for the NRL Dosimetry Capsule in Position 78 of Core No. 54, Tube 2

Axial Position	Experimental Value (dps/target atom)	Calculated Value (dps/target atom)
1	$2.95(10^{-13})$*	2.77
2	3.16	3.00
3	3.33	3.17
4	3.46	3.30
5	3.68	3.45
6	3.76	3.53
7	3.77	3.54
8	3.70	3.49
9	3.64	3.38
10	3.50	3.26
11	3.20	3.15
12	3.04	2.98
13	2.74	2.81

*Read 2.95×10^{-13}

Table 15. Comparison of Experimental and Calculated $^{58}Ni(n,p)$ Reaction Rates for the NRL Dosimetry Capsule in Position 78 of Core No. 54, Tube 2

Axial Position	Experimental Value (dps/target atom)	Calculated Value (dps/target atom)
1	$4.18(10^{-13})$*	3.74
2	4.47	4.05
3	4.66	4.28
4	4.97	4.47
5	5.28	4.67
6	5.40	4.77
7	5.45	4.79
8	5.44	4.72
9	5.11	4.56
10	4.86	4.41
11	4.58	4.26
12	4.30	4.02
13	4.00	3.80

*Read 4.18×10^{-13}

Table 16. Comparison of Experimental and Calculated $^{54}Fe(n,p)$ Reaction Rates for the NRL Dosimetry Capsule in Position 78 of Core No. 54, Tube 3

Axial Position	Experimental Value (dps/target atom)	Calculated value (dps/target atom)
1	$4.05(10^{-13})$*	3.61
2	4.26	3.93
3	4.47	4.17
4	4.72	4.35
5	4.94	4.56
6	5.11	4.66
7	5.06	4.68
8	4.99	4.60
9	4.72	4.44
10	4.59	4.29
11	4.24	4.12
12	3.95	3.86
13	3.71	3.58

*Read 4.05×10^{-13}

Table 17. Comparison of Experimental and Calculated $^{54}Fe(n,p)$ Reaction Rates for the NRL Dosimetry Capsule in Position 78 of Core No. 54, Tube 4

Axial Position	Experimental Value (dps/target atom)	Calculated Value (dps/target atom)
1	$3.67(10^{-13})$*	3.80
2	3.99	4.14
3	4.29	4.39
4	4.48	4.59
5	4.72	4.80
6	4.92	4.91
7	4.96	4.92
8	4.85	4.84
9	4.57	4.68
10	4.27	4.52
11	4.16	4.35
12	3.77	4.07
13	3.56	3.75

*Read 3.67×10^{-13}

Table 18. Comparison of Experimental and Calculated $^{58}Ni(n,p)$ Reaction Rates for the NRL Dosimetry Capsule in Position 78 of Core No. 54, Tube 4

Axial Position	Experimental Value (dps/target atom)	Calculated Value (dps/target atom)
1	$5.21(10^{-13})$*	5.13
2	5.62	5.59
3	6.10	5.94
4	6.44	6.20
5	6.66	6.48
6	6.80	6.63
7	6.96	6.66
8	6.93	6.55
9	6.69	6.33
10	6.42	6.11
11	5.99	5.88
12	5.45	5.50
13	5.01	5.07

*Read 5.21×10^{-13}

Table 19. Comparison of Experimental and Calculated $^{54}Fe(n,p)$ Reaction Rates for the NRL Dosimetry Capsule in Position 78 of Core No. 54, Tube 5

Axial Position	Experimental Value (dps/target atom)	Calculated Value (dps/target atom)
1	$3.06(10^{-13})$*	3.09
2	3.22	3.38
3	3.36	3.59
4	3.55	3.76
5	3.69	3.93
6	3.81	4.02
7	3.85	4.03
8	3.85	3.97
9	3.64	3.84
10	3.54	3.70
11	3.30	3.57
12	3.04	3.35
13	2.86	3.13

*Read 3.06×10^{-13}

Table 20. Comparison of Experimental and Calculated $^{58}Ni(n,p)$ Reaction Rates for the NRL Dosimetry Capsule in Position 78 of Core No. 54, Tube 5

Axial Position	Experimental Value (dps/target atom)	Calculated Value (dps/target atom)
1	$4.29(10^{-13})$*	4.17
2	4.75	4.57
3	4.85	4.86
4	5.07	5.08
5	5.40	5.31
6	5.67	5.43
7	5.59	5.45
8	5.48	5.37
9	5.38	5.18
10	5.07	5.01
11	4.80	4.83
12	4.40	4.53
13	4.10	4.23

*Read 4.29×10^{-13}

Table 21. Comparison of Experimental and Calculated Ratios of the $^{58}Ni(n,p)$ Reaction and the $^{54}Fe(n,p)$ Reaction for Core 37, Tube 5 **

Calculation Description	Reaction Rate $\frac{^{58}Ni(n,p)}{^{54}Fe(n,p)}$ Experimental	Reaction Rate $\frac{^{58}Ni(n,p)}{^{54}Fe(n,p)}$ Calculated
1-D Transport Calc., 40 groups	1.330*	1.329
27 groups	1.330	1.329
15 groups	1.330	1.329
7 groups	1.330	1.331
1-D Diffusion Calc., 40 groups	1.330	1.329
27 groups	1.330	1.329
15 groups	1.330	1.329
7 groups	1.330	1.331
2-D Transport Calc., Quarter Core Symmetry, 7 groups	1.330	1.333
2-D Diffusion Calc., Quarter Core Symmetry, 7 groups	1.330	1.332
Half Core Symmetry, 7 groups	1.330	1.338
Full Core Symmetry, 7 groups	1.330	1.332
Half Core Symmetry, 15 groups	1.330	1.332
Full Core Symmetry, 15 groups	1.330	1.338

Table 21. Comparison of Experimental and Calculated Ratios (Cont'd)

Calculation Description	Reaction Rate	
	$\frac{^{58}Ni(n,p)}{^{54}Fe(n,p)}$	$\frac{^{58}Ni(n,p)}{^{54}Fe(n,p)}$
	Experimental	Calculated
3-D Diffusion Calc., Plane 2, 7 groups	1.313	1.331
3-D Diffusion Calc., Plane 3, 7 groups	1.373	1.332
3-D Diffusion Calc., Plane 4, 7 groups	1.362	1.332
3-D Diffusion Calc., Plane 5, 7 groups	1.298	1.331
3-D Diffusion Calc., Plane 7, 7 groups	1.348	1.332
3-D Diffusion Calc., Plane 8, 7 groups	1.366	1.332
3-D Diffusion Calc., Plane 10, 7 groups	1.458	1.331

*The experimental value for the one- and two-dimensional calculation is an average of planes 4 and 5 for the three-dimensional calculation.

**All comparisons are made for irradiation tube 5.

Table 22. Comparison of Experimental and Calculated Ratios of the $^{58}Ni(n,p)$ Reaction and the $^{54}Fe(n,p)$ Reaction for Core 54 , Tube 5

Calculation Description	Reaction Rate	
	$\frac{^{58}Ni(n,p)}{^{54}Fe(n,p)}$	$\frac{^{58}Ni(n,p)}{^{54}Fe(n,p)}$
	Experimental	Calculated
1-D Transport Calc., 40 groups	1.452*	1.348
27 groups	1.452	1.348
15 groups	1.452	1.348
7 groups	1.452	1.342
1-D Diffusion Calc., 40 groups	1.452	1.344
27 groups	1.452	1.344
15 groups	1.452	1.344
7 groups	1.452	1.342
2-D Diffusion Calc., Quarter Core Symmetry, 7 groups	1.452	1.342
Half Core Symmetry, 7 groups	1.452	1.342
Full Core Symmetry, 7 groups	1.452	1.349
Quarter Core Symmetry, 15 groups	1.452	1.349
Half Core Symmetry, 15 groups	1.452	1.351
Full Core Symmetry, 15 groups	1.452	1.351

Table 22. Comparison of Experimental and Calculated Ratios (Cont'd)

Calculation Description	Reaction Rate	
	$\frac{^{58}Ni(n,p)}{^{54}Fe(n,p)}$	$\frac{^{58}Ni(n,p)}{^{54}Fe(n,p)}$
	Experimental	Calculated
3-D Diffusion Calc., 7 groups, Plane 1	1.402	1.341
2	1.475	1.342
3	1.444	1.342
4	1.428	1.342
5	1.463	1.342
6	1.488	1.342
7	1.452	1.342
8	1.423	1.342
9	1.478	1.342
10	1.432	1.342
11	1.455	1.342
12	1.447	1.342
13	1.434	1.341

*The experimental value for the one- and two-dimensional calculations is the value for plane 7 of the three-dimensional calculation.

Table 23. Spectral Parameters of the One-Dimensional Transport Calculations for Core No. 37; All Group Structures

Parameter	Integration Range	1-D 40-Groups	1-D 27-Groups	1-D 15-Groups	1-D 7-Groups
ϕ (n/cm^2-sec)	Total	$2.91(10^{13})$	$3.15(10^{13})$	$3.05(10^{13})$	$3.08(10^{13})$
	E>0.1 MeV	$1.08(10^{13})$	$1.17(10^{13})$	$1.14(10^{13})$	$1.13(10^{13})$
	E>0.5 MeV	$7.69(10^{12})$	$8.29(10^{12})$	$8.05(10^{12})$	$7.93(10^{12})$
	E>1.0 MeV	$5.28(10^{12})$	$5.68(10^{12})$	$5.55(10^{12})$	$5.44(10^{12})$
^{54}Fe(n,p) σ(cm^2)	Total	$1.80(10^{-26})$	$1.79(10^{-26})$	$1.81(10^{-26})$	$1.76(10^{-26})$
	E>0.1 MeV	$4.86(10^{-26})$	$4.83(10^{-26})$	$4.83(10^{-26})$	$4.81(10^{-26})$
	E>0.5 MeV	$6.82(10^{-26})$	$6.81(10^{-26})$	$6.84(10^{-26})$	$6.84(10^{-26})$
	E>1.0 MeV	$9.93(10^{-26})$	$9.93(10^{-26})$	$9.92(10^{-26})$	$9.98(10^{-26})$
^{58}Ni(n,p) σ(cm^2)	Total	$2.40(10^{-26})$	$2.38(10^{-26})$	$2.40(10^{-26})$	$2.35(10^{-26})$
	E>0.1 MeV	$6.45(10^{-26})$	$6.41(10^{-26})$	$6.42(10^{-26})$	$6.41(10^{-26})$
	E>0.5 MeV	$9.06(10^{-26})$	$9.05(10^{-26})$	$9.09(10^{-26})$	$9.10(10^{-26})$
	E>1.0 MeV	$1.32(10^{-25})$	$1.32(10^{-25})$	$1.32(10^{-25})$	$1.33(10^{-26})$
Fe(dpa) σ(cm^2)	Total	$2.62(10^{-22})$	$2.61(10^{-22})$	$2.66(10^{-22})$	$2.71(10^{-22})$
	E>0.1 MeV	$7.07(10^{-22})$	$7.04(10^{-22})$	$7.12(10^{-22})$	$7.41(10^{-22})$
	E>0.5 MeV	$9.92(10^{-22})$	$9.93(10^{-22})$	$1.01(10^{-21})$	$1.05(10^{-21})$
	E>1.0 MeV	$1.45(10^{-21})$	$1.45(10^{-21})$	$1.46(10^{-21})$	$1.54(10^{-21})$

Table 24. Spectral Parameter of the One-Dimensional Diffusion Calculations for Core No. 37; All Group Structures

Parameter	Integration Range	1-D 40-Groups	1-D 27-Groups	1-D 15-Groups	1-D 7-Groups
ϕ (n/cm^2-sec)	Total	$5.02(10^{13})$	$5.02(10^{13})$	$4.94(10^{13})$	$4.96(10^{13})$
	E>0.1 MeV	$1.93(10^{13})$	$1.93(10^{13})$	$1.91(10^{13})$	$1.90(10^{13})$
	E>0.5 MeV	$1.38(10^{13})$	$1.38(10^{13})$	$1.36(10^{13})$	$1.35(10^{13})$
	E>1.0 MeV	$9.52(10^{12})$	$9.52(10^{12})$	$9.42(10^{12})$	$9.28(10^{12})$
^{54}Fe(n,p) σ(cm^2)	Total	$1.88(10^{-26})$	$1.88(10^{-26})$	$1.90(10^{-26})$	$1.87(10^{-26})$
	E>0.1 MeV	$4.90(10^{-26})$	$4.90(10^{-26})$	$4.90(10^{-26})$	$4.88(10^{-26})$
	E>0.5 MeV	$6.86(10^{-26})$	$6.86(10^{-26})$	$6.87(10^{-26})$	$6.88(10^{-26})$
	E>1.0 MeV	$9.93(10^{-26})$	$9.93(10^{-26})$	$9.94(10^{-26})$	$9.99(10^{-26})$
^{58}Ni(n,p) σ(cm^2)	Total	$2.50(10^{-26})$	$2.50(10^{-26})$	$2.52(10^{-26})$	$2.49(10^{-26})$
	E>0.1 MeV	$6.51(10^{-26})$	$6.51(10^{-26})$	$6.51(10^{-26})$	$6.49(10^{-26})$
	E>0.5 MeV	$9.12(10^{-26})$	$9.12(10^{-26})$	$9.13(10^{-26})$	$9.15(10^{-26})$
	E>1.0 MeV	$1.32(10^{-25})$	$1.32(10^{-25})$	$1.32(10^{-25})$	$1.33(10^{-25})$
Fe(dpa) σ(cm^2)	Total	$2.73(10^{-22})$	$2.73(10^{-22})$	$2.79(10^{-22})$	$2.86(10^{-22})$
	E>0.1 MeV	$7.11(10^{-22})$	$7.11(10^{-22})$	$7.20(10^{-22})$	$7.45(10^{-22})$
	E>0.5 MeV	$9.96(10^{-22})$	$9.96(10^{-22})$	$1.01(10^{-21})$	$1.05(10^{-21})$
	E>1.0 MeV	$1.44(10^{-21})$	$1.44(10^{-21})$	$1.46(10^{-21})$	$1.53(10^{-21})$

Table 25. Spectral Parameters of the Two-Dimensional Transport Calculation for Core No. 37; Quarter Core Symmetry and 7-Groups

Parameter	Integration Range	Tube 3	Tube 4	Tube 5
ϕ (n/cm^2-sec)	Total	$4.36(10^{13})$	$5.37(10^{13})$	$4.38(10^{13})$
	E>0.1 MeV	$2.03(10^{13})$	$2.41(10^{13})$	$2.28(10^{13})$
	E>0.5 MeV	$1.35(10^{13})$	$1.62(10^{13})$	$1.48(10^{13})$
	E>1.0 MeV	$8.26(10^{12})$	$1.03(10^{13})$	$8.81(10^{12})$
^{54}Fe(n,p) σ(cm^2)	Total	$1.66(10^{-26})$	$1.69(10^{-26})$	$1.74(10^{-26})$
	E>0.1 MeV	$3.58(10^{-26})$	$3.78(10^{-26})$	$3.35(10^{-26})$
	E>0.5 MeV	$5.39(10^{-26})$	$5.62(10^{-26})$	$5.16(10^{-26})$
	E>1.0 MeV	$8.78(10^{-26})$	$8.84(10^{-26})$	$8.65(10^{-26})$
^{58}Ni(n,p) σ(cm^2)	Total	$2.22(10^{-26})$	$2.25(10^{-26})$	$2.32(10^{-26})$
	E>0.1 MeV	$4.77(10^{-26})$	$5.03(10^{-26})$	$4.47(10^{-26})$
	E>0.5 MeV	$7.18(10^{-26})$	$7.49(10^{-26})$	$6.88(10^{-26})$
	E>1.0 MeV	$1.17(10^{-25})$	$1.18(10^{-25})$	$1.15(10^{-25})$
Fe(dpa) σ(cm^2)	Total	$3.00(10^{-22})$	$2.99(10^{-22})$	$3.21(10^{-22})$
	E>0.1 MeV	$6.45(10^{-22})$	$6.68(10^{-22})$	$6.19(10^{-22})$
	E>0.5 MeV	$9.71(10^{-22})$	$9.94(10^{-22})$	$9.53(10^{-22})$
	E>1.0 MeV	$1.58(10^{-21})$	$1.37(10^{-21})$	$1.60(10^{-21})$

Table 26. Spectral Parameters of the Two-Dimensional Diffusion Calculation for Core No. 37; Quarter Core Symmetry and 7-Groups

Parameter	Integration Range	Tube 3	Tube 4	Tube 5
	Total	$3.20(10^{13})$	$3.90(10^{13})$	$3.18(10^{13})$
ϕ	E>0.1 MeV	$1.38(10^{13})$	$1.66(10^{13})$	$1.52(10^{13})$
(n/cm^2-sec)	E>0.5 MeV	$9.64(10^{12})$	$1.17(10^{13})$	$1.05(10^{13})$
	E>1.0 MeV	$6.44(10^{12})$	$7.90(10^{12})$	$6.92(10^{12})$
	Total	$1.82(10^{-26})$	$1.85(10^{-26})$	$1.96(10^{-26})$
^{54}Fe(n,p)	E>0.1 MeV	$4.20(10^{-26})$	$4.34(10^{-26})$	$4.11(10^{-26})$
σ(cm^2)	E>0.5 MeV	$6.03(10^{-26})$	$6.16(10^{-26})$	$5.93(10^{-26})$
	E>1.0 MeV	$9.03(10^{-26})$	$9.11(10^{-26})$	$9.00(10^{-26})$
	Total	$2.42(10^{-26})$	$2.46(10^{-26})$	$2.61(10^{-26})$
^{58}Ni(n,p)	E>0.1 MeV	$5.59(10^{-26})$	$5.78(10^{-26})$	$5.47(10^{-26})$
σ(cm^2)	E>0.5 MeV	$8.03(10^{-26})$	$8.20(10^{-26})$	$7.90(10^{-26})$
	E>1.0 MeV	$1.20(10^{-25})$	$1.21(10^{-25})$	$1.20(10^{-25})$
	Total	$3.08(10^{-22})$	$3.09(10^{-22})$	$3.33(10^{-22})$
Fe(dpa)	E>0.1 MeV	$7.12(10^{-22})$	$7.27(10^{-22})$	$6.99(10^{-22})$
σ(cm^2)	E>0.5 MeV	$1.02(10^{-21})$	$1.03(10^{-21})$	$1.01(10^{-21})$
	E>1.0 MeV	$1.53(10^{-21})$	$1.53(10^{-21})$	$1.53(10^{-21})$

Table 27. Spectral Parameters of the Two-Dimensional Diffusion Calculation for Core No. 37; Quarter Core Symmetry and 15-Groups

Parameter	Integration Range	Tube 3	Tube 4	Tube 5
	Total	$3.28(10^{13})$	$3.96(10^{13})$	$3.28(10^{13})$
ϕ	E>0.1 MeV	$1.43(10^{13})$	$1.71(10^{13})$	$1.57(10^{13})$
$(n/cm^2\text{-sec})$	E>0.5 MeV	$1.00(10^{13})$	$1.21(10^{13})$	$1.09(10^{13})$
	E>1.0 MeV	$6.74(10^{12})$	$8.28(10^{12})$	$7.26(10^{12})$
	Total	$1.83(10^{-26})$	$1.90(10^{-26})$	$1.91(10^{-26})$
$^{54}Fe(n,p)$	E>0.1 MeV	$4.19(10^{-26})$	$4.40(10^{-26})$	$3.99(10^{-26})$
$\sigma(cm^2)$	E>0.5 MeV	$5.98(10^{-26})$	$6.22(10^{-26})$	$5.73(10^{-26})$
	E>1.0 MeV	$8.91(10^{-26})$	$9.10(10^{-26})$	$8.62(10^{-26})$
	Total	$2.44(10^{-26})$	$2.53(10^{-26})$	$2.55(10^{-26})$
$^{58}Ni(n,p)$	E>0.1 MeV	$5.58(10^{-26})$	$5.84(10^{-26})$	$5.33(10^{-26})$
$\sigma(cm^2)$	E>0.5 MeV	$7.97(10^{-26})$	$8.26(10^{-26})$	$7.66(10^{-26})$
	E>1.0 MeV	$1.19(10^{-25})$	$1.21(10^{-25})$	$1.15(10^{-25})$
	Total	$3.02(10^{-22})$	$3.05(10^{-22})$	$3.23(10^{-22})$
Fe(dpa)	E>0.1 MeV	$6.90(10^{-22})$	$7.04(10^{-22})$	$6.75(10^{-22})$
$\sigma(cm^2)$	E>0.5 MeV	$9.86(10^{-22})$	$9.95(10^{-22})$	$1.10(10^{-21})$
	E>1.0 MeV	$1.47(10^{-21})$	$1.46(10^{-21})$	$1.46(10^{-21})$

Table 28. Spectral Parameters of the Two-Dimensional Diffusion Calculation for Core No. 37; Half Core Symmetry and 7-Groups

Parameter	Integration Range	Tube 1	Tube 2	Tube 3	Tube 4	Tube 5
	Total	$4.36(10^{13})$	$3.44(10^{13})$	$3.60(10^{13})$	$4.50(10^{13})$	$3.56(10^{13})$
ϕ	E>0.1 MeV	$1.87(10^{13})$	$1.51(10^{13})$	$1.56(10^{13})$	$1.92(10^{13})$	$1.71(10^{13})$
$(n/cm^2\text{-sec})$	E>0.5 MeV	$1.32(10^{13})$	$1.05(10^{13})$	$1.09(10^{13})$	$1.35(10^{13})$	$1.18(10^{13})$
	E>1.0 MeV	$8.92(10^{12})$	$6.94(10^{12})$	$7.22(10^{12})$	$9.16(10^{12})$	$7.78(10^{12})$
	Total	$1.55(10^{-26})$	$1.52(10^{-26})$	$1.52(10^{-26})$	$1.55(10^{-26})$	$1.64(10^{-26})$
$^{54}Fe(n,p)$	E>0.1 MeV	$3.62(10^{-26})$	$3.47(10^{-26})$	$3.50(10^{-26})$	$3.63(10^{-26})$	$3.42(10^{-26})$
$\sigma(cm^2)$	E>0.5 MeV	$5.13(10^{-26})$	$5.00(10^{-26})$	$5.02(10^{-26})$	$5.15(10^{-26})$	$4.94(10^{-26})$
	E>1.0 MeV	$7.59(10^{-26})$	$7.53(10^{-26})$	$7.56(10^{-26})$	$7.60(10^{-26})$	$7.51(10^{-26})$
	Total	$2.07(10^{-26})$	$2.02(10^{-26})$	$2.02(10^{-26})$	$2.06(10^{-26})$	$2.19(10^{-26})$
$^{58}Ni(n,p)$	E>0.1 MeV	$4.81(10^{-26})$	$4.62(10^{-26})$	$4.66(10^{-26})$	$4.83(10^{-26})$	$4.56(10^{-26})$
$\sigma(cm^2)$	E>0.5 MeV	$6.84(10^{-26})$	$6.66(10^{-26})$	$6.69(10^{-26})$	$6.86(10^{-26})$	$6.58(10^{-26})$
	E>1.0 MeV	$1.01(10^{-25})$	$1.00(10^{-25})$	$1.01(10^{-25})$	$1.01(10^{-25})$	$1.00(10^{-25})$
	Total	$3.12(10^{-22})$	$3.10(10^{-22})$	$3.08(10^{-22})$	$3.10(10^{-22})$	$3.35(10^{-22})$
Fe(dpa)	E>0.1 MeV	$7.27(10^{-22})$	$7.08(10^{-22})$	$7.10(10^{-22})$	$7.28(10^{-22})$	$6.98(10^{-22})$
$\sigma(cm^2)$	E>0.5 MeV	$1.03(10^{-21})$	$1.02(10^{-21})$	$1.02(10^{-21})$	$1.03(10^{-21})$	$1.01(10^{-21})$
	E>1.0 MeV	$1.53(10^{-21})$	$1.54(10^{-21})$	$1.54(10^{-21})$	$1.52(10^{-21})$	$1.53(10^{-21})$

Table 29. Spectral Parameters of the Two-Dimensional Diffusion Calculation for Core No. 37; Half Core Symmetry and 15-Groups

Parameter	Integration Range	Tube 1	Tube 2	Tube 3	Tube 4	Tube 5
	Total	$4.44(10^{13})$	$3.54(10^{13})$	$3.68(10^{13})$	$4.56(10^{13})$	$3.70(10^{13})$
ϕ	E>0.1 MeV	$1.93(10^{13})$	$1.56(10^{13})$	$1.61(10^{13})$	$1.98(10^{13})$	$1.77(10^{13})$
$(n/cm^2\text{-sec})$	E>0.5 MeV	$1.36(10^{13})$	$1.09(10^{13})$	$1.13(10^{13})$	$1.40(10^{13})$	$1.23(10^{13})$
	E>1.0 MeV	$9.30(10^{12})$	$7.28(10^{12})$	$7.56(10^{12})$	$9.56(10^{12})$	$8.14(10^{12})$
	Total	$1.58(10^{-26})$	$1.51(10^{-26})$	$1.52(10^{-26})$	$1.59(10^{-26})$	$1.90(10^{-26})$
$^{54}Fe(n,p)$	E>0.1 MeV	$3.64(10^{-26})$	$3.43(10^{-26})$	$3.48(10^{-26})$	$3.67(10^{-26})$	$3.98(10^{-26})$
$\sigma(cm^2)$	E>0.5 MeV	$5.15(10^{-26})$	$4.90(10^{-26})$	$4.97(10^{-26})$	$5.19(10^{-26})$	$5.73(10^{-26})$
	E>1.0 MeV	$7.56(10^{-26})$	$7.34(10^{-26})$	$7.42(10^{-26})$	$7.59(10^{-26})$	$8.63(10^{-26})$
	Total	$2.11(10^{-26})$	$2.01(10^{-26})$	$2.03(10^{-26})$	$2.12(10^{-26})$	$2.11(10^{-26})$
$^{58}Ni(n,p)$	E>0.1 MeV	$4.84(10^{-26})$	$4.57(10^{-26})$	$4.63(10^{-26})$	$4.88(10^{-26})$	$4.42(10^{-26})$
$\sigma(cm^2)$	E>0.5 MeV	$6.85(10^{-26})$	$6.54(10^{-26})$	$6.62(10^{-26})$	$6.90(10^{-26})$	$6.36(10^{-26})$
	E>1.0 MeV	$1.01(10^{-25})$	$9.79(10^{-26})$	$9.88(10^{-26})$	$1.01(10^{-25})$	$9.58(10^{-26})$
	Total	$3.05(10^{-22})$	$3.02(10^{-22})$	$3.02(10^{-22})$	$3.05(10^{-22})$	$3.21(10^{-22})$
Fe(dpa)	E>0.1 MeV	$7.01(10^{-22})$	$6.78(10^{-22})$	$6.89(10^{-22})$	$7.03(10^{-22})$	$6.73(10^{-22})$
$\sigma(cm^2)$	E>0.5 MeV	$9.93(10^{-22})$	$9.71(10^{-22})$	$9.84(10^{-22})$	$9.94(10^{-22})$	$9.69(10^{-22})$
	E>1.0 MeV	$1.46(10^{-21})$	$1.45(10^{-21})$	$1.47(10^{-21})$	$1.45(10^{-21})$	$1.46(10^{-21})$

Table 30. Spectral Parameters of the Two-Dimensional Diffusion Calculation for Core No. 37; Full Core Symmetry and 7-Groups

Parameter	Integration Range	Tube 1	Tube 2	Tube 3	Tube 4	Tube 5
ϕ (n/cm^2-sec)	Total	$3.20(10^{13})$	$2.34(10^{13})$	$2.64(10^{13})$	$3.44(10^{13})$	$2.58(10^{13})$
	E>0.1 MeV	$1.47(10^{13})$	$1.11(10^{13})$	$1.23(10^{13})$	$1.56(10^{13})$	$1.34(10^{13})$
	E>0.5 MeV	$1.03(10^{13})$	$7.66(10^{12})$	$8.50(10^{12})$	$1.10(10^{12})$	$9.20(10^{12})$
	E>1.0 MeV	$6.94(10^{12})$	$5.00(10^{12})$	$5.62(10^{12})$	$7.44(10^{12})$	$6.02(10^{12})$
^{54}Fe(n,p) σ(cm^2)	Total	$2.13(10^{-26})$	$2.07(10^{-26})$	$2.08(10^{-26})$	$2.13(10^{-26})$	$2.26(10^{-26})$
	E>0.1 MeV	$4.64(10^{-26})$	$4.36(10^{-26})$	$4.49(10^{-26})$	$4.69(10^{-26})$	$4.36(10^{-26})$
	E>0.5 MeV	$6.62(10^{-26})$	$6.34(10^{-26})$	$6.47(10^{-26})$	$6.67(10^{-26})$	$6.35(10^{-26})$
	E>1.0 MeV	$9.84(10^{-26})$	$9.71(10^{-26})$	$9.79(10^{-26})$	$9.85(10^{-26})$	$9.70(10^{-26})$
^{58}Ni(n,p) σ(cm^2)	Total	$2.84(10^{-26})$	$2.76(10^{-26})$	$2.77(10^{-26})$	$2.84(10^{-26})$	$3.01(10^{-26})$
	E>0.1 MeV	$6.18(10^{-26})$	$5.80(10^{-26})$	$5.97(10^{-26})$	$6.24(10^{-26})$	$5.80(10^{-26})$
	E>0.5 MeV	$8.81(10^{-26})$	$8.44(10^{-26})$	$8.62(10^{-26})$	$8.88(10^{-26})$	$8.45(10^{-26})$
	E>1.0 MeV	$1.31(10^{-25})$	$1.29(10^{-25})$	$1.30(10^{-25})$	$1.31(10^{-25})$	$1.29(10^{-25})$
Fe(dpa) σ(cm^2)	Total	$3.31(10^{-22})$	$3.29(10^{-22})$	$3.27(10^{-22})$	$3.29(10^{-22})$	$3.57(10^{-22})$
	E>0.1 MeV	$7.19(10^{-22})$	$6.91(10^{-22})$	$7.05(10^{-22})$	$7.25(10^{-22})$	$7.18(10^{-22})$
	E>0.5 MeV	$1.03(10^{-21})$	$1.01(10^{-21})$	$1.02(10^{-21})$	$1.03(10^{-21})$	$1.05(10^{-21})$
	E>1.0 MeV	$1.52(10^{-21})$	$1.54(10^{-21})$	$1.54(10^{-21})$	$1.52(10^{-22})$	$1.60(10^{-21})$

Table 31. Spectral Parameters of the Two-Dimensional Diffusion Calculation for Core No. 37; Full Core Symmetry and 15-Groups

Parameter	Integration Range	Tube 1	Tube 2	Tube 3	Tube 4	Tube 5
ϕ (n/cm^2-sec)	Total	$3.54(10^{13})$	$2.68(10^{13})$	$3.00(10^{13})$	$3.78(10^{13})$	$2.96(10^{13})$
	E>0.1 MeV	$1.54(10^{13})$	$1.19(10^{13})$	$1.31(10^{13})$	$1.64(10^{13})$	$1.42(10^{13})$
	E>0.5 MeV	$1.09(10^{13})$	$8.24(10^{12})$	$9.14(10^{12})$	$1.16(10^{13})$	$9.82(10^{12})$
	E>1.0 MeV	$7.40(10^{12})$	$5.44(10^{12})$	$6.12(10^{12})$	$7.94(10^{12})$	$6.50(10^{12})$
$^{54}Fe(n,p)$ $\sigma(cm^2)$	Total	$2.05(10^{-26})$	$1.90(10^{-26})$	$1.96(10^{-26})$	$2.07(10^{-26})$	$2.03(10^{-26})$
	E>0.1 MeV	$4.69(10^{-26})$	$4.28(10^{-26})$	$4.49(10^{-26})$	$4.79(10^{-26})$	$4.25(10^{-26})$
	E>0.5 MeV	$6.64(10^{-26})$	$6.18(10^{-26})$	$6.43(10^{-26})$	$6.75(10^{-26})$	$6.13(10^{-26})$
	E>1.0 MeV	$9.79(10^{-26})$	$9.36(10^{-26})$	$9.60(10^{-26})$	$9.87(10^{-26})$	$9.26(10^{-26})$
$^{58}Ni(n,p)$ $\sigma(cm^2)$	Total	$2.72(10^{-26})$	$2.54(10^{-26})$	$2.61(10^{-26})$	$2.75(10^{-26})$	$2.72(10^{-26})$
	E>0.1 MeV	$6.24(10^{-26})$	$5.71(10^{-26})$	$5.98(10^{-26})$	$6.36(10^{-26})$	$5.69(10^{-26})$
	E>0.5 MeV	$8.84(10^{-26})$	$8.25(10^{-26})$	$8.56(10^{-26})$	$8.98(10^{-26})$	$8.20(10^{-26})$
	E>1.0 MeV	$1.30(10^{-25})$	$1.25(10^{-25})$	$1.28(10^{-25})$	$1.31(10^{-25})$	$1.24(10^{-25})$
Fe(dpa) $\sigma(cm^2)$	Total	$3.05(10^{-22})$	$2.99(10^{-22})$	$2.99(10^{-22})$	$3.05(10^{-22})$	$3.21(10^{-22})$
	E>0.1 MeV	$6.99(10^{-22})$	$6.74(10^{-22})$	$6.87(10^{-22})$	$7.05(10^{-22})$	$6.71(10^{-22})$
	E>0.5 MeV	$9.91(10^{-22})$	$9.73(10^{-22})$	$9.82(10^{-22})$	$9.95(10^{-22})$	$9.67(10^{-22})$
	E>1.0 MeV	$1.46(10^{-21})$	$1.47(10^{-21})$	$1.47(10^{-21})$	$1.45(10^{-21})$	$1.46(10^{-21})$

Table 32. Spectral Parameters of Tube 3 at Various Axial Irradiation Positions of the Three-Dimensional Diffusion Calculation; Quarter Core Symmetry and 7-Groups; Core No. 37

Parameter	Integration Range	Plane 2	Plane 4	Plane 5	Plane 6	Plane 8
	Total	$3.74(10^{13})$	$3.86(10^{13})$	$4.72(10^{13})$	$4.02(10^{13})$	$3.04(10^{13})$
ϕ	E>0.1 MeV	$1.59(10^{13})$	$1.64(10^{13})$	$1.64(10^{13})$	$1.55(10^{13})$	$1.33(10^{13})$
$(n/cm^2\text{-sec})$	E>0.5 MeV	$1.11(10^{13})$	$1.15(10^{13})$	$1.16(10^{13})$	$1.09(10^{13})$	$9.26(10^{12})$
	E>1.0 MeV	$7.48(10^{12})$	$7.70(10^{12})$	$7.88(10^{12})$	$7.34(10^{12})$	$6.20(10^{12})$
	Total	$1.81(10^{-26})$	$1.81(10^{-26})$	$1.53(10^{-26})$	$1.67(10^{-26})$	$1.85(10^{-26})$
$^{54}Fe(n,p)$	E>0.1 MeV	$4.26(10^{-26})$	$4.24(10^{-26})$	$4.41(10^{-26})$	$4.35(10^{-26})$	$4.23(10^{-26})$
$\sigma(cm^2)$	E>0.5 MeV	$6.09(10^{-26})$	$6.07(10^{-26})$	$6.26(10^{-26})$	$6.19(10^{-26})$	$6.06(10^{-26})$
	E>1.0 MeV	$9.07(10^{-26})$	$9.06(10^{-26})$	$9.18(10^{-26})$	$9.16(10^{-26})$	$9.05(10^{-26})$
	Total	$2.41(10^{-26})$	$2.41(10^{-26})$	$2.04(10^{-26})$	$2.23(10^{-26})$	$2.46(10^{-26})$
$^{58}Ni(n,p)$	E>0.1 MeV	$5.67(10^{-26})$	$5.65(10^{-26})$	$5.87(10^{-26})$	$5.81(10^{-26})$	$5.63(10^{-26})$
$\sigma(cm^2)$	E>0.5 MeV	$8.11(10^{-26})$	$8.08(10^{-26})$	$8.33(10^{-26})$	$8.24(10^{-26})$	$8.07(10^{-26})$
	E>1.0 MeV	$1.21(10^{-25})$	$1.21(10^{-25})$	$1.22(10^{-25})$	$1.22(10^{-25})$	$1.21(10^{-25})$
	Total	$3.06(10^{-22})$	$3.05(10^{-22})$	$2.57(10^{-22})$	$2.80(10^{-22})$	$3.12(10^{-22})$
Fe(dpa)	E>0.1 MeV	$7.19(10^{-22})$	$7.17(10^{-22})$	$7.39(10^{-22})$	$7.28(10^{-22})$	$7.15(10^{-22})$
$\sigma(cm^2)$	E>0.5 MeV	$1.03(10^{-21})$	$1.02(10^{-21})$	$1.05(10^{-21})$	$1.04(10^{-21})$	$1.02(10^{-21})$
	E>1.0 MeV	$1.53(10^{-21})$	$1.53(10^{-21})$	$1.54(10^{-21})$	$1.53(10^{-21})$	$1.53(10^{-21})$

Table 33. Spectral Parameters of Tube 4 at Various Axial Irradiation Positions of the Three-Dimensional Diffusion Calculation; Quarter Core Symmetry and 7-Groups; Core No. 37

Parameter	Integration Range	Plane 2	Plane 4	Plane 5	Plane 6	Plane 8
	Total	$4.54(10^{13})$	$4.68(10^{13})$	$5.32(10^{13})$	$4.68(10^{13})$	$3.70(10^{13})$
ϕ	E>0.1 MeV	$1.91(10^{13})$	$1.97(10^{13})$	$1.95(10^{13})$	$1.84(10^{13})$	$1.59(10^{13})$
$(n/cm^2\text{-sec})$	E>0.5 MeV	$1.35(10^{13})$	$1.39(10^{13})$	$1.38(10^{13})$	$1.30(10^{13})$	$1.12(10^{13})$
	E>1.0 MeV	$9.22(10^{12})$	$9.48(10^{12})$	$9.50(10^{12})$	$8.92(10^{12})$	$7.62(10^{12})$
	Total	$1.85(10^{-26})$	$1.85(10^{-26})$	$1.65(10^{-26})$	$1.75(10^{-26})$	$1.88(10^{-26})$
$^{54}Fe(n,p)$	E>0.1 MeV	$4.39(10^{-26})$	$4.38(10^{-26})$	$4.50(10^{-26})$	$4.45(10^{-26})$	$4.37(10^{-26})$
$\sigma(cm^2)$	E>0.5 MeV	$6.21(10^{-26})$	$6.20(10^{-26})$	$6.34(10^{-26})$	$6.29(10^{-26})$	$6.19(10^{-26})$
	E>1.0 MeV	$9.12(10^{-26})$	$9.11(10^{-26})$	$9.21(10^{-26})$	$9.19(10^{-26})$	$9.11(10^{-26})$
	Total	$2.46(10^{-26})$	$2.46(10^{-26})$	$2.19(10^{-26})$	$2.33(10^{-26})$	$2.50(10^{-26})$
$^{58}Ni(n,p)$	E>0.1 MeV	$5.85(10^{-26})$	$5.83(10^{-26})$	$5.98(10^{-26})$	$5.93(10^{-26})$	$5.81(10^{-26})$
$\sigma(cm^2)$	E>0.5 MeV	$8.26(10^{-26})$	$8.25(10^{-26})$	$8.44(10^{-26})$	$8.37(10^{-26})$	$8.24(10^{-26})$
	E>1.0 MeV	$1.21(10^{-25})$	$1.21(10^{-25})$	$1.23(10^{-25})$	$1.22(10^{-25})$	$1.21(10^{-25})$
	Total	$3.09(10^{-22})$	$3.09(10^{-22})$	$2.73(10^{-22})$	$2.91(10^{-22})$	$3.14(10^{-22})$
Fe(dpa)	E>0.1 MeV	$7.34(10^{-22})$	$7.32(10^{-22})$	$7.46(10^{-22})$	$7.38(10^{-22})$	$7.30(10^{-22})$
$\sigma(cm^2)$	E>0.5 MeV	$1.04(10^{-21})$	$1.04(10^{-21})$	$1.05(10^{-21})$	$1.04(10^{-21})$	$1.03(10^{-21})$
	E>1.0 MeV	$1.52(10^{-21})$	$1.52(10^{-21})$	$1.53(10^{-21})$	$1.52(10^{-21})$	$1.52(10^{-21})$

Table 34. Spectral Parameters of Tube 5 at Various Axial Irradiation Positions of the Three-Dimensional Diffusion Calculations; Quarter Core Symmetry and 7-Groups; Core No. 37

Parameters	Integration Range	Plane 2	Plane 4	Plane 5	Plane 6	Plane 8
	Total	$3.72(10^{13})$	$3.84(10^{13})$	$4.88(10^{13})$	$4.10(10^{13})$	$3.00(10^{13})$
ϕ	E>0.1 MeV	$1.74(10^{13})$	$1.80(10^{13})$	$1.79(10^{13})$	$1.69(10^{13})$	$1.45(10^{13})$
$(n/cm^2\text{-sec})$	E>0.5 MeV	$1.21(10^{13})$	$1.25(10^{13})$	$1.25(10^{13})$	$1.19(10^{13})$	$1.01(10^{13})$
	E>1.0 MeV	$8.06(10^{12})$	$8.32(10^{12})$	$8.50(10^{12})$	$7.98(10^{12})$	$6.66(10^{12})$
	Total	$1.95(10^{-26})$	$1.95(10^{-26})$	$1.59(10^{-26})$	$1.76(10^{-26})$	$2.00(10^{-26})$
$^{54}Fe(n,p)$	E>0.1 MeV	$4.17(10^{-26})$	$4.16(10^{-26})$	$4.35(10^{-26})$	$4.26(10^{-26})$	$4.14(10^{-26})$
$\sigma(cm^2)$	E>0.5 MeV	$6.00(10^{-26})$	$5.98(10^{-26})$	$6.20(10^{-26})$	$6.09(10^{-26})$	$5.96(10^{-26})$
	E>1.0 MeV	$9.02(10^{-26})$	$9.00(10^{-26})$	$9.14(10^{-26})$	$9.04(10^{-26})$	$9.01(10^{-26})$
	Total	$2.60(10^{-26})$	$2.60(10^{-26})$	$2.12(10^{-26})$	$2.34(10^{-26})$	$2.66(10^{-26})$
$^{58}Ni(n,p)$	E>0.1 MeV	$5.56(10^{-26})$	$5.54(10^{-26})$	$5.78(10^{-26})$	$5.67(10^{-26})$	$5.51(10^{-26})$
$\sigma(cm^2)$	E>0.5 MeV	$7.99(10^{-26})$	$7.96(10^{-26})$	$8.25(10^{-26})$	$8.10(10^{-26})$	$7.94(10^{-26})$
	E>1.0 MeV	$1.20(10^{-25})$	$1.20(10^{-25})$	$1.22(10^{-25})$	$1.20(10^{-25})$	$1.20(10^{-25})$
	Total	$3.29(10^{-22})$	$3.30(10^{-22})$	$2.67(10^{-22})$	$2.97(10^{-22})$	$3.39(10^{-22})$
Fe(dpa)	E>0.1 MeV	$7.06(10^{-22})$	$7.04(10^{-22})$	$7.29(10^{-22})$	$7.19(10^{-22})$	$7.02(10^{-22})$
$\sigma(cm^2)$	E>0.5 MeV	$1.02(10^{-21})$	$1.01(10^{-21})$	$1.04(10^{-21})$	$1.04(10^{-21})$	$1.01(10^{-21})$
	E>1.0 MeV	$1.53(10^{-21})$	$1.52(10^{-21})$	$1.53(10^{-21})$	$1.53(10^{-21})$	$1.53(10^{-21})$

Table 35. Spectral Parameters of the One-Dimensional Transport Calculations for Core No. 54, All Group Structures

Parameter	Integration Range	1-D 40-Groups	1-D 27-Groups	1-D 15-Groups	1-D 7-Groups
ϕ (n/cm^2-sec)	Total	$2.59(10^{13})$	$2.77(10^{13})$	$2.77(10^{13})$	$2.77(10^{13})$
	E>0.1 MeV	$1.10(10^{13})$	$1.17(10^{13})$	$1.19(10^{13})$	$1.18(10^{13})$
	E>0.5 MeV	$7.45(10^{12})$	$7.92(10^{12})$	$7.99(10^{12})$	$7.99(10^{12})$
	E>1.0 MeV	$4.78(10^{12})$	$5.10(10^{12})$	$5.15(10^{12})$	$5.10(10^{12})$
^{54}Fe(n,p) σ(cm^2)	Total	$1.61(10^{-26})$	$1.60(10^{-26})$	$1.61(10^{-26})$	$1.66(10^{-26})$
	E>0.1 MeV	$3.77(10^{-26})$	$3.78(10^{-26})$	$3.77(10^{-26})$	$3.90(10^{-26})$
	E>0.5 MeV	$5.58(10^{-26})$	$5.59(10^{-26})$	$5.59(10^{-26})$	$5.76(10^{-26})$
	E>1.0 MeV	$8.69(10^{-26})$	$8.70(10^{-26})$	$8.68(10^{-26})$	$9.02(10^{-26})$
^{58}Ni (n,p) σ(cm^2)	Total	$2.17(10^{-26})$	$2.16(10^{-26})$	$2.17(10^{-26})$	$2.23(10^{-26})$
	E>0.1 MeV	$5.08(10^{-26})$	$5.09(10^{-26})$	$5.08(10^{-26})$	$5.23(10^{-26})$
	E>0.5 MeV	$7.52(10^{-26})$	$7.54(10^{-26})$	$7.54(10^{-26})$	$7.73(10^{-26})$
	E>1.0 MeV	$1.17(10^{-25})$	$1.17(10^{-25})$	$1.17(10^{-25})$	$1.21(10^{-25})$
Fe(dpa) σ(cm^2)	Total	$2.74(10^{-22})$	$2.73(10^{-22})$	$2.77(10^{-22})$	$2.87(10^{-22})$
	E>0.1 MeV	$6.43(10^{-22})$	$6.45(10^{-22})$	$6.48(10^{-22})$	$6.72(10^{-22})$
	E>0.5 MeV	$9.52(10^{-22})$	$9.55(10^{-22})$	$9.63(10^{-22})$	$9.93(10^{-22})$
	E>1.0 MeV	$1.48(10^{-21})$	$1.49(10^{-21})$	$1.49(10^{-21})$	$1.56(10^{-21})$

Table 36. Spectral Parameters of the One-Dimensional Diffusion Calculations for Core No. 54; All Group Structures

Parameter	Integration Range	1-D 40-Groups	1-D 27-Groups	1-D 15-Groups	1-D 7-Groups
ϕ (n/cm^2-sec)	Total	$5.34(10^{13})$	$5.34(10^{13})$	$5.36(10^{13})$	$5.42(10^{13})$
	E>0.1 MeV	$2.36(10^{13})$	$2.34(10^{13})$	$2.38(10^{13})$	$2.42(10^{13})$
	E>0.5 MeV	$1.61(10^{13})$	$1.61(10^{13})$	$1.63(10^{13})$	$1.66(10^{13})$
	E>1.0 MeV	$1.05(10^{13})$	$1.05(10^{13})$	$1.07(10^{13})$	$1.09(10^{13})$
^{54}Fe(n,p) σ(cm^2)	Total	$1.76(10^{-26})$	$1.76(10^{-26})$	$1.77(10^{-26})$	$1.82(10^{-26})$
	E>0.1 MeV	$3.99(10^{-26})$	$4.02(10^{-26})$	$4.02(10^{-26})$	$4.08(10^{-26})$
	E>0.5 MeV	$5.85(10^{-26})$	$5.85(10^{-26})$	$5.85(10^{-26})$	$5.94(10^{-26})$
	E>1.0 MeV	$8.95(10^{-26})$	$8.95(10^{-26})$	$8.95(10^{-26})$	$9.09(10^{-26})$
^{58}Ni(n,p) σ(cm^2)	Total	$2.37(10^{-26})$	$2.37(10^{-26})$	$2.40(10^{-26})$	$2.44(10^{-26})$
	E>0.1 MeV	$5.36(10^{-26})$	$5.41(10^{-26})$	$5.40(10^{-26})$	$5.47(10^{-26})$
	E>0.5 MeV	$7.86(10^{-26})$	$7.86(10^{-26})$	$7.88(10^{-26})$	$7.97(10^{-26})$
	E>1.0 MeV	$1.20(10^{-25})$	$1.20(10^{-25})$	$1.20(10^{-25})$	$1.22(10^{-25})$
Fe(dpa) σ(cm^2)	Total	$2.89(10^{-22})$	$2.89(10^{-22})$	$2.94(10^{-22})$	$3.09(10^{-22})$
	E>0.1 MeV	$6.53(10^{-22})$	$6.59(10^{-22})$	$6.61(10^{-22})$	$6.91(10^{-22})$
	E>0.5 MeV	$9.58(10^{-22})$	$9.58(10^{-22})$	$9.63(10^{-22})$	$1.01(10^{-21})$
	E>1.0 MeV	$1.47(10^{-21})$	$1.47(10^{-21})$	$1.47(10^{-21})$	$1.54(10^{-21})$

Table 37. Spectral Parameters of the Two-Dimensional Diffusion Calculation for Core No. 54, Quarter Core Symmetry and 15-Groups

Parameter	Integration Range	Tube 1	Tube 2	Tube 3	Tube 4	Tube 5
	Total	$2.12(10^{13})$	$1.84(10^{13})$	$2.46(10^{13})$	$2.64(10^{13})$	$2.12(10^{13})$
ϕ	E>0.1 MeV	$9.92(10^{12})$	$9.04(10^{12})$	$1.11(10^{13})$	$1.17(10^{13})$	$1.04(10^{13})$
$(n/cm^2\text{-sec})$	E>0.5 MeV	$6.68(10^{12})$	$6.14(10^{12})$	$7.70(10^{12})$	$8.04(10^{12})$	$7.02(10^{12})$
	E>1.0 MeV	$4.26(10^{12})$	$3.92(10^{12})$	$5.10(10^{12})$	$5.28(10^{12})$	$4.48(10^{12})$
	Total	$1.95(10^{-26})$	$2.10(10^{-26})$	$2.18(10^{-26})$	$2.07(10^{-26})$	$2.04(10^{-26})$
$^{54}Fe(n,p)$	E>0.1 MeV	$4.17(10^{-26})$	$4.27(10^{-26})$	$4.81(10^{-26})$	$4.65(10^{-26})$	$4.15(10^{-26})$
$\sigma(cm^2)$	E>0.5 MeV	$6.19(10^{-26})$	$6.29(10^{-26})$	$6.96(10^{-26})$	$6.79(10^{-26})$	$6.17(10^{-26})$
	E>1.0 MeV	$9.71(10^{-26})$	$9.85(10^{-26})$	$1.05(10^{-25})$	$1.03(10^{-26})$	$9.66(10^{-26})$
	Total	$2.63(10^{-26})$	$2.83(10^{-26})$	$2.91(10^{-26})$	$2.77(10^{-26})$	$2.75(10^{-26})$
$^{58}Ni(n,p)$	E>0.1 MeV	$5.62(10^{-26})$	$5.75(10^{-26})$	$6.42(10^{-26})$	$6.22(10^{-26})$	$5.60(10^{-26})$
$\sigma(cm^2)$	E>0.5 MeV	$8.35(10^{-26})$	$8.47(10^{-26})$	$9.29(10^{-26})$	$9.09(10^{-26})$	$8.32(10^{-26})$
	E>1.0 MeV	$1.31(10^{-25})$	$1.33(10^{-25})$	$1.40(10^{-25})$	$1.38(10^{-25})$	$1.30(10^{-25})$
	Total	$3.00(10^{-22})$	$3.17(10^{-22})$	$3.05(10^{-22})$	$2.96(10^{-22})$	$3.14(10^{-22})$
Fe(dpa)	E>0.1 MeV	$6.41(10^{-22})$	$6.43(10^{-22})$	$6.73(10^{-22})$	$6.66(10^{-22})$	$6.39(10^{-22})$
$\phi(cm^2)$	E>0.5 MeV	$9.52(10^{-22})$	$9.48(10^{-22})$	$9.74(10^{-22})$	$9.73(10^{-22})$	$9.49(10^{-22})$
	E>1.0 MeV	$1.49(10^{-21})$	$1.48(10^{-21})$	$1.47(10^{-21})$	$1.48(10^{-21})$	$1.49(10^{-21})$

Table 38. Spectral Parameters of the Two-Dimensional Diffusion Calculation for Core No. 54; Quarter Core Symmetry and 7-Groups

Parameter	Integration Range	Tube 1	Tube 2	Tube 3	Tube 4	Tube 5
	Total	$2.06(10^{13})$	$1.80(10^{13})$	$2.44(10^{13})$	$2.62(10^{13})$	$2.06(10^{13})$
ϕ	E>0.1 MeV	$9.74(10^{12})$	$8.88(10^{12})$	$1.10(10^{13})$	$1.16(10^{13})$	$1.03(10^{13})$
(n/cm^2-sec)	E>0.5 MeV	$6.56(10^{12})$	$6.02(10^{12})$	$7.60(10^{12})$	$7.94(10^{12})$	$6.92(10^{12})$
	E>1.0 MeV	$4.20(10^{12})$	$3.84(10^{12})$	$5.02(10^{12})$	$5.22(10^{12})$	$4.40(10^{12})$
	Total	$2.07(10^{-26})$	$2.17(10^{-26})$	$2.12(10^{-26})$	$2.05(10^{-26})$	$2.16(10^{-26})$
^{54}Fe(n,p)	E>0.1 MeV	$4.37(10^{-26})$	$4.40(10^{-26})$	$4.70(10^{-26})$	$4.63(10^{-26})$	$4.35(10^{-26})$
σ(cm^2)	E>0.5 MeV	$6.49(10^{-26})$	$6.48(10^{-26})$	$6.80(10^{-26})$	$6.76(10^{-26})$	$6.44(10^{-26})$
	E>1.0 MeV	$1.01(10^{-25})$	$1.02(10^{-25})$	$1.03(10^{-25})$	$1.03(10^{-25})$	$1.01(10^{-25})$
	Total	$2.77(10^{-26})$	$2.91(10^{-26})$	$2.84(10^{-26})$	$2.75(10^{-26})$	$2.90(10^{-26})$
^{58}Ni(n,p)	E>0.1 MeV	$5.86(10^{-26})$	$5.90(10^{-26})$	$6.31(10^{-26})$	$6.21(10^{-26})$	$5.83(10^{-26})$
σ(cm^2)	E>0.5 MeV	$8.71(10^{-26})$	$8.70(10^{-26})$	$9.12(10^{-26})$	$9.07(10^{-26})$	$8.65(10^{-26})$
	E>1.0 MeV	$1.36(10^{-25})$	$1.36(10^{-25})$	$1.38(10^{-25})$	$1.38(10^{-25})$	$1.36(10^{-25})$
	Total	$3.17(10^{-22})$	$3.32(10^{-22})$	$3.16(10^{-22})$	$3.08(10^{-22})$	$3.32(10^{-22})$
Fe(dpa)	E>0.1 MeV	$6.69(10^{-22})$	$6.71(10^{-22})$	$7.03(10^{-22})$	$6.97(10^{-22})$	$6.67(10^{-22})$
σ(cm^2)	E>0.5 MeV	$9.94(10^{-22})$	$9.90(10^{-22})$	$1.02(10^{-21})$	$1.02(10^{-21})$	$9.88(10^{-22})$
	E>1.0 MeV	$1.55(10^{-21})$	$1.55(10^{-21})$	$1.54(10^{-21})$	$1.55(10^{-21})$	$1.55(10^{-21})$

Table 39. Spectral Parameters of the Two-Dimensional Diffusion Calculation for Core No. 54; Half Core Symmetry and 15-Groups

Parameter	Integration Range	Tube 1	Tube 2	Tube 3	Tube 4	Tube 5
	Total	$2.74(10^{13})$	$2.42(10^{13})$	$3.08(10^{13})$	$3.28(10^{13})$	$2.70(10^{13})$
ϕ	E>0.1 MeV	$1.30(10^{13})$	$1.20(10^{13})$	$1.42(10^{13})$	$1.48(10^{13})$	$1.34(10^{13})$
(n/cm^2-sec)	E>0.5 MeV	$8.80(10^{12})$	$8.16(10^{12})$	9.78(o0^{12})	$1.01(10^{13})$	$9.06(10^{12})$
	E>1.0 MeV	$5.62(10^{12})$	$5.24(10^{12})$	$6.46(10^{12})$	$6.58(10^{12})$	$5.76(10^{12})$
	Total	$1.78(10^{-26})$	$1.90(10^{-26})$	$1.95(10^{-26})$	$1.83(10^{-26})$	$1.83(10^{-26})$
^{54}Fe(n,p)	E>0.1 MeV	$3.73(10^{-26})$	$3.83(10^{-26})$	$4.23(10^{-26})$	$4.08(10^{-26})$	$3.68(10^{-26})$
σ(cm^2)	E>0.5 MeV	$5.53(10^{-26})$	$5.64(10^{-26})$	$6.14(10^{-26})$	$5.97(10^{-26})$	$5.46(10^{-26})$
	E>1.0 MeV	$8.66(10^{-26})$	$8.79(10^{-26})$	$9.29(10^{-26})$	$9.14(10^{-26})$	$8.59(10^{-26})$
	Total	$2.40(10^{-26})$	$2.56(10^{-26})$	$2.60(10^{-26})$	$2.46(10^{-26})$	$2.47(10^{-26})$
^{58}Ni(n,p)	E>0.1 MeV	$5.04(10^{-26})$	$5.16(10^{-26})$	$5.67(10^{-26})$	$5.47(10^{-26})$	$4.97(10^{-26})$
σ(cm^2)	E>0.5 MeV	$7.47(10^{-26})$	$7.61(10^{-26})$	$8.22(10^{-26})$	$8.00(10^{-26})$	$7.38(10^{-26})$
	E>1.0 MeV	$1.17(10^{-25})$	$1.18(10^{-25})$	$1.24(10^{-25})$	$1.23(10^{-25})$	$1.16(10^{-25})$
	Total	$3.05(10^{-22})$	$3.21(10^{-22})$	$3.08(10^{-22})$	$2.98(10^{-22})$	$3.17(10^{-22})$
Fe(dpa)	E>0.1 MeV	$6.41(10^{-22})$	$6.46(10^{-22})$	$6.70(10^{-22})$	$6.61(10^{-22})$	$6.37(10^{-22})$
σ(cm^2)	E>0.5 MeV	$9.50(10^{-22})$	$9.51(10^{-22})$	$9.71(10^{-22})$	$9.68(10^{-22})$	$9.45(10^{-22})$
	E>1.0 MeV	$1.49(10^{-21})$	$1.48(10^{-21})$	$1.47(10^{-21})$	$1.48(10^{-21})$	$1.49(10^{-21})$

Table 40. Spectral Parameters of the Two-Dimensional Diffusion Calculation for Core No. 54; Half Core Symmetry and 7-Groups

Parameter	Integration Range	Tube 1	Tube 2	Tube 3	Tube 4	Tube 5
	Total	$2.70(10^{13})$	$2.38(10^{13})$	$3.06(10^{13})$	$3.26(10^{13})$	$2.64(10^{13})$
ϕ	E>0.1 MeV	$1.30(10^{13})$	$1.19(10^{13})$	$1.41(10^{13})$	$1.47(10^{13})$	$1.34(10^{13})$
$(n/cm^2\text{-sec})$	E>0.5 MeV	$8.74(10^{12})$	$8.10(10^{12})$	$9.74(10^{12})$	$1.01(10^{13})$	$9.00(10^{12})$
	E>1.0 MeV	$5.60(10^{12})$	$5.20(10^{12})$	$6.42(10^{12})$	$6.58(10^{12})$	$5.74(10^{12})$
	Total	$1.89(10^{-26})$	$1.99(10^{-26})$	$1.94(10^{-26})$	$1.86(10^{-26})$	$1.97(10^{-26})$
$^{54}Fe(n,p)$	E>0.1 MeV	$3.94(10^{-26})$	$3.97(10^{-26})$	$4.19(10^{-26})$	$4.12(10^{-26})$	$3.89(10^{-26})$
$\sigma(cm^2)$	E>0.5 MeV	$5.84(10^{-26})$	$5.86(10^{-26})$	$6.08(10^{-26})$	$6.02(10^{-26})$	$5.79(10^{-26})$
	E>1.0 MeV	$9.11(10^{-26})$	$9.12(10^{-26})$	$9.22(10^{-26})$	$9.21(10^{-26})$	$9.07(10^{-26})$
	Total	$2.53(10^{-26})$	$2.67(10^{-26})$	$2.60(10^{-26})$	$2.49(10^{-26})$	$2.65(10^{-26})$
$^{58}Ni(n,p)$	E>0.1 MeV	$5.28(10^{-26})$	$5.33(10^{-26})$	$5.63(10^{-26})$	$5.53(10^{-26})$	$5.22(10^{-26})$
$\sigma(cm^2)$	E>0.5 MeV	$7.83(10^{-26})$	$7.86(10^{-26})$	$8.16(10^{-26})$	$8.08(10^{-26})$	$7.77(10^{-26})$
	E>1.0 MeV	$1.22(10^{-25})$	$1.22(10^{-25})$	$1.24(10^{-25})$	$1.24(10^{-25})$	$1.22(10^{-25})$
	Total	$3.22(10^{-22})$	$3.38(10^{-22})$	$3.22(10^{-22})$	$3.12(10^{-22})$	$3.37(10^{-22})$
Fe(dpa)	E>0.1 MeV	$6.71(10^{-22})$	$6.73(10^{-22})$	$6.98(10^{-22})$	$6.93(10^{-22})$	$6.65(10^{-22})$
$\sigma(cm^2)$	E>0.5 MeV	$9.95(10^{-22})$	$1.07(10^{-21})$	$1.01(10^{-21})$	$1.01(10^{-21})$	$9.89(10^{-22})$
	E>1.0 MeV	$1.55(10^{-21})$	$1.55(10^{-21})$	$1.54(10^{-21})$	$1.55(10^{-21})$	$1.55(10^{-21})$

Table 41. Spectral Parameters of the Two-Dimensional Diffusion Calculation for Core No. 54; Full Core Symmetry Core Position 76, and 15-Groups

Parameter	Integration Range	Tube 1	Tube 2	Tube 3	Tube 4	Tube 5
	Total	$2.42(10^{13})$	$2.82(10^{13})$	$3.40(10^{13})$	$3.08(10^{13})$	$2.74(10^{13})$
ϕ	E>0.1 MeV	$1.19(10^{13})$	$1.33(10^{13})$	$1.54(10^{13})$	$1.39(10^{13})$	$1.36(10^{13})$
(n/cm^2-sec)	E>0.5 MeV	$8.08(10^{12})$	$9.00(10^{12})$	$1.06(10^{13})$	$9.52(10^{12})$	$9.14(10^{12})$
	E>1.0 MeV	$5.16(10^{12})$	$5.76(10^{12})$	$6.90(10^{12})$	$6.26(10^{12})$	$5.80(10^{12})$
	Total	$1.85(10^{-26})$	$1.75(10^{-26})$	$1.83(10^{-26})$	$1.87(10^{-26})$	$1.80(10^{-26})$
^{54}Fe(n,p)	E>0.1 MeV	$3.76(10^{-26})$	$3.70(10^{-26})$	$4.04(10^{-26})$	$4.16(10^{-26})$	$3.63(10^{-26})$
σ(cm^2)	E>0.5 MeV	$5.55(10^{-26})$	$5.48(10^{-26})$	$5.90(10^{-26})$	$6.06(10^{-26})$	$5.39(10^{-26})$
	E>1.0 MeV	$8.69(10^{-26})$	$8.56(10^{-26})$	$9.02(10^{-26})$	$9.21(10^{-26})$	$8.49(10^{-26})$
	Total	$2.50(10^{-26})$	$2.36(10^{-26})$	$2.46(10^{-26})$	$2.51(10^{-26})$	$2.43(10^{-26})$
^{58}Ni(n,p)	E>0.1 MeV	$5.07(10^{-26})$	$4.99(10^{-26})$	$5.42(10^{-26})$	$5.57(10^{-26})$	$4.90(10^{-26})$
σ(cm^2)	E>0.5 MeV	$7.48(10^{-26})$	$7.40(10^{-26})$	$7.91(10^{-26})$	$8.11(10^{-26})$	$7.29(10^{-26})$
	E>1.0 MeV	$1.17(10^{-25})$	$1.16(10^{-25})$	$1.21(10^{-25})$	$1.23(10^{-25})$	$1.15(10^{-25})$
	Total	$3.17(10^{-22})$	$3.03(10^{-22})$	$3.00(10^{-22})$	$3.00(10^{-22})$	$3.15(10^{-22})$
Fe(dpa)	E>0.1 MeV	$6.43(10^{-22})$	$6.40(10^{-22})$	$6.61(10^{-22})$	$6.67(10^{-22})$	$6.35(10^{-22})$
σ(cm^2)	E>0.5 MeV	$9.48(10^{-22})$	$9.49(10^{-22})$	$9.66(10^{-22})$	$9.71(10^{-22})$	$9.43(10^{-22})$
	E>1.0 MeV	$1.48(10^{-21})$	$1.48(10^{-21})$	$1.48(10^{-21})$	$1.48(10^{-21})$	$1.49(10^{-21})$

Table 42. Spectral Parameters of the Two-Dimensional Diffusion Calculation for Core No. 54: Full Core Symmetry, Core Position 76, and 7-Groups

Parameter	Integration Range	Tube 1	Tube 2	Tube 3	Tube 4	Tube 5
	Total	$2.40(10^{13})$	$2.78(10^{13})$	$3.38(10^{13})$	$3.06(10^{13})$	$2.70(10^{13})$
ϕ	E>0.1 Mev	$1.20(10^{13})$	$1.33(10^{13})$	$1.54(10^{13})$	$1.39(10^{13})$	$1.36(10^{13})$
(n/cm^2-sec)	E>0.5 MeV	$8.12(10^{12})$	$8.98(10^{12})$	$1.06(10^{13})$	$9.56(10^{12})$	$9.16(10^{12})$
	E>1.0 MeV	$5.20(10^{12})$	$5.76(10^{12})$	$6.92(10^{12})$	$6.30(10^{12})$	$5.82(10^{12})$
	Total	$1.96(10^{-26})$	$1.87(10^{-26})$	$1.87(10^{-26})$	$1.88(10^{-26})$	$1.95(10^{-26})$
^{54}Fe(n,p)	E>0.1 MeV	$3.93(10^{-26})$	$3.91(10^{-26})$	$4.09(10^{-26})$	$4.15(10^{-26})$	$3.86(10^{-26})$
σ(cm^2)	E>0.5 Mev	$5.80(10^{-26})$	$5.79(10^{-26})$	$5.99(10^{-26})$	$6.03(10^{-26})$	$5.73(10^{-26})$
	E>1.0 MeV	$9.06(10^{-26})$	$9.03(10^{-26})$	$9.14(10^{-26})$	$9.15(10^{-26})$	$9.03(10^{-26})$
	Total	$2.64(10^{-26})$	$2.51(10^{-26})$	$2.51(10^{-26})$	$2.53(10^{-26})$	$2.61(10^{-26})$
^{58}Ni(n,p)	E>0.1 MeV	$5.28(10^{-26})$	$5.24(10^{-26})$	$5.49(10^{-26})$	$5.56(10^{-26})$	$5.18(10^{-26})$
σ(cm^2)	E>0.5 MeV	$7.79(10^{-26})$	$7.78(10^{-26})$	$8.03(10^{-26})$	$8.09(10^{-26})$	$7.70(10^{-26})$
	E>1.0 MeV	$1.22(10^{-25})$	$1.21(10^{-25})$	$1.23(10^{-25})$	$1.23(10^{-25})$	$1.21(10^{-25})$
	Total	$3.36(10^{-22})$	$3.22(10^{-22})$	$3.17(10^{-22})$	$3.18(10^{-22})$	$3.36(10^{-22})$
Fe(dpa)	E>0.1 MeV	$6.73(10^{-22})$	$6.71(10^{-22})$	$6.93(10^{-22})$	$6.99(10^{-22})$	$6.66(10^{-22})$
σ(cm^2)	E>0.5 MeV	$9.93(10^{-22})$	$9.96(10^{-22})$	$1.01(10^{-21})$	$1.02(10^{-21})$	$9.89(10^{-22})$
	E>1.0 MeV	$1.55(10^{-21})$	$1.55(10^{-21})$	$1.55(10^{-21})$	$1.54(10^{-21})$	$1.56(10^{-21})$

Table 43. Spectral Parameters of the Two-Dimensional Diffusion Calculation for Core No. 54; Full Core Symmetry, Core Position 78, and 15-Groups

Parameters	Integration Range	Tube 1	Tube 2	Tube 3	Tube 4	Tube 5
	Total	$2.86(10^{13})$	$2.54(10^{13})$	$3.24(10^{13})$	$3.44(10^{13})$	$2.84(10^{13})$
ϕ	E 0.1 MeV	$1.37(10^{13})$	$1.27(10^{13})$	$1.49(10^{13})$	$1.55(10^{13})$	$1.41(10^{13})$
$(n/cm^2\text{-sec})$	E 0.5 MeV	$9.24(10^{12})$	$8.60(10^{12})$	$1.03(10^{13})$	$1.06(10^{13})$	$9.52(10^{12})$
	E 1.0 MeV	$5.90(10^{12})$	$5.52(10^{12})$	$6.80(10^{12})$	$6.90(10^{12})$	$6.06(10^{12})$
	Total	$1.77(10^{-26})$	$1.89(10^{-26})$	$1.94(10^{-26})$	$1.82(10^{-26})$	$1.81(10^{-26})$
$^{54}Fe(n,p)$	E 0.1 MeV	$3.70(10^{-26})$	$3.80(10^{-26})$	$4.20(10^{-26})$	$4.04(10^{-26})$	$3.65(10^{-26})$
$\sigma(cm^2)$	E 0.5 MeV	$5.48(10^{-26})$	$5.59(10^{-26})$	$6.08(10^{-26})$	$5.91(10^{-26})$	$5.41(10^{-26})$
	E 1.0 MeV	$8.58(10^{-26})$	$8.72(10^{-26})$	$9.23(10^{-26})$	$9.06(10^{-26})$	$8.51(10^{-26})$
	Total	$2.39(10^{-26})$	$2.55(10^{-26})$	$2.59(10^{-26})$	$2.44(10^{-26})$	$2.45(10^{-26})$
$^{58}Ni(n,p)$	E 0.1 MeV	$5.00(10^{-26})$	$5.12(10^{-26})$	$5.62(10^{-26})$	$5.42(10^{-26})$	$4.93(10^{-26})$
$\sigma(cm^2)$	E 0.5 MeV	$7.40(10^{-26})$	$7.54(10^{-26})$	$8.14(10^{-26})$	$7.93(10^{-26})$	$7.32(10^{-26})$
	E 1.0 MeV	$1.16(10^{-25})$	$1.17(10^{-25})$	$1.24(10^{-25})$	$1.22(10^{-25})$	$1.15(10^{-25})$
	Total	$3.06(10^{-22})$	$3.21(10^{-22})$	$3.09(10^{-22})$	$2.98(10^{-22})$	$3.16(10^{-22})$
Fe(dpa)	E 0.1 MeV	$6.40(10^{-22})$	$6.45(10^{-22})$	$6.69(10^{-22})$	$6.61(10^{-22})$	$6.35(10^{-22})$
$\sigma(cm^2)$	E 0.5 MeV	$9.48(10^{-22})$	$9.49(10^{-22})$	$9.69(10^{-22})$	$9.68(10^{-22})$	$9.43(10^{-22})$
	E 1.0 MeV	$1.48(10^{-21})$	$1.48(10^{-21})$	$1.47(10^{-21})$	$1.48(10^{-21})$	$1.48(10^{-21})$

Table 44. Spectral Parameters of the Two-Dimensional Diffusion Calculation for Core No. 54; Fuel Core Symmetry, Core Position 78, and 7-Groups

Parameters	Integration Range	Tube 1	Tube 2	Tube 3	Tube 4	Tube 5
	Total	$2.82(10^{13})$	$2.50(10^{13})$	$3.22(10^{13})$	$3.42(10^{13})$	$2.76(10^{13})$
ϕ	E>0.1 MeV	$1.36(10^{13})$	$1.26(10^{13})$	$1.49(10^{13})$	$1.54(10^{13})$	$1.41(10^{13})$
(n/cm^2-sec)	E>0.5 MeV	$9.18(10^{12})$	$8.54(10^{12})$	$1.03(10^{13})$	$1.05(10^{13})$	$9.46(10^{12})$
	E>1.0 MeV	$5.86(10^{12})$	$5.48(10^{12})$	$6.76(10^{12})$	$6.90(10^{12})$	$6.02(10^{12})$
	Total	$1.88(10^{-26})$	$1.98(10^{-26})$	$1.92(10^{-26})$	$1.84(10^{-26})$	$1.97(10^{-26})$
^{54}Fe(n,p)	E>0.1 MeV	$3.90(10^{-26})$	$3.94(10^{-26})$	$4.16(10^{-26})$	$4.08(10^{-26})$	$3.86(10^{-26})$
σ(cm^2)	E>0.5 MeV	$5.78(10^{-26})$	$5.80(10^{-26})$	$6.03(10^{-26})$	$5.98(10^{-26})$	$5.74(10^{-26})$
	E>1.0 MeV	$9.05(10^{-26})$	$9.03(10^{-26})$	$9.15(10^{-26})$	$9.14(10^{-26})$	$9.02(10^{-26})$
	Total	$2.52(10^{-26})$	$2.66(10^{-26})$	$2.58(10^{-26})$	$2.47(10^{-26})$	$2.64(10^{-26})$
^{58}Ni(n,p)	E>0.1 MeV	$5.23(10^{-26})$	$5.29(10^{-26})$	$5.58(10^{-26})$	$5.48(10^{-26})$	$5.18(10^{-26})$
σ(cm^2)	E>0.5 MeV	$7.75(10^{-26})$	$7.78(10^{-26})$	$8.09(10^{-26})$	$8.02(10^{-26})$	$7.70(10^{-26})$
	E>1.0 MeV	$1.21(10^{-25})$	$1.21(10^{-25})$	$1.23(10^{-25})$	$1.23(10^{-25})$	$1.21(10^{-25})$
	Total	$3.23(10^{-22})$	$3.38(10^{-22})$	$3.22(10^{-22})$	$3.12(10^{-22})$	$3.38(10^{-22})$
Fe(dpa)	E 0.1 MeV	$6.71(10^{-22})$	$6.74(10^{-22})$	$6.99(10^{-22})$	$6.92(10^{-22})$	$6.64(10^{-22})$
σ(cm^2)	E 0.5 MeV	$9.93(10^{-22})$	$9.91(10^{-22})$	$1.01(10^{-21})$	$1.01(10^{-21})$	$9.87(10^{-22})$
	E 1.0 MeV	$1.56(10^{-21})$	$1.54(10^{-21})$	$1.54(10^{-21})$	$1.55(10^{-21})$	$1.55(10^{-21})$

Table 45. Spectral Parameters of Plane 3 of the Three-Dimensional Diffusion Calculation for Core No. 54; Quarter Core Symmetry and 7-Groups

Parameter	Integration Range	Tube 1	Tube 2	Tube 3	Tube 4	Tube 5
	Total	$2.22(10^{13})$	$1.90(10^{13})$	$2.62(10^{13})$	$2.86(10^{13})$	$2.14(10^{13})$
ϕ	E>0.1 MeV	$9.98(10^{12})$	$9.02(10^{12})$	$1.12(10^{13})$	$1.20(10^{13})$	$1.04(10^{13})$
(n/cm^2-sec)	E>0.5 MeV	$6.86(10^{12})$	$6.24(10^{12})$	$7.88(10^{12})$	$8.38(10^{12})$	$7.16(10^{12})$
	E>1.0 MeV	$4.52(10^{12})$	$4.12(10^{12})$	$5.34(10^{12})$	$5.64(10^{12})$	$4.68(10^{12})$
	Total	$2.09(10^{-26})$	$2.23(10^{-26})$	$2.12(10^{-26})$	$2.05(10^{-26})$	$2.24(10^{-26})$
^{54}Fe(n,p)	E>0.1 MeV	$4.64(10^{-26})$	$4.69(10^{-26})$	$4.96(10^{-26})$	$4.88(10^{-26})$	$4.59(10^{-26})$
σ(cm^2)	E>0.5 Mev	$6.76(10^{-26})$	$6.77(10^{-26})$	$7.05(10^{-26})$	$6.99(10^{-26})$	$6.70(10^{-26})$
	E>1.0 MeV	$1.03(10^{-25})$	$1.03(10^{-25})$	$1.04(10^{-25})$	$1.04(10^{-25})$	$1.02(10^{-25})$
	Total	$2.80(10^{-26})$	$2.99(10^{-26})$	$2.85(10^{-26})$	$2.75(10^{-26})$	$3.01(10^{-26})$
^{58}Ni(n,p)	E>0.1 MeV	$6.23(10^{-26})$	$6.29(10^{-26})$	$6.66(10^{-26})$	$6.54(10^{-26})$	$6.16(10^{-26})$
σ(cm^2)	E>0.5 Mev	$9.07(10^{-26})$	$9.09(10^{-26})$	$9.46(10^{-26})$	$9.38(10^{-26})$	$8.98(10^{-26})$
	E>1.0 MeV	$1.38(10^{-25})$	$1.38(10^{-25})$	$1.40(10^{-25})$	$1.39(10^{-25})$	$1.37(10^{-25})$
	Total	$3.14(10^{-22})$	$3.33(10^{-22})$	$3.11(10^{-22})$	$3.05(10^{-22})$	$3.36(10^{-22})$
Fe(dpa)	E>0.1 Mev	$6.97(10^{-22})$	$6.98(10^{-22})$	$7.29(10^{-22})$	$7.22(10^{-22})$	$6.90(10^{-22})$
σ(cm^2)	E>0.5 MeV	$1.01(10^{-21})$	$1.01(10^{-21})$	$1.04(10^{-21})$	$1.04(10^{-21})$	$1.01(10^{-21})$
	E>1.0 MeV	$1.54(10^{-21})$	$1.53(10^{-21})$	$1.53(10^{-21})$	$1.54(10^{-21})$	$1.54(10^{-21})$

Table 46. Spectral Parameters of Plane 5 of the Three-Dimensional Diffusion Calculation for Core No. 54; Quarter Core Symmetry and 7-Groups

Parameter	Integration Range	Tube 1	Tube 2	Tube 3	Tube 4	Tube 5
ϕ (n/cm^2-sec)	Total	$2.42(10^{13})$	$2.08(10^{13})$	$2.88(10^{13})$	$3.12(10^{13})$	$2.36(10^{13})$
	E>0.1 MeV	$1.10(10^{13})$	$9.92(10^{12})$	$1.23(10^{13})$	$1.32(10^{13})$	$1.15(10^{13})$
	E>0.5 MeV	$7.52(10^{12})$	$6.84(10^{12})$	$8.64(10^{12})$	$9.20(10^{12})$	$7.88(10^{12})$
	E>1.0 MeV	$4.92(10^{12})$	$4.48(10^{12})$	$5.84(10^{12})$	$6.18(10^{12})$	$5.12(10^{12})$
$^{54}Fe(n,p)$ $\sigma(cm^2)$	Total	$2.09(10^{-26})$	$2.21(10^{-26})$	$2.11(10^{-26})$	$2.05(10^{-26})$	$2.22(10^{-26})$
	E>0.1 MeV	$4.60(10^{-26})$	$4.64(10^{-26})$	$4.93(10^{-26})$	$4.84(10^{-26})$	$4.55(10^{-26})$
	E>0.5 MeV	$6.71(10^{-26})$	$6.73(10^{-26})$	$7.03(10^{-26})$	$6.95(10^{-26})$	$6.65(10^{-26})$
	E>1.0 MeV	$1.03(10^{-25})$	$1.03(10^{-25})$	$1.04(10^{-25})$	$1.04(10^{-25})$	$1.02(10^{-25})$
$^{58}Ni(n,p)$ $\sigma(cm^2)$	Total	$2.80(10^{-26})$	$2.97(10^{-26})$	$2.83(10^{-26})$	$2.75(10^{-26})$	$2.98(10^{-26})$
	E>0.1 MeV	$6.17(10^{-26})$	$6.23(10^{-26})$	$6.62(10^{-26})$	$6.49(10^{-26})$	$6.10(10^{-26})$
	E>0.5 Mev	$9.00(10^{-26})$	$9.03(10^{-26})$	$9.43(10^{-26})$	$9.33(10^{-26})$	$8.92(10^{-26})$
	E>1.0 MeV	$1.38(10^{-25})$	$1.38(10^{-25})$	$1.40(10^{-25})$	$1.39(10^{-25})$	$1.37(10^{-25})$
Fe(dpa) $\sigma(cm^2)$	Total	$3.14(10^{-22})$	$3.32(10^{-22})$	$3.11(10^{-22})$	$3.05(10^{-22})$	$3.35(10^{-22})$
	E>0.1 MeV	$6.92(10^{-22})$	$6.96(10^{-22})$	$7.27(10^{-22})$	$7.19(10^{-22})$	$6.86(10^{-22})$
	E>0.5 MeV	$1.01(10^{-21})$	$1.01(10^{-21})$	$1.04(10^{-21})$	$1.03(10^{-21})$	$1.01(10^{-21})$
	E>1.0 MeV	$1.54(10^{-21})$	$1.54(10^{-21})$	$1.53(10^{-21})$	$1.54(10^{-21})$	$1.54(10^{-21})$

Table 47. Spectral Parameters of Plane 7 of the Three-Dimensional Diffusion Calculation for Core No. 54; Quarter Core Symmetry and 7-Groups

Parameter	Integration Range	Tube 1	Tube 2	Tube 3	Tube 4	Tube 5
ϕ (n/cm^2-sec)	Total	$2.50(10^{13})$	$2.14(10^{13})$	$2.96(10^{13})$	$3.20(10^{13})$	$2.42(10^{13})$
	E>0.1 MeV	$1.13(10^{13})$	$1.02(10^{13})$	$1.27(10^{13})$	$1.36(10^{13})$	$1.18(10^{13})$
	E>0.5 MeV	$7.72(10^{12})$	$7.02(10^{12})$	$8.88(10^{12})$	$9.44(10^{12})$	$8.10(10^{12})$
	E>1.0 Mev	$5.06(10^{12})$	$4.60(10^{12})$	$6.00(10^{12})$	$6.34(10^{12})$	$5.26(10^{12})$
^{54}Fe(n,p) σ(cm^2)	Total	$2.07(10^{-26})$	$2.21(10^{-26})$	$2.11(10^{-26})$	$2.05(10^{-26})$	$2.22(10^{-26})$
	E>0.1 MeV	$4.59(10^{-26})$	$4.64(10^{-26})$	$4.93(10^{-26})$	$4.83(10^{-26})$	$4.54(10^{-26})$
	E>0.5 MeV	$6.71(10^{-26})$	$6.74(10^{-26})$	$7.03(10^{-26})$	$6.96(10^{-26})$	$6.64(10^{-26})$
	E>1.0 MeV	$1.02(10^{-25})$	$1.03(10^{-25})$	$1.04(10^{-25})$	$1.04(10^{-25})$	$1.02(10^{-25})$
^{58}Ni (n,p) σ(cm^2)	Total	$2.78(10^{-26})$	$2.96(10^{-26})$	$2.83(10^{-26})$	$2.75(10^{-26})$	$2.98(10^{-26})$
	E>0.1 MeV	$6.16(10^{-26})$	$6.22(10^{-26})$	$6.61(10^{-26})$	$6.48(10^{-26})$	$6.09(10^{-26})$
	E>0.5 MeV	$9.00(10^{-26})$	$9.04(10^{-26})$	$9.43(10^{-26})$	$9.33(10^{-26})$	$8.91(10^{-26})$
	E>1.0 MeV	$1.37(10^{-25})$	$1.38(10^{-25})$	$1.39(10^{-25})$	$1.39(10^{-25})$	$1.37(10^{-25})$
Fe(dpa) σ(cm^2)	Total	$3.12(10^{-22})$	$3.31(10^{-22})$	$3.11(10^{-22})$	$3.05(10^{-22})$	$3.36(10^{-22})$
	E>0.1 MeV	$6.91(10^{-22})$	$6.94(10^{-22})$	$7.27(10^{-22})$	$7.18(10^{-22})$	$6.86(10^{-22})$
	E>0.5 MeV	$1.01(10^{-21})$	$1.01(10^{-21})$	$1.04(10^{-21})$	$1.03(10^{-21})$	$1.00(10^{-21})$
	E>1.0 MeV	$1.54(10^{-21})$	$1.54(10^{-21})$	$1.53(10^{-21})$	$1.54(10^{-21})$	$1.54(10^{-21})$

Table 48. Spectral Parameters of Plane 9 of the Three-Dimensional Diffusion Calculation for Core No. 54, Quarter Core Symmetry and 7-Groups

Parameter	Integration Range	Tube 1	Tube 2	Tube 3	Tube 4	Tube 5
ϕ (n/cm^2-sec)	Total	$2.38(10^{13})$	$2.04(10^{13})$	$2.80(10^{13})$	$3.04(10^{13})$	$2.30(10^{13})$
	E>0.1 MeV	$1.07(10^{13})$	$9.68(10^{12})$	$1.20(10^{13})$	$1.29(10^{13})$	$1.12(10^{13})$
	E>0.5 MeV	$7.36(10^{12})$	$6.68(10^{12})$	$8.44(10^{12})$	$8.96(10^{12})$	$7.68(10^{12})$
	E>1.0 MeV	$4.82(10^{12})$	$4.38(10^{12})$	$5.70(10^{12})$	$6.02(10^{12})$	$5.00(10^{12})$
$^{54}Fe(n,p)$ $\sigma(cm^2)$	Total	$2.07(10^{-26})$	$2.21(10^{-26})$	$2.12(10^{-26})$	$2.05(10^{-26})$	$2.22(10^{-26})$
	E>0.1 MeV	$4.60(10^{-26})$	$4.65(10^{-26})$	$4.93(10^{-26})$	$4.84(10^{-26})$	$4.55(10^{-26})$
	E>0.5 MeV	$6.71(10^{-26})$	$6.74(10^{-26})$	$7.02(10^{-26})$	$6.97(10^{-26})$	$6.66(10^{-26})$
	E>1.0 MeV	$1.02(10^{-25})$	$1.03(10^{-25})$	$1.04(10^{-25})$	$1.04(10^{-25})$	$1.02(10^{-25})$
$^{58}Ni(n,p)$ $\sigma(cm^2)$	Total	$2.78(10^{-26})$	$2.96(10^{-26})$	$2.84(10^{-26})$	$2.76(10^{-26})$	$2.98(10^{-26})$
	E>0.1 MeV	$6.18(10^{-26})$	$6.24(10^{-26})$	$6.61(10^{-26})$	$6.49(10^{-26})$	$6.11(10^{-26})$
	E>0.5 MeV	$9.00(10^{-26})$	$9.04(10^{-26})$	$9.41(10^{-26})$	$9.35(10^{-26})$	$8.94(10^{-26})$
	E>1.0 MeV	$1.37(10^{-25})$	$1.38(10^{-25})$	$1.39(10^{-25})$	$1.39(10^{-25})$	$1.37(10^{-25})$
Fe(dpa) $\sigma(cm^2)$	Total	$3.13(10^{-22})$	$3.30(10^{-22})$	$3.11(10^{-22})$	$3.05(10^{-22})$	$3.35(10^{-22})$
	E>0.1 MeV	$6.94(10^{-22})$	$6.96(10^{-22})$	$7.25(10^{-22})$	$7.18(10^{-22})$	$6.85(10^{-22})$
	E>0.5 MeV	$1.01(10^{-21})$	$1.01(10^{-21})$	$1.03(10^{-21})$	$1.03(10^{-21})$	$1.00(10^{-21})$
	E>1.0 MeV	$1.54(10^{-21})$	$1.54(10^{-21})$	$1.53(10^{-21})$	$1.54(10^{-21})$	$1.54(10^{-21})$

Table 49. Spectral Parameters of Plane 11 if the Three-Dimensional Diffusion Calculation for Core No. 54; Quarter Core Symmetry and 7-Groups

Parameter	Integration Range	Tube 1	Tube 2	Tube 3	Tube 4	Tube 5
ϕ (n/cm^2-sec)	Total	$2.20(10^{13})$	$1.89(10^{13})$	$2.60(10^{13})$	$2.82(10^{13})$	$2.12(10^{13})$
	E>0.1 MeV	$9.94(10^{12})$	$8.98(10^{12})$	$1.11(10^{13})$	$1.19(10^{13})$	$1.04(10^{13})$
	E>0.5 MeV	$6.84(10^{12})$	$6.22(10^{12})$	$7.80(10^{12})$	$8.32(10^{12})$	$7.12(10^{12})$
	E>1.0 MeV	$4.50(10^{12})$	$4.10(10^{12})$	$5.30(10^{12})$	$5.60(10^{12})$	$4.66(10^{12})$
^{54}Fe(n,p) σ(cm^2)	Total	$2.10(10^{-26})$	$2.23(10^{-26})$	$2.12(10^{-26})$	$2.06(10^{-26})$	$2.25(10^{-26})$
	E>0.1 MeV	$4.64(10^{-26})$	$4.68(10^{-26})$	$4.96(10^{-26})$	$4.86(10^{-26})$	$4.58(10^{-26})$
	E>0.5 MeV	$6.74(10^{-26})$	$6.76(10^{-26})$	$7.05(10^{-26})$	$6.98(10^{-26})$	$6.69(10^{-26})$
	E>1.0 MeV	$1.02(10^{-25})$	$1.03(10^{-25})$	$1.04(10^{-25})$	$1.04(10^{-25})$	$1.02(10^{-25})$
^{58}Ni(n,p) σ(cm^2)	Total	$2.81(10^{-26})$	$2.99(10^{-26})$	$2.84(10^{-26})$	$2.76(10^{-26})$	$3.01(10^{-26})$
	E>0.1 MeV	$6.22(10^{-26})$	$6.28(10^{-26})$	$6.65(10^{-26})$	$6.52(10^{-26})$	$6.14(10^{-26})$
	E>0.5 MeV	$9.04(10^{-26})$	$9.07(10^{-26})$	$9.46(10^{-26})$	$9.36(10^{-26})$	$8.97(10^{-26})$
	E>1.0 MeV	$1.37(10^{-25})$	$1.38(10^{-25})$	$1.39(10^{-25})$	$1.39(10^{-25})$	$1.37(10^{-25})$
Fe(dpa) σ(cm^2)	Total	$3.15(10^{-22})$	$3.33(10^{-22})$	$3.12(10^{-22})$	$3.05(10^{-22})$	$3.38(10^{-22})$
	E>0.1 MeV	$6.96(10^{-22})$	$6.99(10^{-22})$	$7.30(10^{-22})$	$7.20(10^{-22})$	$6.88(10^{-22})$
	E>0.5 MeV	$1.01(10^{-21})$	$1.01(10^{-21})$	$1.04(10^{-21})$	$1.03(10^{-21})$	$1.01(10^{-21})$
	E>1.0 MeV	$1.54(10^{-21})$	$1.53(10^{-21})$	$1.53(10^{-21})$	$1.54(10^{-21})$	$1.54(10^{-21})$

Table 50. Center Point Group Fluxes by Core Element Position for BSR Core No. 54.
[Two-dimensional, full core VENTURE calculation used.]

Group No.	Core Position Number							
	89	79	69	59	49	39	29	19
1	7.16(10)	1.54(11)	2.54(11)	2.87(11)	2.66(11)	2.17(11)	1.49(11)	7.17(10)
2	1.29(11)	2.88(11)	4.90(11)	5.54(11)	5.07(11)	4.11(11)	2.76(11)	1.27(11)
3	4.23(11)	9.60(11)	1.65(12)	1.85(12)	1.68(12)	1.35(12)	9.00(11)	4.05(11)
4	3.72(11)	7.97(11)	1.34(12)	1.51(12)	1.37(12)	1.11(12)	7.42(11)	3.52(11)
5	9.25(11)	1.91(12)	3.16(12)	3.53(12)	3.19(12)	2.57(12)	1.73(12)	8.37(11)
6	5.07(11)	9.82(11)	1.59(12)	1.76(12)	1.59(12)	1.28(12)	8.62(11)	4.44(11)
7	1.14(12)	2.13(12)	3.38(12)	3.75(12)	3.40(12)	2.74(12)	1.85(12)	9.74(11)
8	5.28(11)	9.05(11)	1.41(12)	1.57(12)	1.42(12)	1.14(12)	7.76(11)	4.46(11)
9	6.77(11)	1.27(12)	1.98(12)	2.21(12)	2.00(12)	1.62(12)	1.09(12)	5.69(11)
10	3.11(11)	5.15(11)	7.91(11)	8.83(11)	8.03(11)	6.49(11)	4.41(11)	2.60(11)
11	9.54(11)	1.67(12)	2.58(12)	2.88(12)	2.63(12)	2.13(12)	1.45(12)	8.02(11)
12	1.75(12)	3.01(12)	4.63(12)	5.23(12)	4.80(12)	3.91(12)	2.66(12)	1.50(12)
13	1.51(12)	2.55(12)	3.84(12)	4.34(12)	4.02(12)	3.30(12)	2.24(12)	1.32(12)
14	4.69(11)	7.76(11)	1.18(12)	1.33(12)	1.23(12)	1.02(12)	6.89(11)	4.11(11)
15	6.35(12)	7.90(12)	1.05(13)	1.19(13)	1.05(13)	1.01(13)	6.78(12)	5.43(12)

Table 50. Center Point Group Fluxes (Cont'd)

Group No.	Core Position Number							
	88	78	68	58	48	38	28	18
1	1.22(11)	1.32(11)	2.76(11)	3.63(11)	3.08(11)	2.78(11)	1.87(11)	1.31(11)
2	2.31(11)	2.17(11)	4.97(11)	6.98(11)	5.70(11)	5.25(11)	3.39(11)	2.43(11)
3	7.90(11)	7.38(11)	1.56(12)	2.32(12)	1.83(12)	1.72(12)	1.07(12)	7.90(11)
4	6.68(11)	7.05(11)	1.30(12)	1.91(12)	1.53(12)	1.42(12)	9.03(11)	6.54(11)
5	1.66(12)	1.98(12)	2.92(12)	4.44(12)	3.48(12)	3.29(12)	2.05(12)	1.53(12)
6	8.73(11)	1.18(12)	1.40(12)	2.20(12)	1.70(12)	1.63(12)	1.00(12)	7.63(11)
7	1.94(12)	2.83(12)	3.09(12)	4.74(12)	3.72(12)	3.51(12)	2.20(12)	1.64(12)
8	8.28(11)	1.29(12)	1.30(12)	1.99(12)	1.58(12)	1.48(12)	9.37(11)	6.92(11)
9	1.17(12)	1.74(12)	1.96(12)	2.83(12)	2.30(12)	2.11(12)	1.37(12)	9.79(11)
10	4.74(11)	7.41(11)	8.01(11)	1.14(12)	9.52(11)	8.56(11)	5.66(11)	3.94(11)
11	1.54(11)	2.13(12)	2.78(12)	3.78(12)	3.22(12)	2.84(12)	1.92(12)	1.29(12)
12	2.79(12)	3.87(12)	5.49(12)	7.05(12)	6.29(12)	5.38(12)	3.75(12)	2.40(12)
13	2.30(12)	3.09(12)	5.02(12)	5.96(12)	5.30(12)	4.59(12)	3.18(12)	2.02(12)
14	6.99(11)	7.20(11)	1.61(12)	1.83(12)	1.53(12)	1.41(12)	9.21(11)	6.17(11)
15	5.93(12)	1.87(12)	3.73(13)	1.73(13)	4.65(12)	1.19(13)	2.98(12)	5.39(12)

Table 50. Center Point Group Fluxes (Cont'd)

Group No.	Core Position Number							
	87	77	67	57	47	37	27	17
1	1.39(11)	1.61(11)	3.42(11)	4.12(11)	3.70(11)	3.22(11)	2.32(11)	1.54(11)
2	2.71(11)	2.96(11)	6.63(11)	8.06(11)	7.10(11)	6.20(11)	4.40(11)	2.91(11)
3	9.32(11)	1.01(12)	2.24(12)	2.71(12)	2.35(12)	2.06(12)	1.45(12)	9.57(11)
4	7.84(11)	9.15(11)	1.85(12)	2.23(12)	1.94(12)	1.70(12)	1.20(12)	7.85(11)
5	1.93(12)	2.38(12)	4.41(12)	5.24(12)	4.52(12)	3.97(12)	2.78(12)	1.83(12)
6	1.01(12)	1.34(12)	2.23(12)	2.62(12)	2.25(12)	1.98(12)	1.38(12)	9.12(11)
7	2.22(12)	3.09(12)	4.80(12)	5.61(12)	4.84(12)	4.24(12)	2.97(12)	1.95(12)
8	9.55(11)	1.46(12)	2.02(12)	2.35(12)	2.03(12)	1.78(12)	1.25(12)	8.19(11)
9	1.33(12)	1.85(12)	2.84(12)	3.32(12)	2.89(12)	2.52(12)	1.78(12)	1.16(12)
10	5.44(11)	8.59(11)	1.14(12)	1.33(12)	1.17(12)	1.01(12)	7.19(11)	4.66(11)
11	1.77(12)	2.58(12)	3.74(12)	4.37(12)	3.86(12)	3.33(12)	2.37(12)	1.52(12)
12	3.31(12)	4.60(12)	6.80(12)	7.99(12)	7.21(12)	6.15(12)	4.44(12)	2.85(12)
13	2.86(12)	3.90(12)	5.63(12)	6.62(12)	6.09(12)	5.15(12)	3.76(12)	2.40(12)
14	8.77(11)	1.17(12)	1.72(12)	2.02(12)	1.86(12)	1.58(12)	1.15(12)	7.37(11)
15	8.21(12)	8.31(12)	1.51(13)	1.63(13)	1.50(13)	1.25(13)	8.88(12)	7.14(12)

Table 50. Center Point Group Fluxes (Cont'd)

Group No.	Core Position Number							
	86	76	66	56	46	36	26	16
1	1.16(11)	1.26(11)	2.66(11)	3.50(11)	2.95(11)	2.67(11)	1.79(11)	1.26(11)
2	2.20(11)	2.07(11)	4.80(11)	6.74(11)	5.47(11)	5.05(11)	3.26(11)	2.33(11)
3	7.53(11)	7.06(11)	1.51(12)	2.24(12)	1.75(12)	1.65(12)	1.03(12)	7.58(11)
4	6.37(11)	6.75(11)	1.26(12)	1.84(12)	1.47(12)	1.37(12)	8.68(11)	6.27(11)
5	1.59(12)	1.90(12)	2.84(12)	4.30(12)	3.34(12)	3.17(12)	1.97(12)	1.46(12)
6	8.34(11)	1.13(12)	1.36(12)	2.14(12)	1.63(12)	1.57(12)	9.66(11)	7.31(11)
7	1.86(12)	2.73(12)	3.02(12)	4.60(12)	3.58(12)	3.39(12)	2.12(12)	1.57(12)
8	7.93(11)	1.24(12)	1.27(12)	1.93(12)	1.52(12)	1.42(12)	9.02(11)	6.64(11)
9	1.12(12)	1.67(12)	1.91(12)	2.75(12)	2.22(12)	2.03(12)	1.32(12)	9.42(11)
10	4.56(11)	7.16(11)	7.83(11)	1.11(12)	9.16(11)	8.25(11)	5.46(11)	3.80(11)
11	1.49(12)	2.06(12)	2.71(12)	3.64(12)	3.10(12)	2.74(12)	1.85(12)	1.25(12)
12	2.73(12)	3.79(12)	5.38(12)	6.86(12)	6.07(12)	5.21(12)	3.64(12)	2.35(12)
13	2.26(12)	3.03(12)	4.92(12)	5.78(12)	5.13(12)	4.46(12)	3.10(12)	1.98(12)
14	6.89(11)	7.06(11)	1.58(12)	1.77(12)	1.49(12)	1.37(12)	8.99(11)	6.08(11)
15	5.68(12)	1.80(12)	3.62(13)	1.64(13)	4.50(12)	1.15(13)	2.90(12)	5.20(12)

Table 50. Center Point Group Fluxes (Cont'd)

Group No.	Core Position Number							
	85	75	65	55	45	35	25	15
1	6.85(10)	1.40(11)	2.35(11)	2.65(11)	2.45(11)	2.04(11)	1.40(11)	7.04(10)
2	1.25(11)	2.61(11)	4.53(11)	5.08(11)	4.66(11)	3.86(11)	2.58(11)	1.26(11)
3	4.11(11)	8.70(11)	1.52(12)	1.69(12)	1.54(12)	1.27(12)	8.37(12)	4.00(11)
4	3.63(11)	7.28(11)	1.24(12)	1.38(12)	1.26(12)	1.04(12)	6.94(11)	3.48(11)
5	9.09(11)	1.76(12)	2.92(12)	3.23(12)	2.93(12)	2.42(12)	1.61(12)	8.25(11)
6	5.00(11)	9.08(11)	1.47(12)	1.61(12)	1.46(12)	1.20(12)	8.02(11)	4.36(11)
7	1.16(12)	2.02(12)	3.15(12)	3.48(12)	3.16(12)	2.60(12)	1.75(12)	9.76(11)
8	5.45(11)	8.65(11)	1.33(12)	1.47(12)	1.33(12)	1.10(12)	7.43(11)	4.58(11)
9	7.39(11)	1.25(12)	1.90(12)	2.11(12)	1.92(12)	1.59(12)	1.07(12)	6.20(11)
10	3.53(11)	5.13(11)	7.68(11)	8.56(11)	7.82(11)	6.46(11)	4.41(11)	2.95(11)
11	1.12(12)	1.71(12)	2.54(12)	2.84(12)	2.61(12)	2.16(12)	1.48(12)	9.44(11)
12	1.91(12)	3.18(12)	4.69(12)	5.36(12)	4.93(12)	4.08(12)	2.82(12)	1.65(12)
13	1.58(12)	2.64(12)	3.90(12)	4.46(12)	4.15(12)	3.46(12)	2.39(12)	1.39(12)
14	4.77(11)	7.99(11)	1.19(12)	1.36(12)	1.27(12)	1.06(12)	7.29(11)	4.23(11)
15	4.44(12)	6.44(12)	9.87(12)	1.15(13)	9.48(12)	9.09(12)	6.09(12)	3.91(12)

Table 51. Center Point Group Fluxes by Core Element Position on the North Face of the BSR for Core No. 54. [Two-dimensional, full core symmetry VENTURE calculation used.]

Group No.	Core Position Number				
	19	18	17	16	15
1	4.84(10)	9.55(10)	1.11(11)	9.19(10)	4.42(10)
2	8.38(10)	1.73(11)	2.03(11)	1.67(11)	7.74(10)
3	2.61(11)	5.56(11)	6.54(11)	5.34(11)	2.40(11)
4	2.26(11)	4.55(11)	5.32(11)	4.37(11)	2.08(11)
5	5.19(11)	1.05(12)	1.21(12)	1.00(12)	4.73(11)
6	2.79(11)	5.20(11)	6.01(11)	4.99(11)	2.55(11)
7	6.06(11)	1.11(12)	1.28(12)	1.07(12)	5.66(11)
8	2.77(11)	4.65(11)	5.34(11)	4.47(11)	2.68(11)
9	3.62(11)	6.60(11)	7.62(11)	6.35(11)	3.72(11)
10	1.67(11)	2.64(11)	3.04(11)	2.54(11)	1.80(11)
11	5.53(11)	8.70(11)	1.01(12)	8.41(11)	6.24(11)
12	1.26(12)	1.67(12)	1.94(12)	1.63(12)	1.35(12)
13	1.15(12)	1.45(12)	1.69(12)	1.43(12)	1.18(12)
14	3.63(11)	4.55(11)	5.31(11)	4.48(11)	3.65(11)
15	5.56(12)	6.51(12)	7.94(12)	6.29(12)	4.07(12)

Table 52. Center Point Group Fluxes by Core Element Position on the East Face of the BSR for Core No. 54. [Two-dimensional, full core symmetry VENTURE calculation used.]

Group No.	Core Position Number							
	85	75	65	55	45	35	25	15
1	4.95(10)	1.05(11)	1.65(11)	1.84(11)	1.76(11)	1.45(11)	9.97(10)	4.89(10)
2	8.88(10)	1.90(11)	3.05(11)	3.40(11)	3.22(11)	2.63(11)	1.79(11)	8.65(10)
3	2.83(11)	6.16(11)	9.96(11)	1.10(12)	1.04(12)	8.39(11)	5.65(11)	2.68(11)
4	2.48(11)	5.10(11)	8.13(11)	8.95(11)	8.48(11)	6.88(11)	4.66(11)	2.32(11)
5	5.86(11)	1.18(12)	1.85(12)	2.01(12)	1.91(12)	1.55(12)	1.05(12)	5.26(11)
6	3.24(11)	5.99(11)	9.30(11)	1.00(12)	9.49(11)	7.69(11)	5.24(11)	2.83(11)
7	7.66(11)	1.37(12)	2.09(12)	2.25(12)	2.13(12)	1.73(12)	1.18(12)	6.53(11)
8	3.86(11)	6.20(11)	9.36(11)	1.01(12)	9.56(11)	7.77(11)	5.34(11)	3.28(11)
9	5.99(11)	1.00(12)	1.50(12)	1.64(12)	1.54(12)	1.26(12)	8.66(11)	5.09(11)
10	3.05(11)	4.43(11)	6.58(11)	7.18(11)	6.77(11)	5.52(11)	3.83(11)	2.58(11)
11	1.04(12)	1.57(12)	2.30(12)	2.52(12)	2.38(12)	1.95(12)	1.36(12)	8.78(11)
12	1.73(12)	2.67(12)	3.87(12)	4.31(12)	4.05(12)	3.33(12)	2.33(12)	1.48(12)
13	1.40(12)	2.08(12)	2.99(12)	3.35(12)	3.16(12)	2.62(12)	1.84(12)	1.23(12)
14	4.23(11)	6.16(11)	8.83(11)	9.95(11)	9.39(11)	7.82(11)	5.50(11)	3.73(11)
15	4.18(12)	4.67(12)	6.09(12)	7.23(12)	6.57(12)	6.02(12)	4.43(12)	3.69(12)

Table 53. Center Point Group Fluxes by Core Element Position on the West Face of the BSR for Core No. 54. [Two-dimensional, full core symmetry VENTURE calculation used.]

Group No.	Core Position Number							
	89	79	69	59	49	39	29	19
1	5.72(10)	1.26(11)	2.00(11)	2.26(11)	2.13(11)	1.72(11)	1.18(11)	5.56(10)
2	9.93(10)	2.30(11)	3.77(11)	4.24(11)	3.96(11)	3.17(11)	2.14(11)	9.59(10)
3	3.18(11)	7.48(11)	1.24(12)	1.39(12)	1.29(12)	1.02(12)	6.82(11)	2.99(11)
4	2.76(11)	6.14(11)	1.01(12)	1.13(12)	1.04(12)	8.30(11)	5.58(11)	2.57(11)
5	6.57(11)	1.43(12)	2.32(12)	2.58(12)	2.39(12)	1.89(12)	1.28(12)	5.92(11)
6	3.58(11)	7.21(11)	1.16(12)	1.28(12)	1.18(12)	9.34(11)	6.34(11)	3.15(11)
7	7.93(11)	1.55(12)	2.46(12)	2.72(12)	2.51(12)	1.99(12)	1.35(12)	6.83(11)
8	3.64(11)	6.55(11)	1.03(12)	1.13(12)	1.05(12)	8.29(11)	5.67(11)	3.11(11)
9	4.80(11)	9.27(11)	1.45(12)	1.60(12)	1.48(12)	1.18(12)	8.02(11)	4.08(11)
10	2.20(11)	3.73(11)	5.80(11)	6.42(11)	5.92(11)	4.72(11)	3.23(11)	1.86(11)
11	7.21(11)	1.23(12)	1.91(12)	2.12(12)	1.96(12)	1.56(12)	1.07(12)	6.10(11)
12	1.54(12)	2.32(12)	3.55(12)	3.97(12)	3.67(12)	2.96(12)	2.01(12)	1.32(12)
13	1.38(12)	2.03(12)	3.04(12)	3.41(12)	3.17(12)	2.58(12)	1.76(12)	1.19(12)
14	4.32(11)	6.31(11)	9.45(11)	1.06(12)	9.89(11)	8.07(11)	5.50(11)	3.77(11)
15	6.56(12)	9.41(12)	1.24(13)	1.41(13)	1.32(13)	1.18(13)	8.06(12)	5.61(12)

APPENDIX B

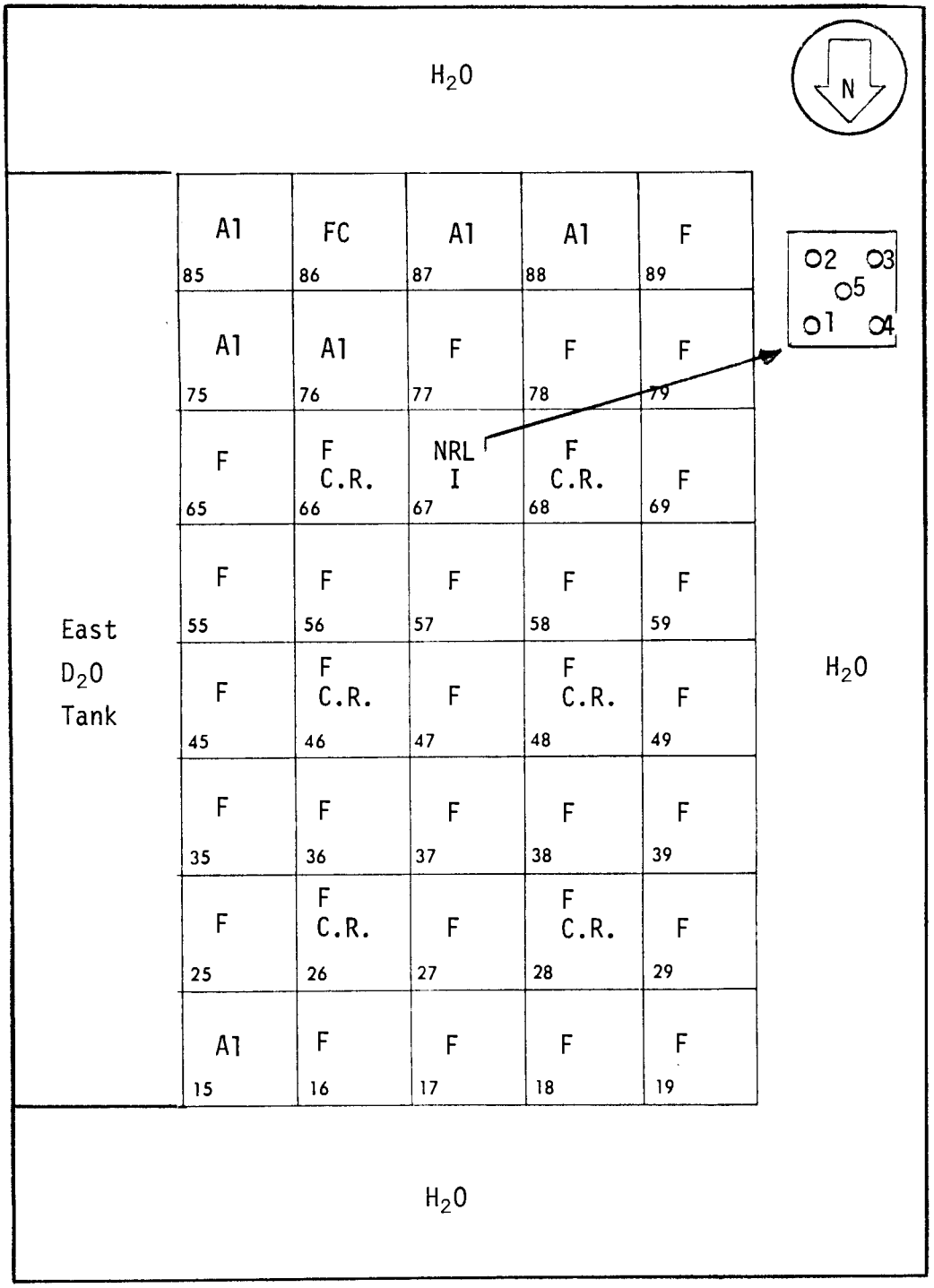

Fig. 1. BSR Core Configuration for Core No. 37

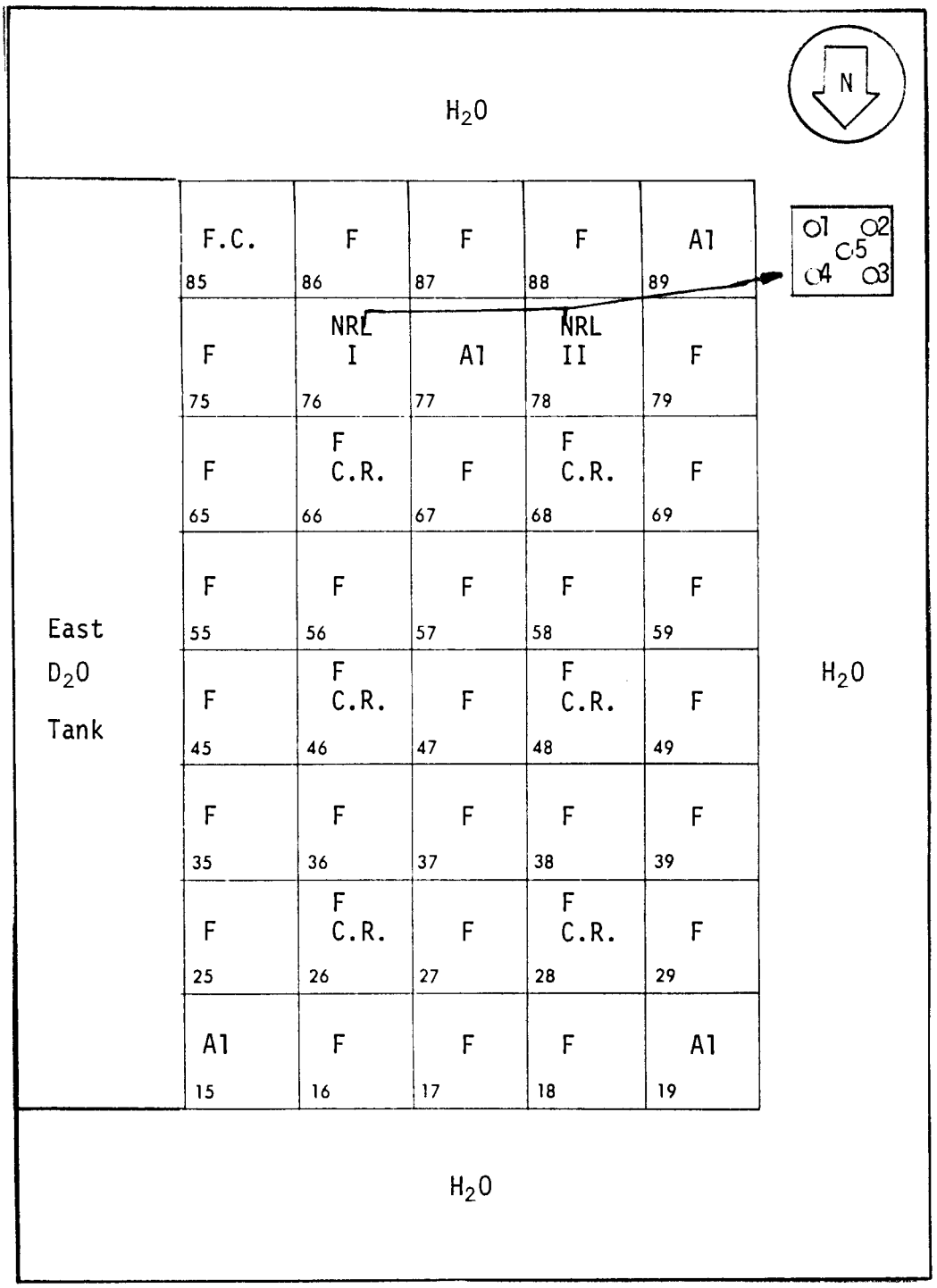

Fig. 2. BSR Core Configuration for Core No. 54

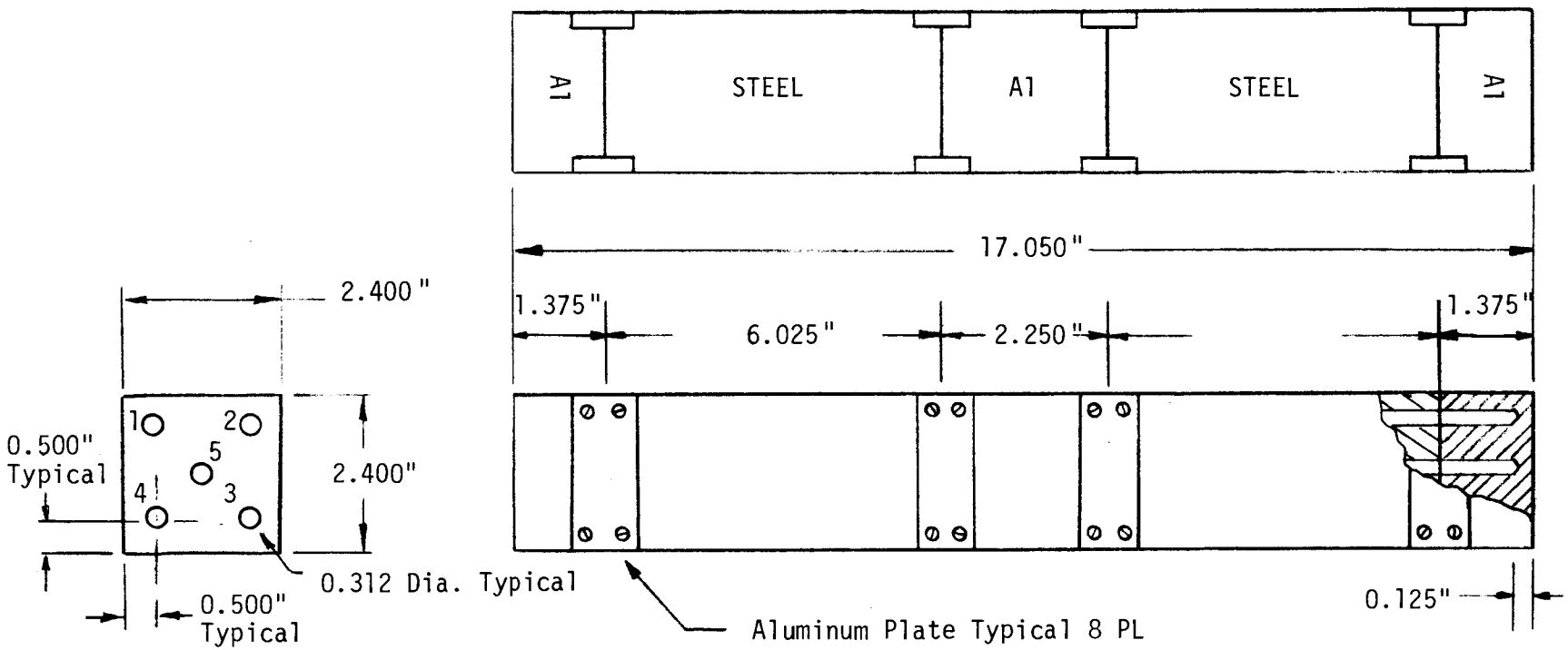

Fig. 3. Simplified Drawing of the NRL Dosimetry Capsule for Core No. 37

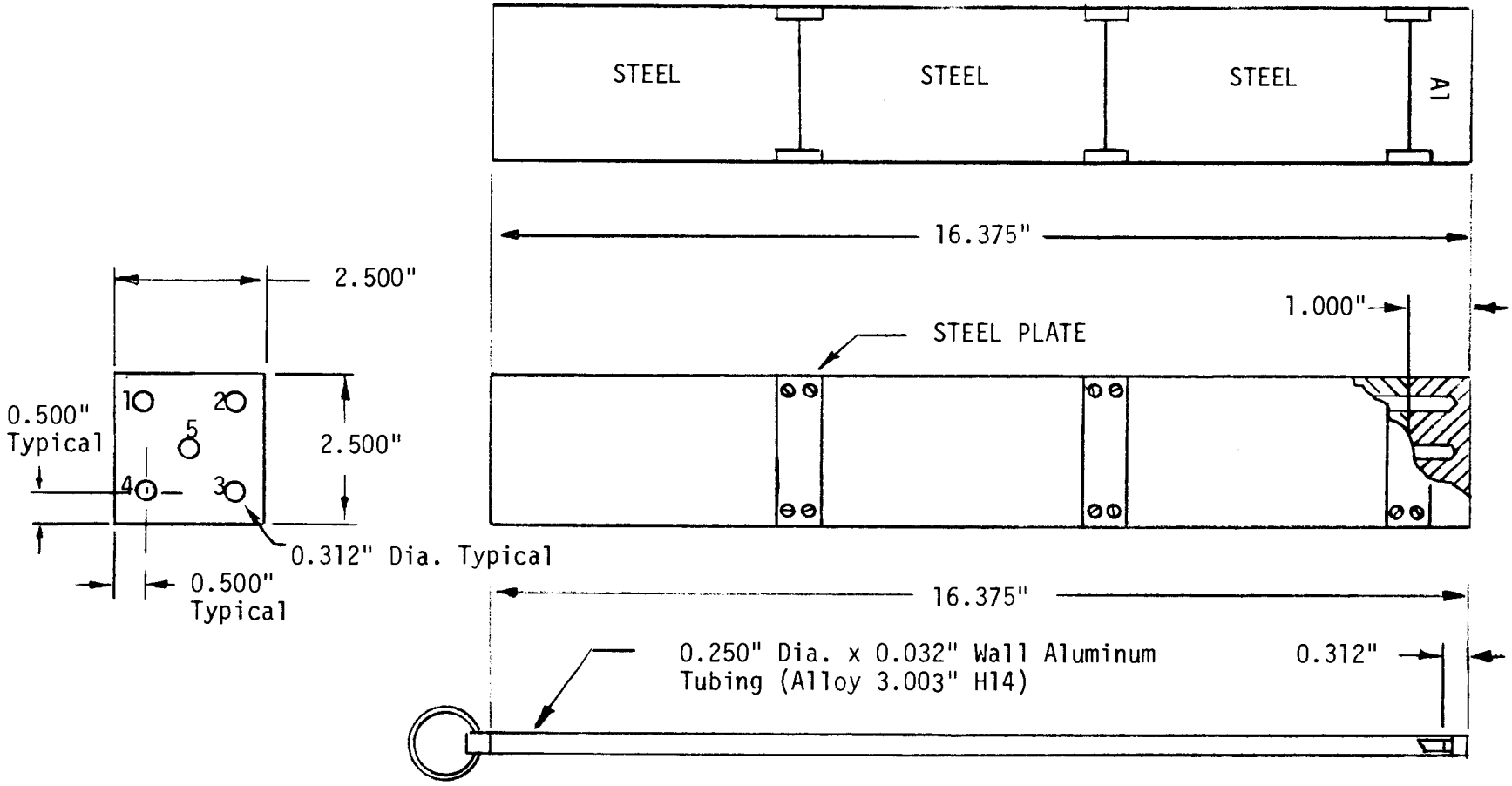

Fig. 4. Simplified Drawing of the NRL Dosimetry Capsule for Core No. 54

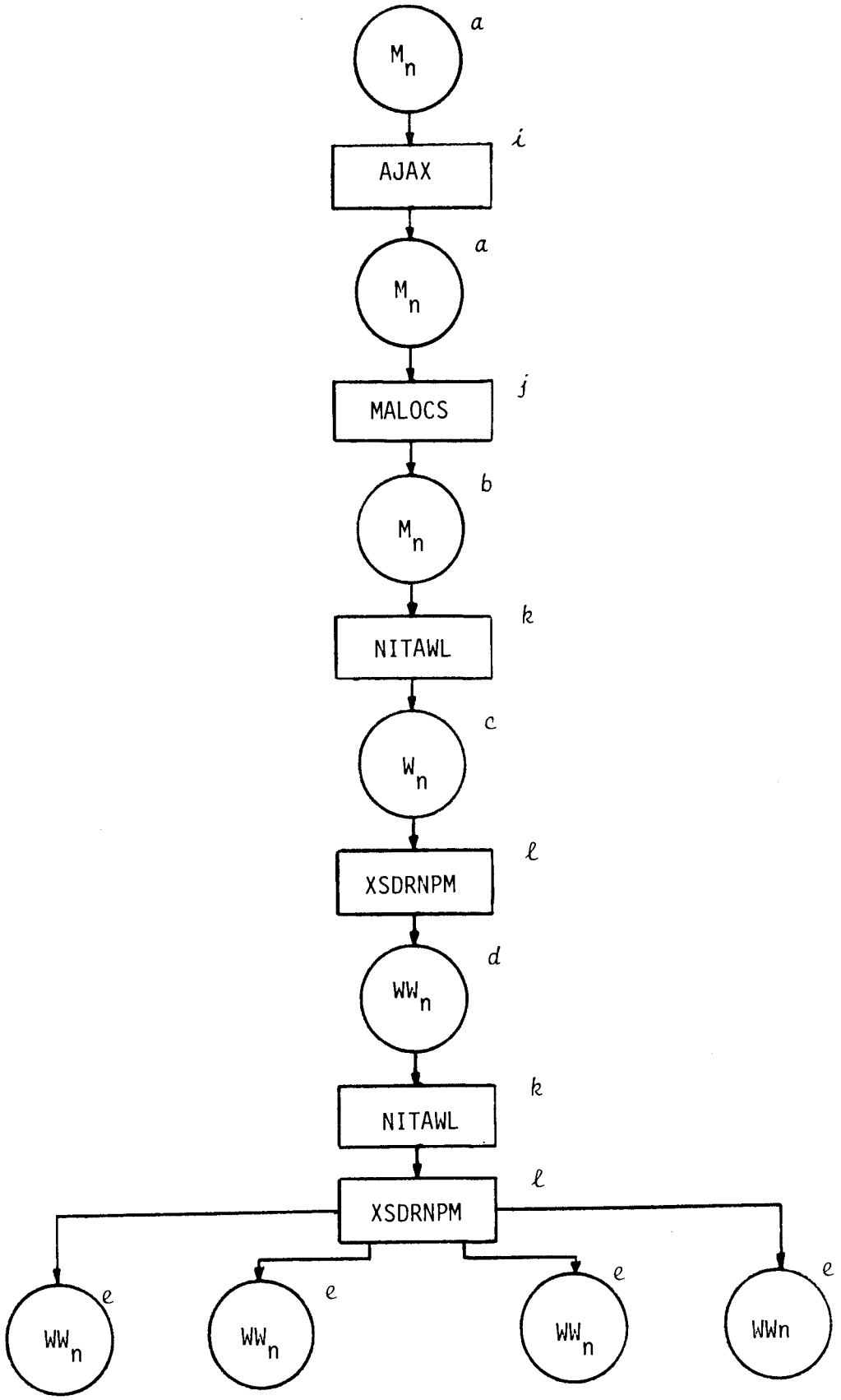

Fig. 5. Block Diagram of the Cross Section Library Generation Used in the NRL Calculational Model

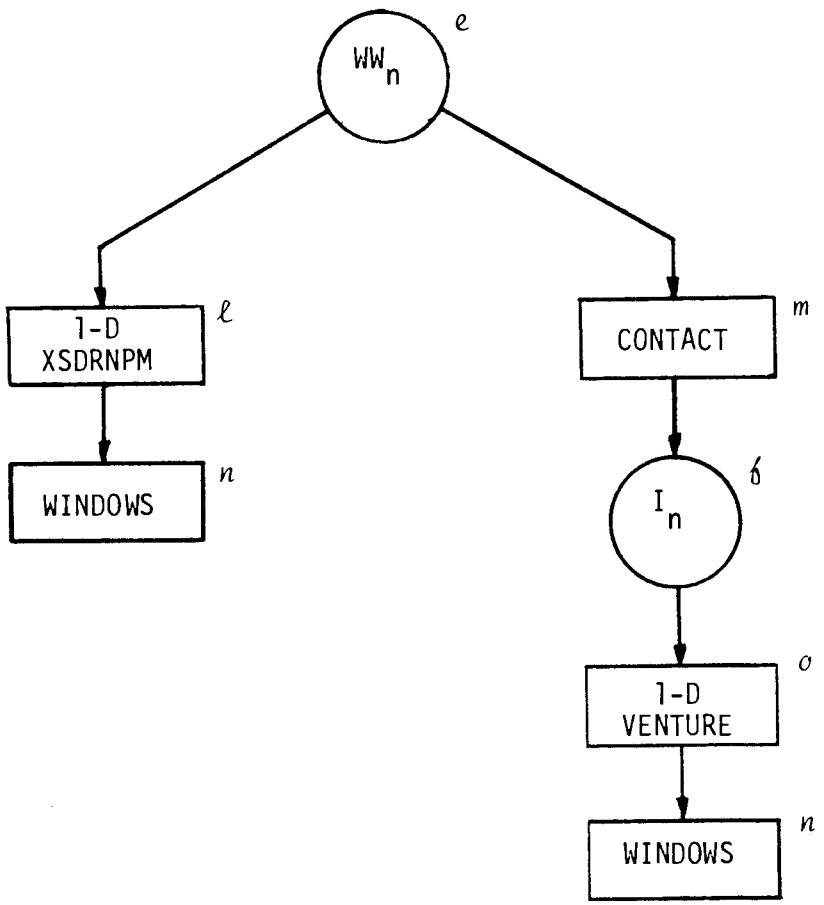

Fig. 6. Block Diagram of the Neutronics Calculations Utilizing the 40- and 27-Group Libraries

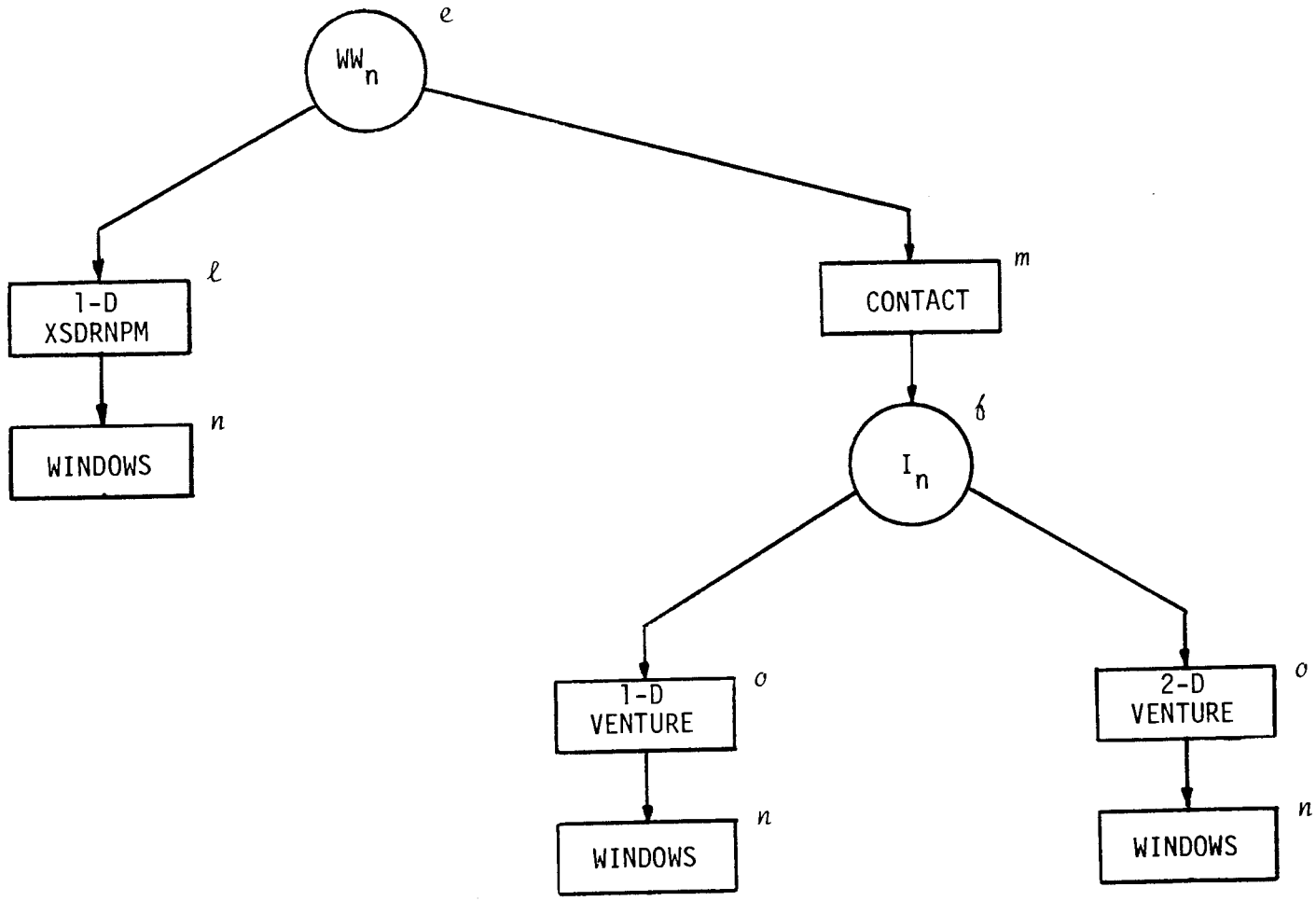

Fig. 7. Block Diagram of the Neutronics Calculations Utilizing the 15-Group Library

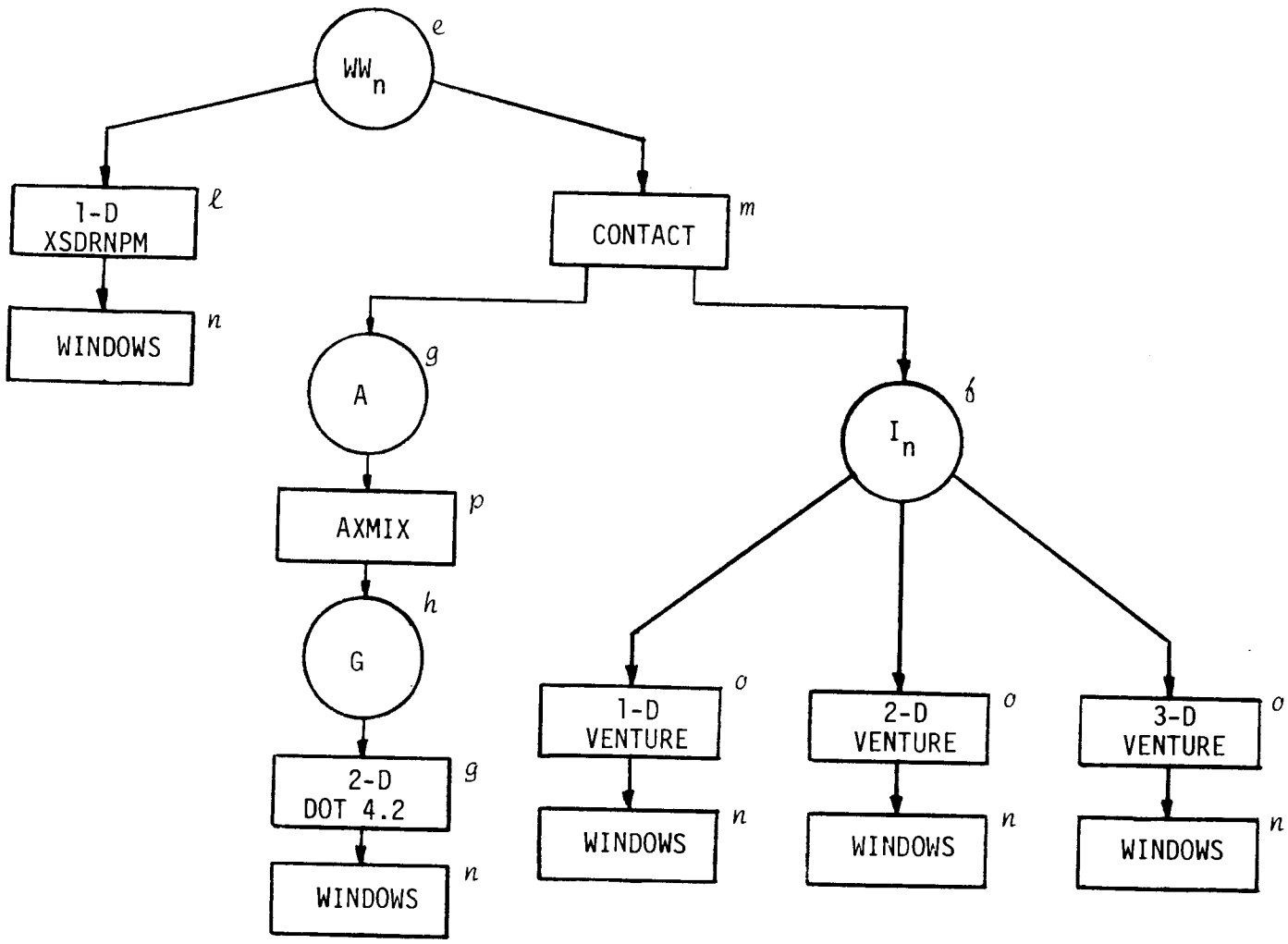

Fig. 8. Block Diagram of the Neutronics Calculations Utilizing the 7-Group Library

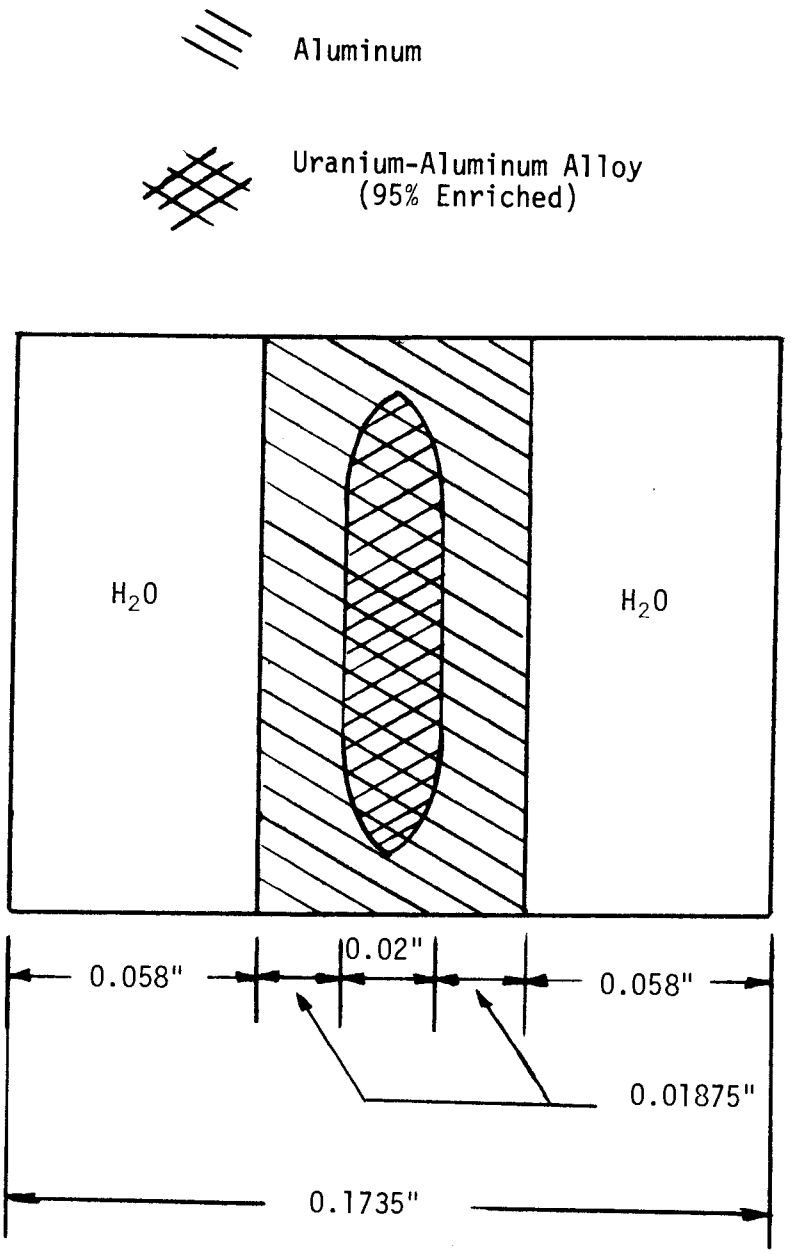

Fig. 9. Model Used for One-Dimensional Cell-Weighting Calculation (Not to Scale)

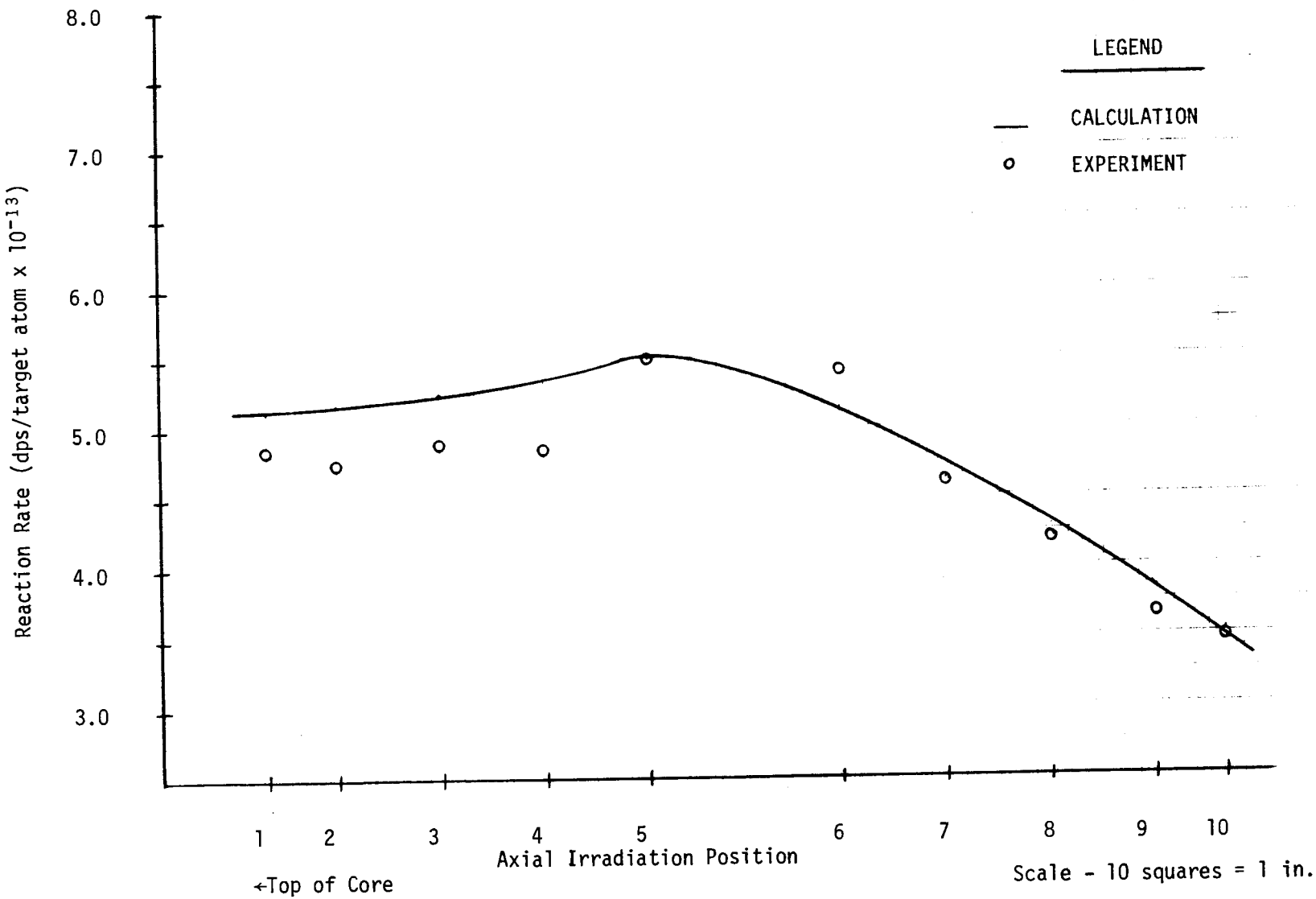

Fig. 10. Axial Distribution of the Absolute Activity of the $^{54}Fe(n,p)$ Reaction for Core No. 37, Tube 3

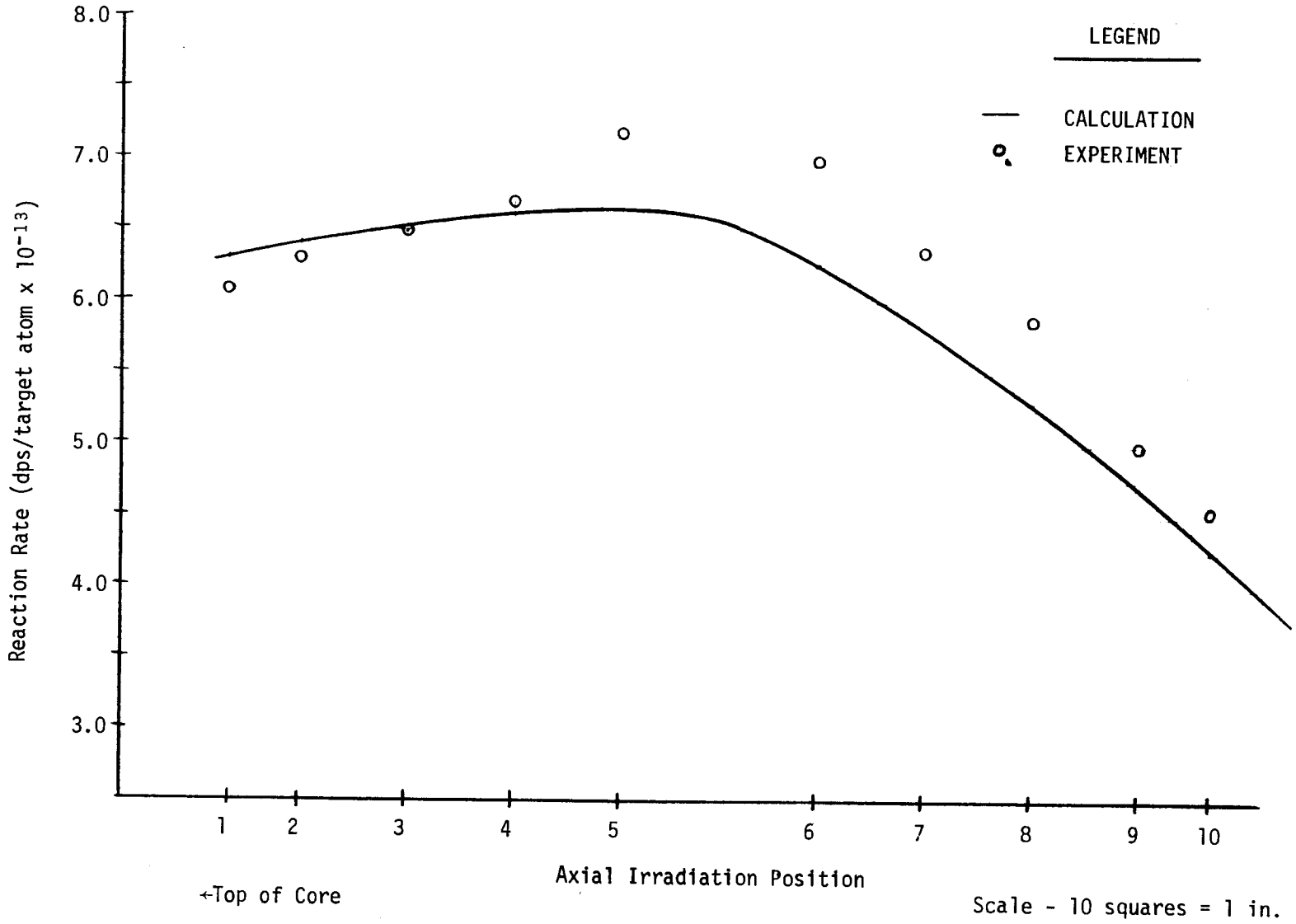

Fig. 11. Axial Distribution of the Absolute Activity of the $^{54}Fe(n,p)$ Reaction for Core No. 37, Tube 4

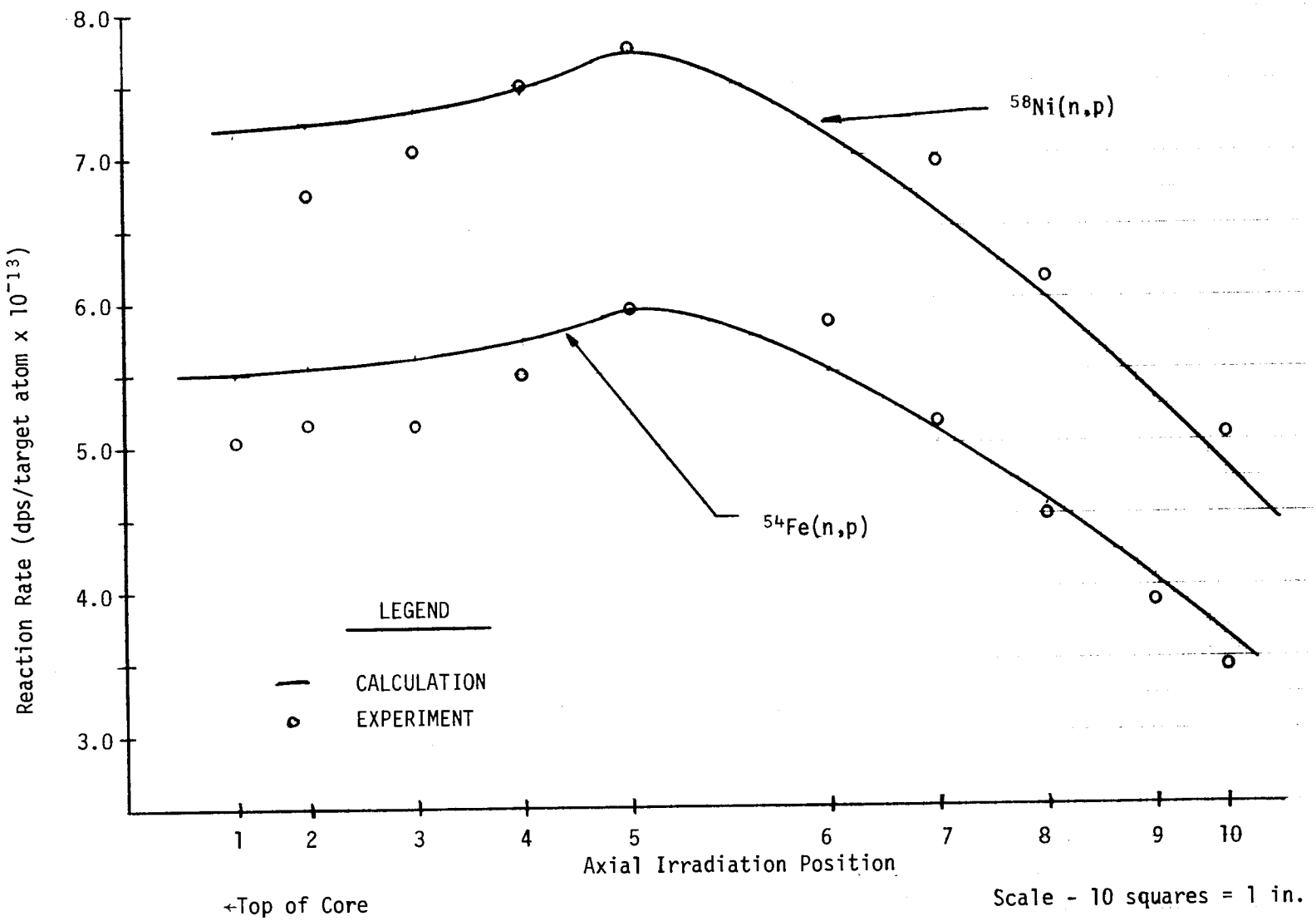

Fig. 12. Axial Distribution of the Absolute Activities of the ^{54}Fe(n,p) Reaction and ^{58}Ni(n,p) Reaction for Core No.37, Tube 5

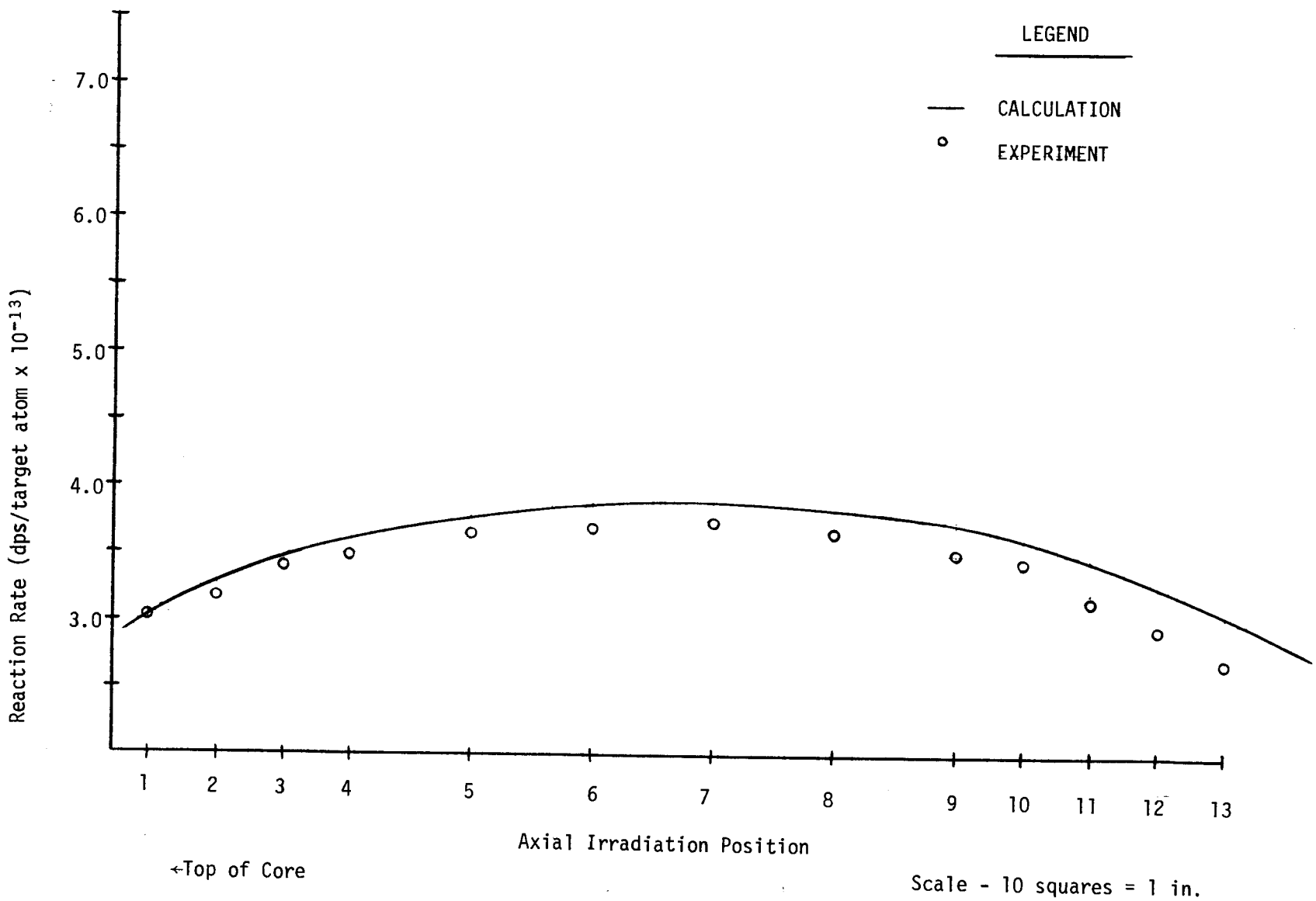

Fig. 13. Axial Distribution of the Absolute Activity of the $^{54}Fe(n,p)$ Reaction for Core No. 54, Tube 1

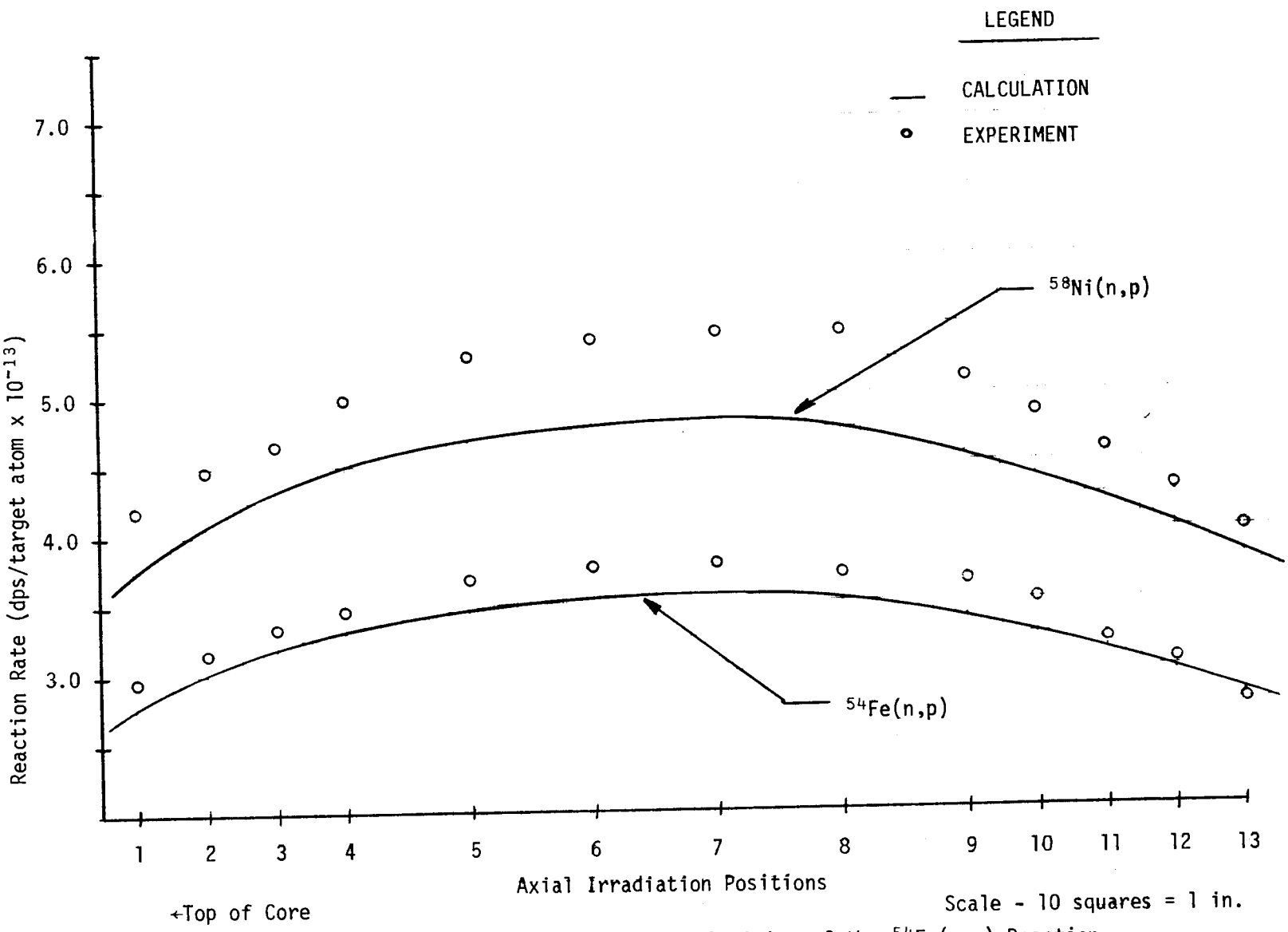

Fig. 14. Axial Distribution of the Absolute Activity of the ^{54}Fe(n,p) Reaction and ^{58}Ni(n,p) Reaction for Core No. 54, Tube 2

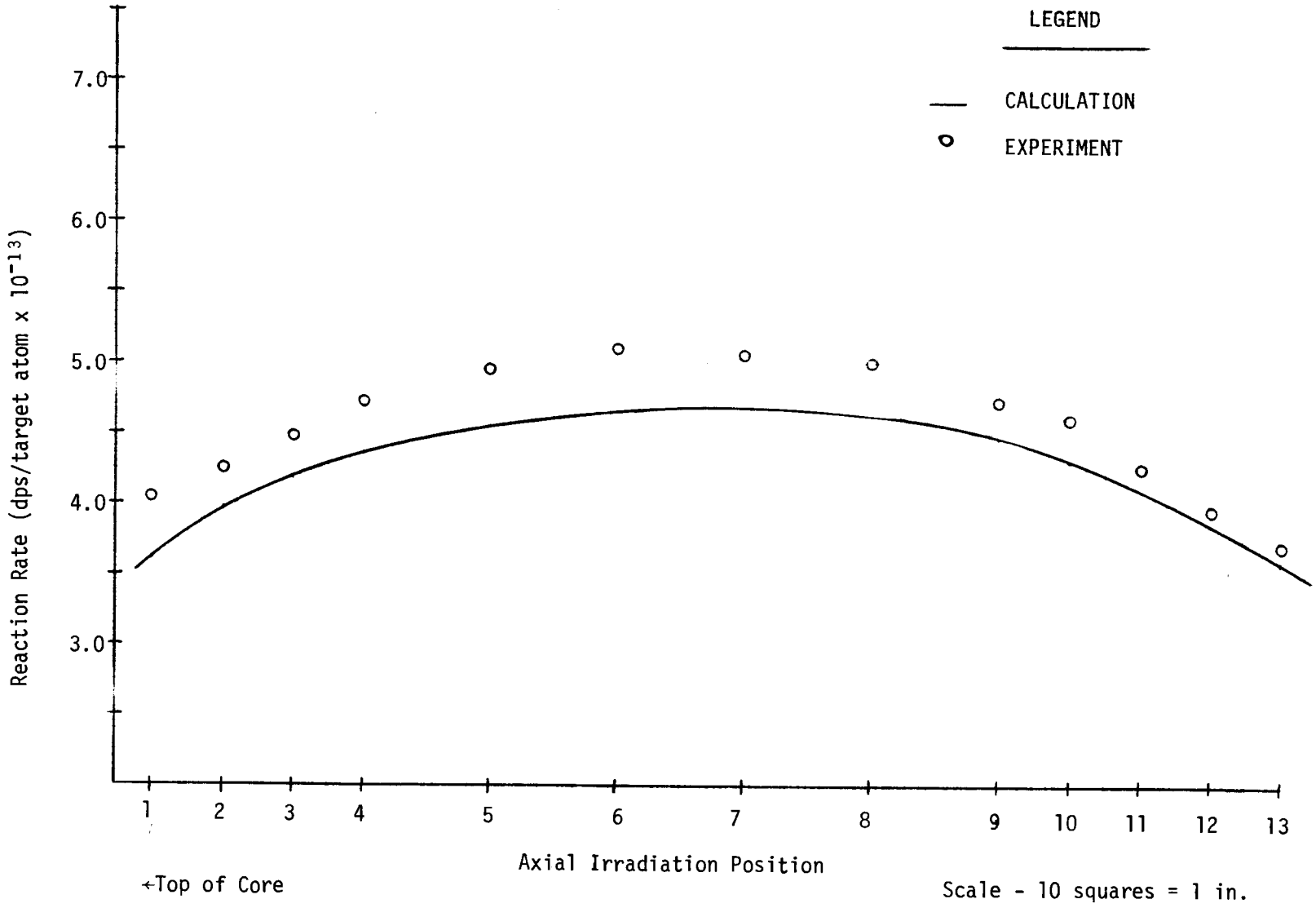

Fig. 15. Axial Distribution of the Absolute Activity of the $^{54}Fe(n,p)$ Reaction for Core No. 54, Tube 3

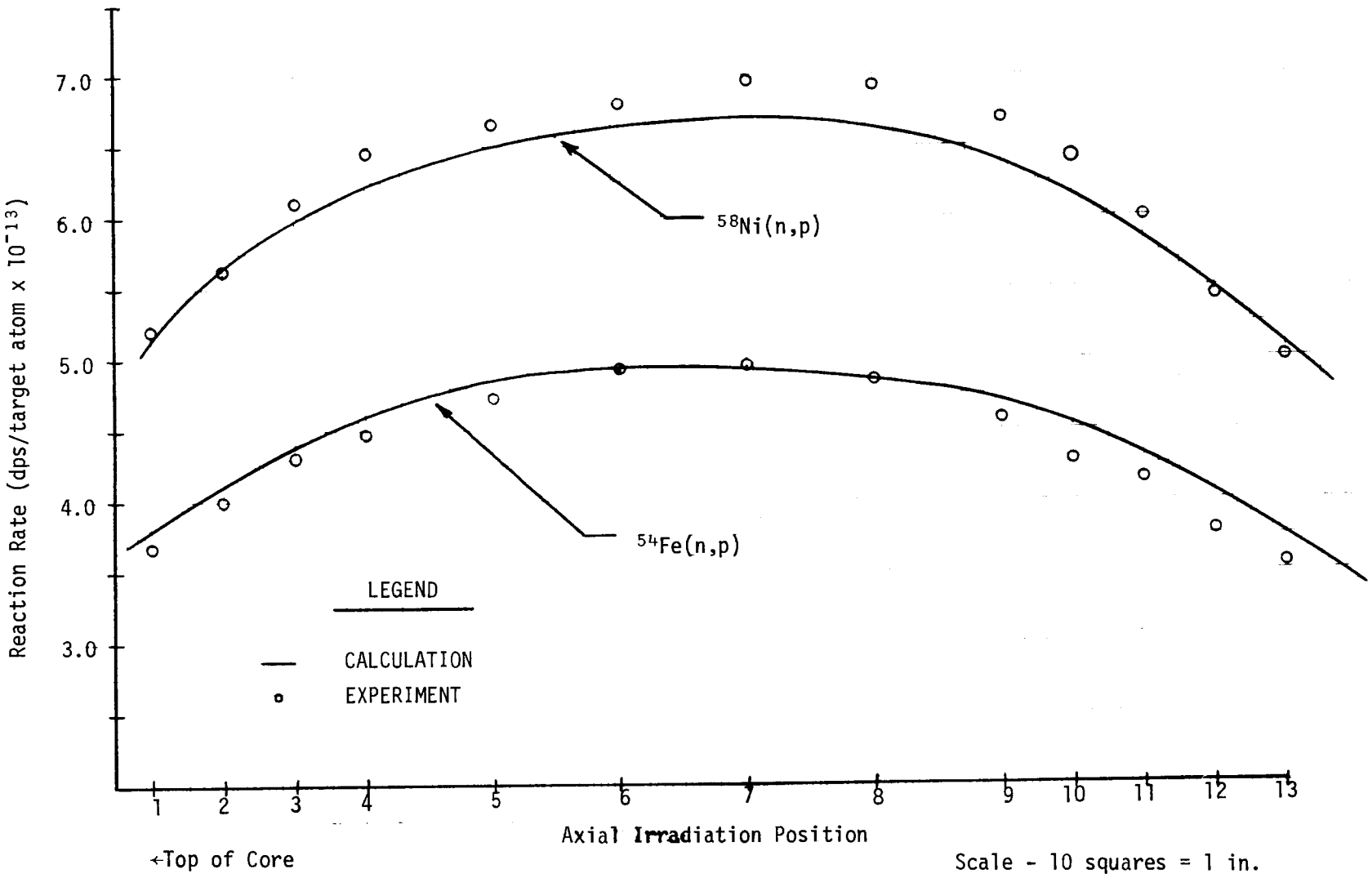

Fig. 16. Axial Distribution of the Absolute Activities of the ^{54}Fe(n,p) Reaction and ^{58}Ni(n,p) Reaction for Core No. 54, Tube 4

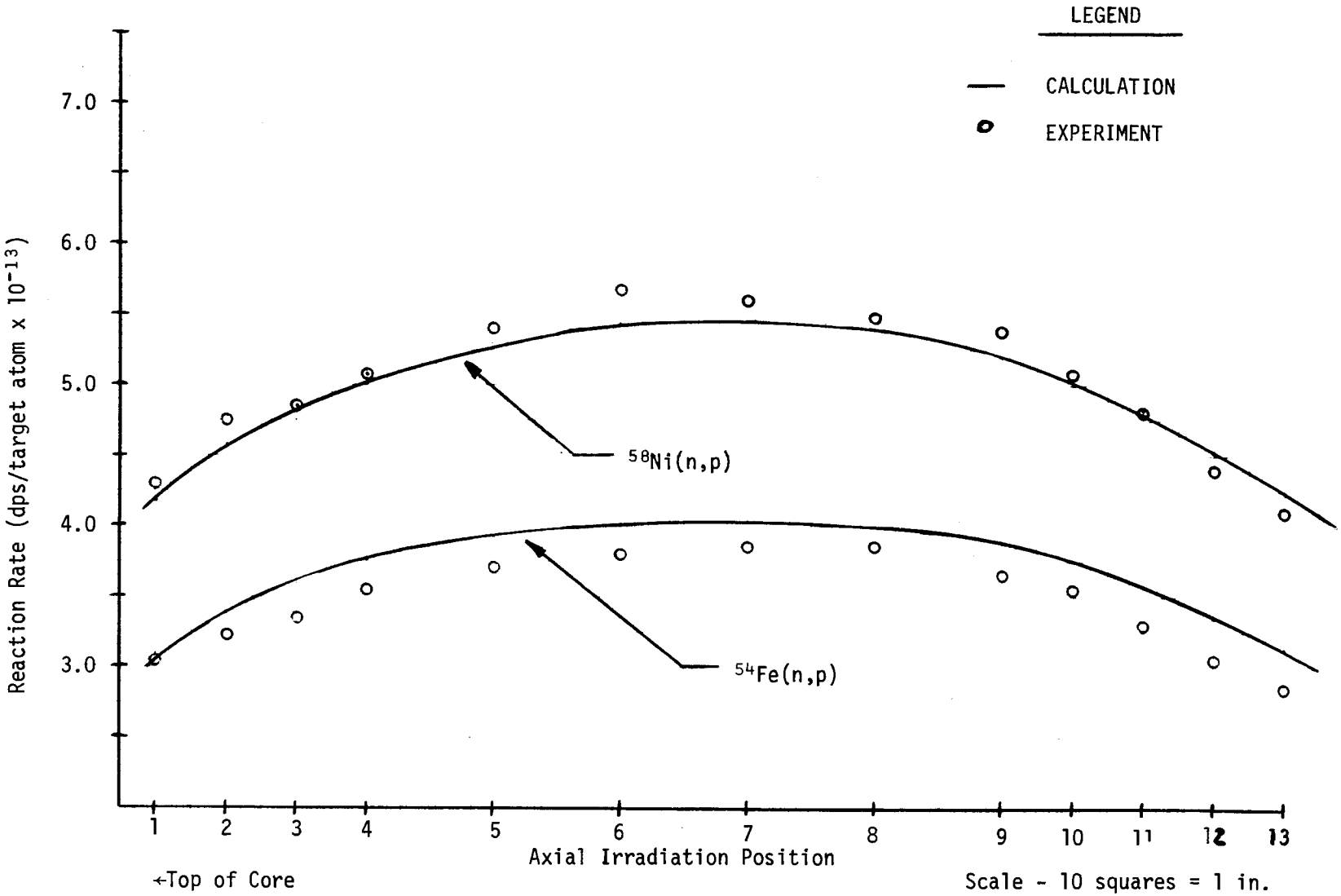

Fig. 17. Axial Distribution of the Absolute Activities of the ^{54}Fe(n,p) Reactions and ^{58}Ni(n,p) Reaction for Core No. 54, Tube 5

ACKNOWLEDGEMENTS

The author would like to express his sincere appreciation to Dr. P. F. Pasqua, Head, Department of Nuclear Engineering, for the opportunity to continue his education under the Graduate Research Program, and F. B. K. Kam, Operations Division, for the funding of this project. He would further like to thank Dr. L. F. Miller, Major Professor, for his expert guidance in the completion of this research, and Charles Baldwin for his help in the plotting packages used.

The work reported within this report is the exclusive work of the author and was performed at the Oak Ridge National Laboratories operated by Union Carbide Corporation.

INTERNAL DISTRIBUTION

1. C. A. Baldwin
2. H. L. Dodds
3. S. S. Hurt
4-8. J. O. Johnson
9-12. F. B. K. Kam
13. R. E. Maerker
14-18. L. F. Miller
19. M. L. Williams
20. Document Reference Section
21. Central Research Library
22-23. Laboratory Records Department
24. Laboratory Records - ORNL R.C.
25. ORNL Patent Office

EXTERNAL DISTRIBUTION

26. P. F. Pasqua, The University of Tennessee, Department of Nuclear Engineering, Knoxville, Tennessee 37916
27. J. A. Lenhard, Office of Assistant Manager for Energy Research and Development Department of Energy, Oak Ridge Operations Office, Oak Ridge, Tennessee 37830

28-54 Technical Information Center, DOE, Oak Ridge, Tennessee 37830